Production, Radiochemical Separation and Chemical Coupling of Radioactive Arsenic Isotopes to Synthesize Radiopharmaceuticals for Molecular Imaging

Dissertation zur Erlangung des Grades
„Doktor der Naturwissenschaften“

am Fachbereich Chemie und Pharmazie
der Johannes Gutenberg-Universität in Mainz

Marc Jennewein
geb. in Mainz

Mainz 2005

D77

Abstract

Noninvasive molecular-imaging technologies are playing a keyrole in drug discovery, development and delivery. Positron Emission Tomography (PET) is such a molecular imaging technology and a powerful tool for the observation of various diseases. However, it is limited by the availability of agents with high selectivity to the target and a physical half-life of the used positron emitting nuclide which matches the biological half-life of the observed process. For the long lasting enrichment of antibodies in tumor tissue few suitable isotopes for PET imaging are currently available. The element arsenic provides a range of isotopes, which could be used for diagnosis and also for endoradiotherapy.
This work describes the development of radiochemical separation procedures to separate arsenic isotopes in no-carrier-added (nca) purity from reactor or cyclotron irradiated targets, the development and evaluation of a labeling chemistry to attach these separated arsenic isotopes to monoclonal antibodies, the *in vitro* and *in vivo* evaluation of antibodies labeled with radioactive arsenic isotopes and the molecular imaging using small animal PET.
More precisely, the major achievements obtained in this thesis are:

1. the development, evaluation and optimization of two different $^{72}Se/^{72}As$ radionuclide generator systems, one based on a cyclic distillation process, separating nca ^{72}As in the form of $^{72}AsCl_3$ in an HCl gas flow from the target solution, the other one based on solid phase extraction of nca $^{72}AsI_3$ from the in $HF_{conc.}$ dissolved target.
2. the development, evaluation and optimization of a direct method to separate cyclotron or reactor produced radioactive arsenic isotopes from germanium oxide targets, based on the solubility of $[GeF_6]^{2-}$ and the solid phase extraction of nca $^{*}AsI_3$ (* = 71,72,73,74,76 or 77).
3. a chemical way of attaching the nca $^{*}AsI_3$ to various biomolecules of interest by using arsenic-sulphur affinity. As an example, a diprotected cysteine was coupled to diphenylarsenic iodide and 1,3-dimercaptopropylarsenic iodide.
4. the development of a labeling method for monoclonal antibodies (mAbs) and the labeling of the vascular targeting phosphatidylserine (PS)-selective mab (ch3G4, Tarvacin®) with $^{*}As$. The mAbs were modified with SATA (N-succinimidyl-S-acetylthioacetate) to introduce additional free thiol-groups to the mab. The labeled mab was tested for *in vitro* stability and immunoreactivity and no degradation of the label could be observed after 72 h incubation in serum and no inhibition of immunoreactivity was observed after SATA-modification and labeling.
5. *in vivo* evaluation of the *As[SATA]ch3G4 in R3327 Dunning prostate AT1 tumor bearing rats using planar scintigraphy on photostimulable plates and small animal PET for molecular imaging. Excellent and antigen specific tumor uptake could be shown and the subsequent biodistribution data corresponded with the imaging data.

This thesis has led to a series of manuscripts, conference proceedings and patents, describing all aspects in detail and implementing new technical and chemical solutions to the various problems arising when introducing new isotopes to nuclear medicine and PET.

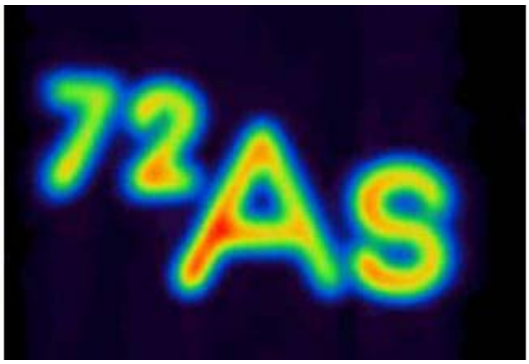
72As

This thesis is based on the following ten manuscripts, referred to by roman numerals:

I. Jennewein, M., A. Schmidt, A.F. Novgorodov, S.M. Qaim, F. Rösch, *A no-carrier-added $^{72}Se/^{72}As$ radionuclide generator based on distillation*, Radiochimica Acta, 92, (2004) 245-249

II. Jennewein, M., A. Hermanne, Mason, R.P., Constantinescu, A., Qaim, S.M., Rösch, F., *A no-carrier-added $^{72}Se/^{72}As$ radionuclide generator based on solid phase extraction*, Radiochimica Acta, submitted

III. Jennewein, M., Qaim, S.M., Hermanne, A., Tsyganov, E., Slavine, N., Seliounine, S., Antich, P.P., Kulkarni, P., Thorpe, P.E., Mason, R.P., and Rösch, F., *A New Method for the Radiochemical Separation of Arsenic from Reactor and Cyclotron Irradiated Germanium Oxide*, Appl. Rad. Isot., submitted

IV. Jennewein, M., Schirrmacher, R., Maus. S., Rösch, F., *Macroscopic Syntheses of arsenoorganic Precursors and first no-carrier-added radioarsenic labelling,* J. Lab. Comp. Radiopharm. 46 (2003) 42

V. Jennewein, M., Schirrmacher, R., Maus. S., Rösch, F., *Synthesis of 1,3-Dimercaptopropyl arsenic-Boc-Cysteine-O-Bzl and Diphenyl arsenic-Boc-Cysteine-O-Bzl and first labelling experiences*, J. Lab. Comp. Radiopharm. 46 (2003) 283

VI. Jennewein, M., Lewis, M., Zhao, D., Kodibagkar, V., Kulkarni, P., Tsyganov, E., Slavine, N., Seliounine, S., Antich, P.P., Qaim, S.M., Hermanne, A., Mason, R.P., Rösch, F., He, J., and Thorpe, P.E, *Vascular imaging of solid tumors in rats with a radioactive arsenic-labeled antibody that binds anionic phospholipids*, manuscript in preparation for Nat. Biotech.

VII. Lewis, M.A., G. Arbique, E. Richer, N. Slavine, M. Jennewein, A. Constantinescu, R. Brekken, J. Guild, E.N. Tsyganov, R.P. Mason, P.P. Antich, *Projection and Pinhole based Data Acquisition for Small Animal SPECT using Storage Phosphor Technology*, Small Animal SPECT Imaging, Chapter 26, Edited by H.H. Barrett and M. Kupinski, Kluwer Academic Publishers, NewYork (2004)

VIII. Tsyganov, E., P. P. Antich, G. Arbique, A. Constantinescu, J. Fernando, M. Jennewein, P. V. Kulkarni, R. P. Mason, R. W. McColl, O. Öz, R. W. Parkey, E. Richer, F. Rösch, S. Y. Seliounine, N. V. Slavine, P.Thorpe, G. Thambi, A. I. Zinchenko, *Performance of the Dallas Small Animal PET Imager*, IEEE Transactions in Nuclear Science, submitted for publication

IX. Jennewein, M., F. Roesch, J. Brockmann, *Verfahren zur Herstellung von trägerfreiem ^{72}As und Vorrichtung zur automatischen Herstellung von trägerfreiem ^{72}As und trägerfreiem ^{72}As (III)-Halogenid sowie deren Verwendung*, Patentschrift DE 103 44 101 B3 2004.12.30, Deutsches Patent- und Markenamt (2004)

X. Jennewein, M., F. Roesch, R. Schirrmacher, *Radioaktives Arsentriiodid und dessen Verwendung zur radioaktiven Markierung*, DE 103 50 397.8, submitted to Deutsches Patent- und Markenamt (2003)

Would it get some wind for the sailboat. And it could get for it is.
It could get the railroad for these workers. And it could be were it is.
It could Franky it could be Franky it could be very fresh and clean.
It could be a ballon.
All these are the days my friends and these are the days my friends.
Would it get some wind for the sailboat. And it could get for it is.
It could get the railroad for these workers. And it could be were it is.
It could Franky it could be Franky it could be very fresh and clean.
It could be a ballon.
All these are the days my friends and these are the days my friends.
It could be those days.

Knee Play 1.

from *‚Einstein on the beach'*, an Opera by Philip Glass.

Table of Contents

1. Introduction

1.1 Arsenic: Drug and Poison throughout the centuries

Arsenic was first used by the Greeks and Chinese more than 2,000 years ago to treat everything from syphilis to cancer, but was also the favourite poison of the Savellis, the Borgias [1, 2], Agatha Christie and famous movie classics, like 'Arsenic and Old Lace' (1944). By the mid-twentieth century, the discoveries of antibiotics and chemotherapy led to the abandonment of arsenic-based treatments, which remained in use only for treating trypanosomiasis [3]. Apart from the radiopharmaceutical studies presented here, the only mention of arsenic today would have been in environmental chemistry [4] in the actual discussions of water contamination [5], had it not been for the discovery of an arsenic-rich Chinese traditional medicine that induced dramatic remissions in acute promyelocytic leukaemia (APL). Arsenic trioxide (As_2O_3) was identified as the active component of this medicine and shown to trigger both the differentiation and apoptosis of leukaemic cells, in a manner similar to that of retinoic acid (RA). Subsequent studies on As_2O_3 increased the knowledge of pathologic pathways of APL dramatically [2, 3, 6-18].

Arsenic is a relatively common element, but pure metallic arsenic is rarely found in nature (so called 'Fliegenstein' or 'Scherbencobalt' [19]). Apart from the organic arsenicals (in which arsenic atoms are covalently bound to carbon-containing molecules), there are three main inorganic arsenic forms: red arsenic (As_4S_4, also known as 'realgar'), yellow arsenic (As_2S_3, also known as 'orpiment'), and white arsenic (arsenic trioxide, As_2O_3) — which is made by burning realgar or orpiment [20]. Arsenic has an impressive reputation as a poison — this conveniently tasteless agent induces acute or chronic illness, mimicking common disorders such as haemorrhagic gastroenteritis, cardiac arrhythmia or even psychiatric diseases. Beginning in the middle ages, As_2O_3 became a common homicide tool [1] and many people believe that Napoleon was poisoned by arsenic-tainted wine, although scientific analysis has disproved this theory [21]. Chronic arsenic exposure through water contaminated by herbicides, pesticides or mining by-products is a public-health problem, owing to its association with bladder, lung, skin and other sorts of cancer [2]. By contrast, arsenic doesn't show carcinogenicity in animal models or cells in culture, so the mechanism by which it promotes tumour development is not understood [2, 22, 23].

Arsenic-derived therapies arose independently in China and Greece (c.f. Fig. 1). Arsenic seems to have been unknown to Egyptian medicine, although it might be the 'stone' referred to as an active agent in the Berlin papyrus. The first mention of arsenicals was made by Hippocrates (460–370 BC), who used realgar and orpiment pastes to treat ulcers. He carefully described the appearance of the naturally occurring sulphur derivatives and the best places to find them. Asclepiade (124–40 BC) extended the use of arsenic to rheumatic diseases. Dioscorides (40–90 AD) later noted that arsenicals caused hair loss but cleared scabies, lice and many skin growths that might have been cancers [2]. He noted that As_2O_3 was a dangerous poison, but at low doses it was effective in treating tuberculosis or emphysema. As the Greeks were exploring the effects of arsenic, this drug was already an ingredient of many folk remedies in central and southern Asia. The Nuei-King treaty (263 BC) described arsenic pills for periodic fever [2]. Sun Simiao (581–682 AD) purified a medicine composed of realgar, orpiment and arsenic trioxide, which he used for the treatment of malaria [2]. Later, the pharmacopeadia of Shi-Zhen Li in the Ming Dynasty described the use of As_2O_3 to treat a variety of diseases. In Persian textbooks, Avicennes (980–1037 AD) described the use of white arsenic to treat fevers. These texts, along with writings by Paracelsus (1493–1541 AD) introduced arsenic therapy to Europe [2].

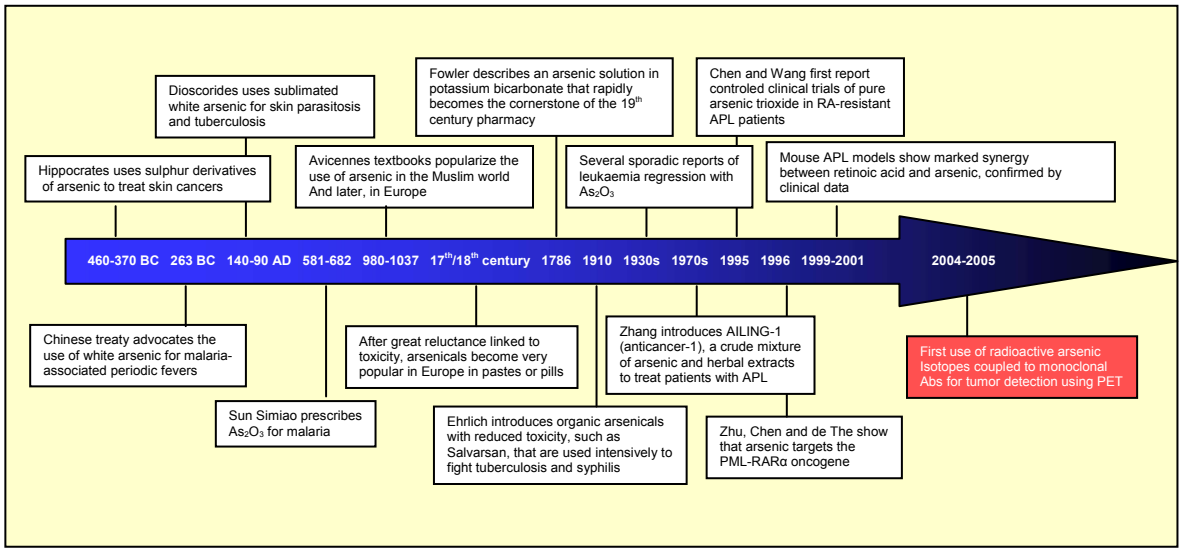

FIGURE 1. Timeline of arsenic as drug and poison throughout the centuries [2]

Although Europeans experimented with arsenic therapy in the sixteenth century, by the seventeenth century, arsenicals were seldom used because of toxicity. In the eighteenth century, William Withering, who extracted a powerful cardiotonic from the flower *Digitalis*, stated that "poisons in small doses are the best medicines and the best medicines in too large doses are poisonous", and accordingly advocated arsenic-based therapies. An amazing number of arsenic-derived preparations flourished throughout that century. For example, in 1774, Lefébure introduced an arsenic-containing paste proposed to be an "established remedy to radically cure all cancers" [2]. In the late eighteenth century, Thomas Fowler created a potassium bicarbonate based solution of arsenic that was originally used to treat periodic fever, and, later, a large variety of diseases. Fowler's liquor, nicknamed 'the mule' for both its strength and its unpredictability, became the cornerstone of nineteenth-century pharmacy [24]. There were fierce debates over dosage — many physicians believed that toxicity had to be achieved for arsenic to have therapeutic effects, whereas others believed that smaller doses were effective. The idea that small quantities of arsenic had therapeutic benefits was supported by the discovery of 'arsenic eaters' in Austria - women, men and even horses that consumed arsenic on a daily basis. This practice supposedly caused obesity and red cheeks in women, making them "attractive", whereas men claimed that arsenic greatly improved their strength. Arsenic self-medication became common throughout Europe, despite a number of dramatic arsenic poisonings that were associated with improper waste management in the emerging chemical industry or with the use of arsenic derivatives as pigments, such as 'vert de Paris'. Arsenic's popularity peaked in 1910 when Paul Ehrlich introduced salvarsan, an organic arsenic-based product that was shown to be effective in treating tuberculosis and syphilis. Other organic arsenicals, such as melarsoprol (2-[4-[(4,6-Diamino-1,3,5-triazin-2-yl)amino]phenyl]-1,3,2-dithiarsolane-4-methanol), are still used to treat trypanosomiasis [25]. As medicine evolved, enthusiasm for arsenic waned, because newer drugs had a greater therapeutic index. In 1930, a brief resurgence in popularity followed a report of patients with chronic leukaemia who responded to As_2O_3 therapy, but later developed chronic poisoning [26]. Since this time, arsenicals remained in pharmacology textbooks as fossils, raising some embarrassment over the continuing use of drugs from another age [24]. In the early 1970s, a group from Harbin Medical University in the northeastern region of China studied more than 1,000 cancer patients and found that intravenous infusions of Ailing-1 — a crude solution of As_2O_3 and trace amounts of mercury — could be used to

treat patients with APL. Complete clinical remission was achieved in two-thirds of patients, with an impressive 30% survival rate after 10 years [27]. Paradoxically, Western school medicine had expressed concern about the presence of mercury and As_2O_3 in Chinese traditional medicines. Nonetheless, the Chinese results were rapidly confirmed in clinical trials that were performed in Japan, Europe and the United States, and the drug is now used worldwide to treat patients with APL who have undergone relapse from their primary therapy [2].

In terms of arsenic-radiopharmacy, there were some early developments in the 1950s and 1960s on ^{74}As. This is a positron emitting isotope ($T_{1/2}$= 17.8 d) with a positron emission rate of 29 % with an extreme low positron energy of E_{β^+mean} = 128 keV and an electron emission rate of 34.2 % and E_{β^-mean} = 137 keV. It was one of the first isotopes used for very preliminary forms of Positron Emission Tomography (PET) in the 1950s and 1960s called positrocephalography in those times [28]. Mainly due to chemical and, with the no-carrier-added (nca) trace amounts used in nuclear medicine more psychological, toxicity problems, radioactive arsenic completely disappeared from nuclear medicine and radiopharmaceutical research until today.

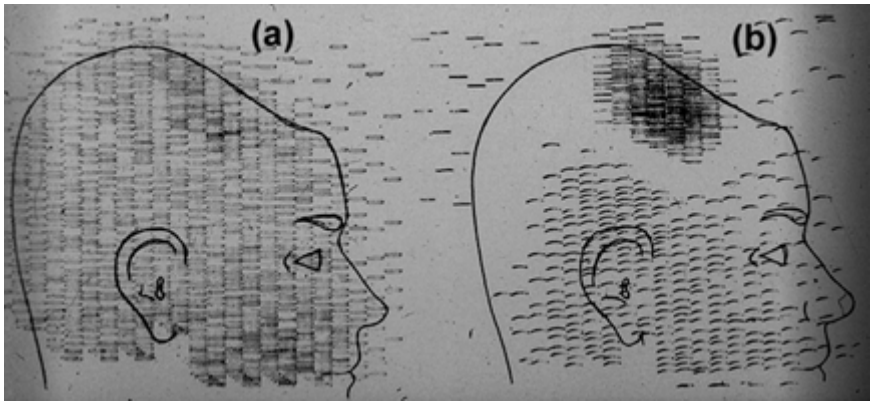

FIGURE 2. Coincidence and unbalance scans of patient with recurring brain tumor using [^{74}As]arsenate. Coincidence scan (a) of a patient showing recurrence of tumor under previous operation site, and unbalance scan (b) showing asymmetry to the left. [28]

1.2 Positron Emission Tomography (PET)

PET is a non invasive, diagnostic imaging technique for measuring the metabolic activity of cells in the human body. It is particulary useful clinically in patients with certain diseases affecting the brain and the heart as well as in patients with certain types of cancer. PET is unique because it produces images of the body's basic biochemistry and functions. By contrast, traditional diagnostic techniques, such as X-rays, CT scans or MRI, mainly produce images of the body's anatomy or structure. The premise with these techniques is, that the change in structure or anatomy that occurs with disease can be observed. Biochemical processes are also altered with disease and may occur long before there is a change in gross anatomy. PET is an imaging technique that is used to visualize some of these processes that change. Even in some diseases, such as Alzheimer's disease, where there is no gross structural abnormality, PET is able to show a biochemical change and therefore a pathological condition.
The following six premises explain the necessity and value of a non-invasive molecular imaging tool like PET for functional imaging versus morphological imaging [29]:

1. The basis of all tissue function is chemical.
2. Diseases result from errors introduced into its chemical systems by viruses, bacteria, genetic abnormalities, drugs, environmental factors, aging, and behavior.
3. The most selective, specific, and appropriate therapy is one chosen from a diagnostic measure of the basic chemical abnormality.
4. Detection of chemical abnormalities provides the earliest identification of disease, even in the presymptomatic stages before the disease process has exhausted the chemical reserves or overridden the compensatory mechanisms of the brain.
5. Assessment of restoration of chemical function provides an objective means for determining the efficacy of therapeutic interventions in the individual patient.
6. The best way to judge whether tissue is normal is by determining its biochemical function.

Chemical compounds followed via PET through the body are labeled with radioactive atoms that decay by emitting positrons. Labeling is defined as a process of attaching some kind of identifying tag to the compound you want to follow, which will later let you

identify where the compound has gone. In principle, the compounds that can be labeled are limited only by the imagination of the investigators and the physical half-life of the positron emitting label.

Another very important attribute of the labelled compound is that it can be used in *trace* quantities. This concept was introduced by Georg de Hevesy (1885-1966) [30]. The main idea is that the labeled compounds can be introduced into the body without pharmacodynamically affecting the normal processes of the body. Hevesy won the Nobel Prize in chemistry 1943 for 'the use of isotopes as probes for the investigation of chemical processe'. He examined the metabolism of plants using the radioactive isotope ^{212}Pb. Today, his discoveries are applied to labelled molecules at nano-molar concentrations for the investigation of physiological processes *in vivo*. PET is sensitive enough to detect trace amounts of a labeled compound and so is well suited to this kind of investigation.

Radiolabeled tracers and the tracer kinetic method are employed throughout the biological sciences to measure such processes as blood flow, membrane transport, metabolism and ligand-receptor interactions; for mapping axonal projection fields through anterograde and retrograde diffusion; measurement of cell birth dates; marker assays using recombinant DNA techniques; radioimmunoassays; and the study of drug interactions with chemical systems of the body. The tracer technique continues to be one of the most sensitive and widely used methodologies for performing assays of biological systems. PET allows the transfer of the tracer assay methodology to the living subject, particularly humans.

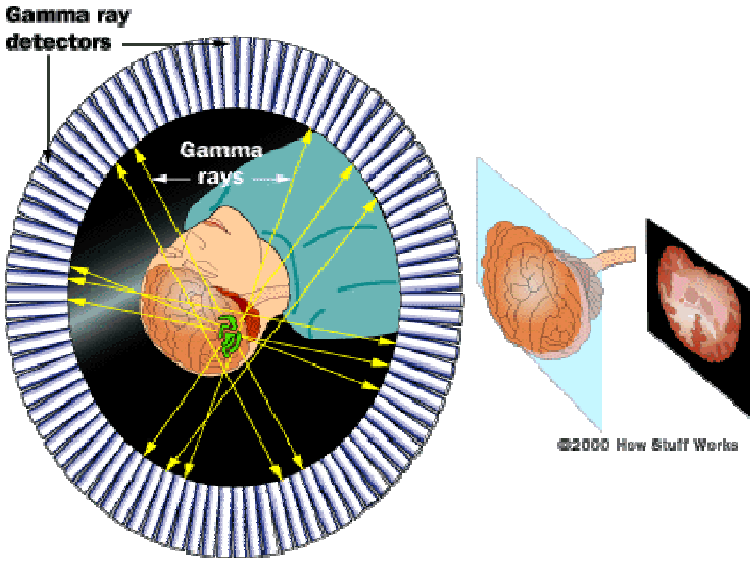

FIGURE 3. Scheme of a PET-system, showing the ring of detectors, surrounding a brain with a positron emitting source.

The mode of positron decay is particularly advantageous for detection and quantification by an external measurement. The decay process begins in the nucleus of a neutron-deficient isotope upon the conversion of a proton to a neutron with simultaneous emission of a positron, or β^+-particle, from the nucleus. The positron is similar to an electron in physical properties except that it is positively rather than negatively charged. The emitted positron is slowed by loss of kinetic energy to the surrounding matter along its path and ultimately combines with an electron. In an intermediate state a positronium with a lifetime of 0.125 ns is formed. In a final interaction, positron annihilation, results in disintegration of both the positron and the electron, with the simultaneous emission of energy equivalent to their combined mass of 1.022 MeV. The emitted energy is in the form of two photons, or γ-rays, with energies of 511 keV that travel in essentially opposite directions [31].

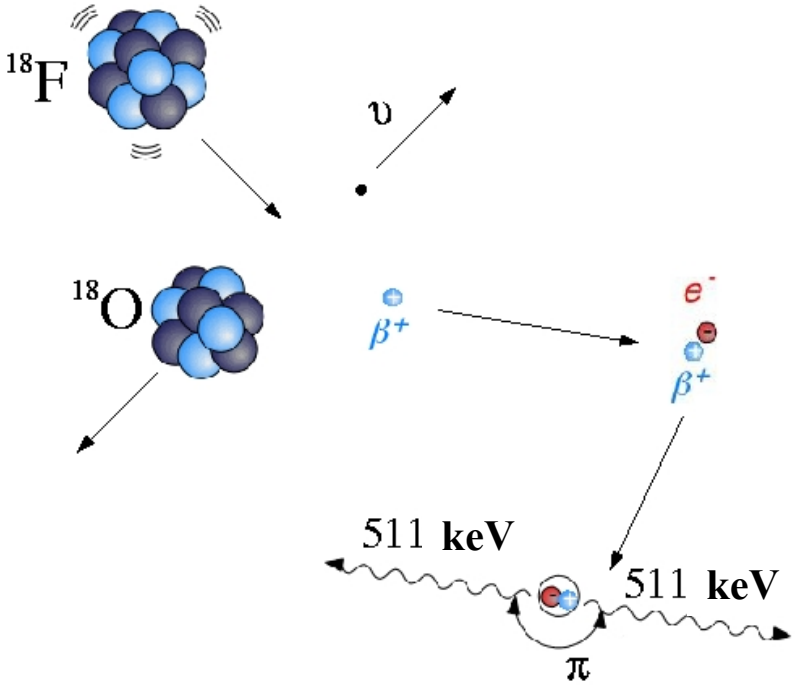

FIGURE 4. Scheme of the β^+-decay of ^{18}F, the most common PET isotope.

Nuclide	Half-Life (min)	Maximum energy (MeV)	Maximum range (mm H_2O)
^{11}C	20.4	0.97	4
^{13}N	9.96	1.20	5
^{15}O	2.04	1.74	8
^{18}F	109.8	0.64	2
^{62}Cu	9.73	2.92	14
^{68}Ga	68.1	1.90	9
^{82}Rb	1.3	3.35	17
Annihilation photon	—	0.511	7,000[a]

[a] Half-value distance.

TABLE 1. Physical Properties of Selected Positron-Emitting Nuclides and Positron Annihilation Photons

Photons, unlike positrons, undergo relatively little interaction with surrounding materials of low density; they are not easily deflected from their course and are readily detected at a distance outside the body. Because of the simultaneous emission of the two photons in exactly opposite directions, coincidence-detection algorithms for quantification of positron decay are employed, resulting in images with a high signal-to-noise ratio [29]. Table 1 shows the physical properties of selected positron-emitting nuclides and positron annihilation photons.

1.3 Phosphatidylserine (PS) as a Marker for Tumor Vasculature

Anionic phospholipids are largely absent from the surface of resting mammalian cells under normal conditions. PS, which is the most abundant anionic phospholipid of the plasma membrane, is tightly segregated to the internal leaflet of the plasma membrane in most cell types [32]. PI (phosphatidylinositol), another major anionic phospholipid, is also situated predominantly in the internal leaflet of the plasma membrane. The minor anionic phospholipids, PA (phophatidic acid) and PG (phosphatidylglycerol), have only been examined in a few cells types, but they also appear to be mainly situated in the internal leaflet of the plasma membrane. CL (cardiolipin), another anionic phospholipid, is present in the mitochondrial membrane and is absent from the plasma membrane. The neutral phospholipids are also asymmetrically distributed in the plasma membrane; PE (phosphatidylethanolamine) is predominately on the internal leaflet, whereas the choline-containing phospholipids, PC (phosphatidylcholine) and SM (spingomyelin), are predominantly on the external leaflet [33]. PS asymmetry, along with that of PE, is maintained by an ATP-dependent aminophospholipid translocase that catalyzes the transport of aminophospholipids from the external leaflet to the internal leaflet of the plasma membrane. Loss of PS and PE asymmetry results from the outward movement of these phospholipids in the plasma membrane and is caused either by inhibition of the translocase or activation of scramblase, a Ca^{2+}-dependent enzyme that transports all of the lipids bidirectionally. Loss of asymmetry is observed under different pathological and physiological conditions, including apoptosis, cell activation, injury, and malignant transformation. Exposure of PS also plays a role in intercellular fusion and cell migration. Endothelial cells externalize PS in response to increased Ca^{2+} fluxes induced by thrombin, calcium ionophore or phorbol esters, hyperlipidemia and nonlytic concentrations of complement proteins C5b-9 [32, 33]. Several major consequences follow membrane PS exposure. Phagocytic macrophages recognize, attach, and eliminate PS-positive senescent and apoptotic cells. PS also mediates attachment of T-lymphocytes to thrombin- activated endothelial cells. The complement system is activated by PS and contributes to the lysis of PS-positive cells. Finally, PS exposure contributes to a procoagulant shift on the endothelium by providing a negatively charged lipid surface for assembly and activation of coagulation complexes.

Antibodies, annexins, and other targeting vectors that bind to anionic phospholipids might be used for the targeting or imaging of tumor blood vessels. Anionic phospholipids are attractive as tumor vessel targets for several reasons: they are abundant (PS is present at 10^6 molecules per cell) [32, 33]; they are on the luminal surface of tumor endothelium, which is directly accessible for binding by vascular targeting agents in the blood; they are present on a significant percentage of tumor endothelial cells in diverse solid tumors; and they appear to be absent from endothelium in all normal tissues. In this thesis, PS-selective antibodies are used for the molecular imaging of tumor blood vessels in syngeneic Dunning prostate R3327AT1 adenocarcinoma in rats.

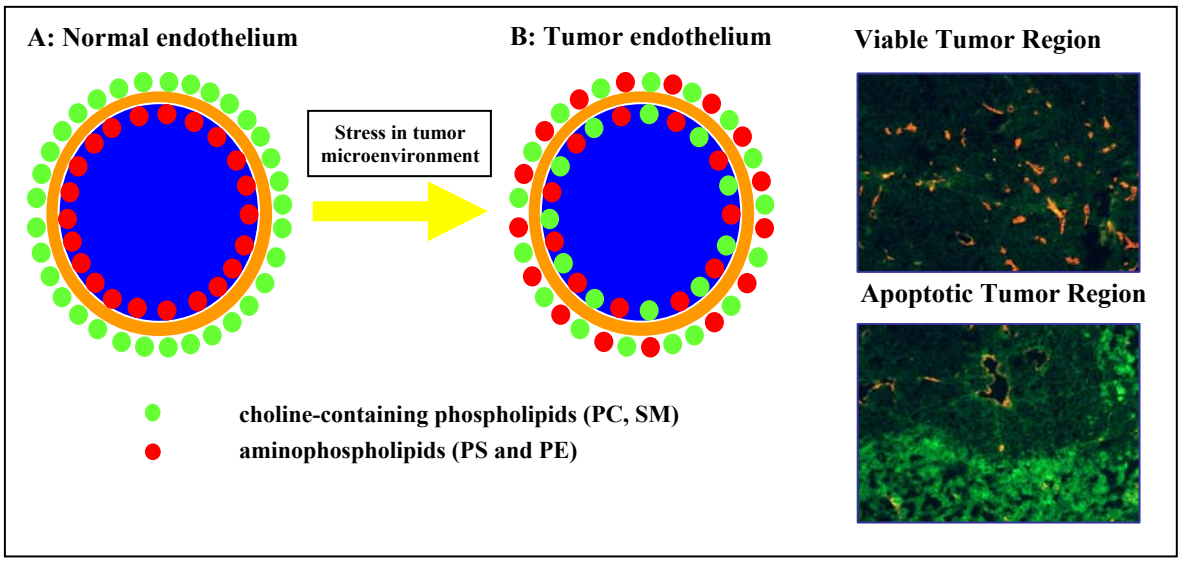

FIGURE 5. Phopholipid distribution on normal and tumor endothelium

2. Problem

Non-invasive molecular-imaging technologies are playing a key role in drug discovery, development and delivery. Positron Emission Tomography (PET) is such a molecular imaging technology and a powerful tool for the observation of various diseases. However, it is limited by the availability of vectors with high selectivity to the target and radionuclides with a physical half-life which matches the biological half-life of the observed process. For the long lasting enrichment of antibodies in tumor tissue, *e.g.*, currently few suitable isotopes for PET imaging are available. The element arsenic provides a range of isotopes, which could be used for diagnosis and also for endoradiotherapy. Once a labeling chemistry is established, the same chemistry could be used for targeting and for treating a tumor with simply exchanging the isotope on the labeled molecule.

Among diagnostic approaches in nuclear medicine oncology PET provides the most accurate technique to localise and to quantify tumour specific biochemical interactions. However, the commonly used "organic" isotope ^{11}C ($T_{½}$ = 20 min), ^{13}N ($T_{½}$ = 10 min), ^{15}O ($T_{½}$ = 2 min) and ^{18}F ($T_{½}$ = 110 min) have short half-lives not useful for immunological problems with labelled monoclonal antibodies, fragments or peptides. Due to their relatively long biological half-life, longer-lived positron emitters would be more adequate. Fortunately, there are some of those longer-lived radioisotopes with sufficiently high positron branching. Among them there are different arsenic radioisotopes: ^{70}As ($T_{½}$ = 52.5 min, 100% β^+), ^{71}As ($T_{½}$ = 64 h, 30% β^+), ^{72}As ($T_{½}$ = 26 h, 85% β^+) and ^{74}As ($T_{½}$ = 17.77 d, 29% β^+). These isotopes can be produced at small cyclotrons. Moreover, ^{72}As is also available via a radioisotope generator system, which could enable a steady availability in medical departments due to its relatively long-lived generator mother nuclide ^{72}Se ($T_{½}$ ≈ 8.2 d).

Positron-emitting isotopes of arsenic have not yet been considered systematically for the preparation of any PET compound. Also in the context of other radiochemical studies those isotopes have been rarely used. Thus very little information is available regarding the production of the isotopes ^{70}As, ^{71}As, ^{72}As and ^{74}As at cyclotrons. Somewhat more information is available on the radiochemical separation of radioarsenic from the corresponding target elements, namely germanium. However, to date these procedures

have never been applied in radiopharmaceutical chemistry. This is also the case for the potential radioisotope generator system $^{72}Se \rightarrow {}^{72}As$. Most importantly, however, seems to be the labeling chemistry for the attachment of arsenic to biochemical molecules. There are no studies on this topic in the context of the preparation of PET radiopharmaceuticals so far and there have been no chemical reactions available to label arsenic isotopes to tumour targeting compounds such as small peptides or larger proteins such as monoclonal antibodies or fragments. Once such a labelling chemistry is developed, one could potentially switch from diagnosis to endoradiotherapy. Using the identical labeling chemistry, this can be done by introducing other arsenic radioisotopes, namely the β^- emitters ^{76}As ($T_{½}$ = 26.4 h, 100% β^-) or ^{77}As ($T_{½}$ = 38.8 h, 100% β^-). Both therapeutic isotopes can be produced with relatively high yields at nuclear reactors.

To introduce new isotopes to radiopharmacy and PET, several steps have to be taken:

1. Optimization of the isotope production via cyclotrons and nuclear reactors
2. Development and evaluation of radiochemical separation procedures suitable for a possible future routine and reliable application in radiopharmacy and nuclear medicine
3. Development and evaluation of a labeling chemistry and the identification of promising biomolecules for labeling
4. *in vitro* and ultimately *in vivo* evaluation of the labeled compounds, namely serum stability, immunoreactivity and biodistribution
5. *in vivo* imaging in an appropriate animal model

This thesis describes all five aspects in detail, gives an in-depth review of the current status of literature and implements new technical and chemical solutions to the various problems arising when introducing new isotopes to nuclear medicine and PET.

References:

1. Micca, G., *Arsenic, or rather arsenious anhydride, the preferred poison of the Borgias.* Minerva Med, 1969. **60**: p. IX-XI.
2. Zhu, J., Z. Chen, V. Lallemand-Breitenbach, and H. de The, *How acute promyelocytic leukaemia revived arsenic.* Nat Rev Cancer, 2002. **2**(9): p. 705-13.
3. Ravandi, F., *Arsenic trioxide: expanding roles for an ancient drug?* Leukemia, 2004. **18**(9): p. 1457-9.
4. Basile, D., C. Birattari, M. Bonardi, L. Goetz, E. Sabbioni, and A. Salomone, *Excitation functions and production of arsenic radioisotopes for environmental toxicology and biomedical purposes.* Int J Appl Radiat Isot, 1981. **32**(6): p. 403-10.
5. Tisler, T. and J. Zagorc-Koncan, *Acute and chronic toxicity of arsenic to some aquatic organism.* Bull Environ Contam Toxicol, 2002. **69**: p. 421-429.
6. Chen, G.Q., X.G. Shi, W. Tang, S.M. Xiong, J. Zhu, X. Cai, Z.G. Han, J.H. Ni, G.Y. Shi, P.M. Jia, M.M. Liu, K.L. He, C. Niu, J. Ma, P. Zhang, T.D. Zhang, P. Paul, T. Naoe, K. Kitamura, W. Miller, S. Waxman, Z.Y. Wang, H. de The, S.J. Chen, and Z. Chen, *Use of arsenic trioxide (As_2O_3) in the treatment of acute promyelocytic leukemia (APL): I. As_2O_3 exerts dose-dependent dual effects on APL cells.* Blood, 1997. **89**(9): p. 3345-53.
7. Chen, G.Q., J. Zhu, X.G. Shi, J.H. Ni, H.J. Zhong, G.Y. Si, X.L. Jin, W. Tang, X.S. Li, S.M. Xong, Z.X. Shen, G.L. Sun, J. Ma, P. Zhang, T.D. Zhang, C. Gazin, T. Naoe, S.J. Chen, Z.Y. Wang, and Z. Chen, *In vitro studies on cellular and molecular mechanisms of arsenic trioxide (As_2O_3) in the treatment of acute promyelocytic leukemia: As_2O_3 induces NB4 cell apoptosis with downregulation of Bcl-2 expression and modulation of PML-RAR alpha/PML proteins.* Blood, 1996. **88**(3): p. 1052-61.
8. Chouchane, S. and E.T. Snow, *In vitro effect of arsenical compounds on glutathione-related enzymes.* Chem Res Toxicol, 2001. **14**(5): p. 517-22.
9. Griffin, R.J., S.H. Lee, K.L. Rood, M.J. Stewart, J.C. Lyons, Y.S. Lew, H. Park, and C.W. Song, *Use of arsenic trioxide as an antivascular and thermosensitizing agent in solid tumors.* Neoplasia, 2000. **2**(6): p. 555-60.

10. Kim, J.H., Y.S. Lew, A. Kolozsvary, S. Ryu, and S.L. Brown, *Arsenic trioxide enhances radiation response of 9L glioma in the rat brain.* Radiat Res, 2003. **160**(6): p. 662-6.
11. Larochette, N., D. Decaudin, E. Jacotot, C. Brenner, I. Marzo, S.A. Susin, N. Zamzami, Z. Xie, J. Reed, and G. Kroemer, *Arsenite induces apoptosis via a direct effect on the mitochondrial permeability transition pore.* Exp Cell Res, 1999. **249**(2): p. 413-21.
12. Miller, W.H., Jr., H.M. Schipper, J.S. Lee, J. Singer, and S. Waxman, *Mechanisms of action of arsenic trioxide.* Cancer Res, 2002. **62**(14): p. 3893-903.
13. Shen, Z.X., G.Q. Chen, J.H. Ni, X.S. Li, S.M. Xiong, Q.Y. Qiu, J. Zhu, W. Tang, G.L. Sun, K.Q. Yang, Y. Chen, L. Zhou, Z.W. Fang, Y.T. Wang, J. Ma, P. Zhang, T.D. Zhang, S.J. Chen, Z. Chen, and Z.Y. Wang, *Use of arsenic trioxide (As_2O_3) in the treatment of acute promyelocytic leukemia (APL): II. Clinical efficacy and pharmacokinetics in relapsed patients.* Blood, 1997. **89**(9): p. 3354-60.
14. Wang, Z.Y., *Arsenic compounds as anticancer agents.* Cancer Chemother Pharmacol, 2001. **48 Suppl 1**: p. S72-6.
15. Zhu, J., M.H. Koken, F. Quignon, M.K. Chelbi-Alix, L. Degos, Z.Y. Wang, Z. Chen, and H. de The, *Arsenic-induced PML targeting onto nuclear bodies: implications for the treatment of acute promyelocytic leukemia.* Proc Natl Acad Sci U S A, 1997. **94**(8): p. 3978-83.
16. Zhu, J., V. Lallemand-Breitenbach, and H. de The, *Pathways of retinoic acid- or arsenic trioxide-induced PML/RARalpha catabolism, role of oncogene degradation in disease remission.* Oncogene, 2001. **20**(49): p. 7257-65.
17. Zhu, J., H. Okumura, S. Ohtake, S. Nakamura, and S. Nakao, *Arsenic trioxide induces apoptosis in leukemia/lymphoma cell lines via the CD95/CD95L system.* Oncol Rep, 2003. **10**(3): p. 705-9.
18. Zhu, X., N.A. Larsen, A. Basran, N.C. Bruce, and I.A. Wilson, *Observation of an arsenic adduct in an acetyl esterase crystal structure.* J Biol Chem, 2003. **278**(3): p. 2008-14.
19. Riedel, E., *Anorganische Chemie*. 3 ed. 1994, Berlin, New York: de Gruyter.
20. Zingaro, R.A., *Arsenic: Inorganic and Organoarsenic Chemistry*, in *Encyclopedia of Inorganic Chemistry*, R.B. King, Editor. 1994, John Wiley&Sons. p. 192-219.

21. Keynes, M., *Did Napoleon die from arsenical poisoning?* Lancet, 1994. **344**: p. 276.
22. Bode, A.M. and Z. Dong, *The paradox of arsenic: molecular mechanisms of cell transformation and chemotherapeutic effects.* Crit Rev Oncol Hematol, 2002. **42**(1): p. 5-24.
23. Huff, J., P. Chan, and A. Nyska, *Is the human carcinogen arsenic carcinogenic to laboratory animals?* Toxicol Sci, 2000. **55**(1): p. 17-23.
24. Waxman, S. and K.C. Anderson, *History of the development of arsenic derivatives in cancer therapy.* Oncologist, 2001. **6 Suppl 2**: p. 3-10.
25. *The Merck Index*. 12 ed, ed. S. Budavari, et al. 1996, New York: Merck Research Laboratories, MERCK&CO., Inc.
26. Kwong, Y.L. and D. Todd, *Delicious poison: arsenic trioxide for the treatment of leukemia.* Blood, 1997. **89**(9): p. 3487-8.
27. Zhang, P., S. Wang, L. Hu, F. Qiu, H. Yang, Y. Xiao, X. Li, X. Han, J. Zhou, and P. Liu, *[Seven years' summary report on the treatment of acute promyelocytic leukemia with arsenic trioxide--an analysis of 242 cases]*. Zhonghua Xue Ye Xue Za Zhi, 2000. **21**(2): p. 67-70.
28. Sweet, W.H. and G.L. Brownell, *Localization of intracranial lesions by scanning with positron-emitting arsenic.* J Am Med Assoc, 1955. **157**(14): p. 1183-1188.
29. Phelps, M.E., *Positron Emission Tomography*. Clinical Brain Imaging: Principles and Application, ed. J. Mazziotta and S. Gilman. 1992, New York: F.A. Davis Company.
30. de Hevesy, G., *Adventures in Radioisotope Research*. Vol. 1. 1962, New York: Pergamon Press.
31. Saha, B.S., *Fundamentals of Nuclear Pharmacy*. 1997, New York, Berlin, Heidelberg: Springer.
32. Ran, S., A. Downes, and P.E. Thorpe, *Increased exposure of anionic phospholipids on the surface of tumor blood vessels.* Cancer Res, 2002. **62**(21): p. 6132-40.
33. Ran, S. and P.E. Thorpe, *Phosphatidylserine is a marker of tumor vasculature and a potential target for cancer imaging and therapy.* Int J Radiat Oncol Biol Phys, 2002. **54**(5): p. 1479-84.

3. Manuscripts

I.

A no-carrier-added ^{72}Se/^{72}As radionuclide generator based on distillation

A no-carrier-added $^{72}Se/^{72}As$ radionuclide generator based on distillation

by M. Jennewein[1], A. Schmidt[1], A.F. Novgorodov[2], S.M. Qaim[3], F. Rösch[1]

Dedicated to the memory of Professor Gerhard L. Stöcklin

[1]Institute for Nuclear Chemistry, Johannes Gutenberg University, Fritz-Strassmann-Weg 2, D-55128 Mainz, Germany;

[2]Joint Institute for Nuclear Research, Laboratory of Nuclear Problems,

RUS-141980 Dubna, Russian Federation

[3]Institut für Nuklearchemie, Forschungszentrum Jülich GmbH, D-52425 Jülich, Germany

Key Words:

As-72, Se-72, Radionuclide generator, Distillation

Summary

Arsenic-72 is a positron emitting isotope with promising properties for future application to syntheses of ^{72}As-labelled radiopharmaceuticals applied to positron emission tomography. This work describes the radiochemical separation of no-carrier-added ^{72}Se from cyclotron irradiated germanium targets and the development of a ^{72}Se/^{72}As radionuclide generator, avoiding the addition of any selenium carrier. Using a vertical quartz tube device, no-carrier-added ^{72}As is nearly quantitatively released from various chloride salt solutions containing ^{72}Se within 10 min at temperatures of 100°C in an HCl gas flow. The distillation kinetics in dependence of temperature and salt-charge of the ^{72}Se/^{72}As isotope generator, as well as the redox-stability of the system, have been extensively studied. Under optimised conditions, ^{72}Se remains almost quantitatively (>99.7%) in solution.

1. Introduction

^{72}As is a positron emitting arsenic isotope, with properties promising for possible application in ^{72}As-labelled radiopharmaceuticals. It has a positron emission rate of 88% with $E_{\beta+max}$ = 2.5 MeV and $E_{\beta+mean}$ = 1.0 MeV [1]. Although the positron emission decay is accompanied by photons of 834 keV (79.5%), 630 keV (7.9%), 1461 keV (1.1%) and others (< 0.5%), the long physical half-life of 26 hours may render ^{72}As as a PET radionuclide of choice for the quantitative imaging of biochemical and physiological processes with longer biological half-lives, e.g. immunoimaging and receptor mapping. In these cases, the half-life of ^{72}As may meet the radiopharmacological requirements resulting from the slower localization kinetics of the targeting vectors. The versatile chemistry of arsenic would permit the radiolabelling of a broad spectrum of potentially valuable pharmaceuticals.

The radionuclide ^{72}As can be produced directly at medium-energy cyclotrons via the ^{72}Ge(p,n), ^{72}Ge(d,2n), ^{69}Ga(α,n), ^{71}Ga(α,3n), and ^{71}Ga(^{3}He,2n) reactions. Indirectly, it can be produced as a daughter radionuclide of the relatively long-lived ^{72}Se ($T_{1/2}$ = 8.5 d). Various ways for the production of ^{72}Se have been described but mainly in the context of ^{73}Se productions. Both deuteron- and proton-induced reactions on arsenic, and α- and ^{3}He-induced reactions on germanium have been investigated [2-4]. Alternatively, ^{72}Se can be obtained via proton induced spallation of RbBr [5].

Radionuclide generator systems play a key role in providing both diagnostic and therapeutic radioisotopes [6] for various applications in nuclear medicine, oncology and interventional cardiology. In particular, the application of positron emission tomography (PET) at centers lacking a cyclotron to produce the necessary radionuclides depends on the availability of biomedical PET radionuclide generators.

Fig.1 illustrates the transient radionuclide generator kinetics for the system ^{72}Se/^{72}As. The time where the daughter activity is maximum can be calculated to 88.6 h. However, already after 48 h, i.e. every second day, it is theoretically possible to elute around 70% of the maximum daughter activity.

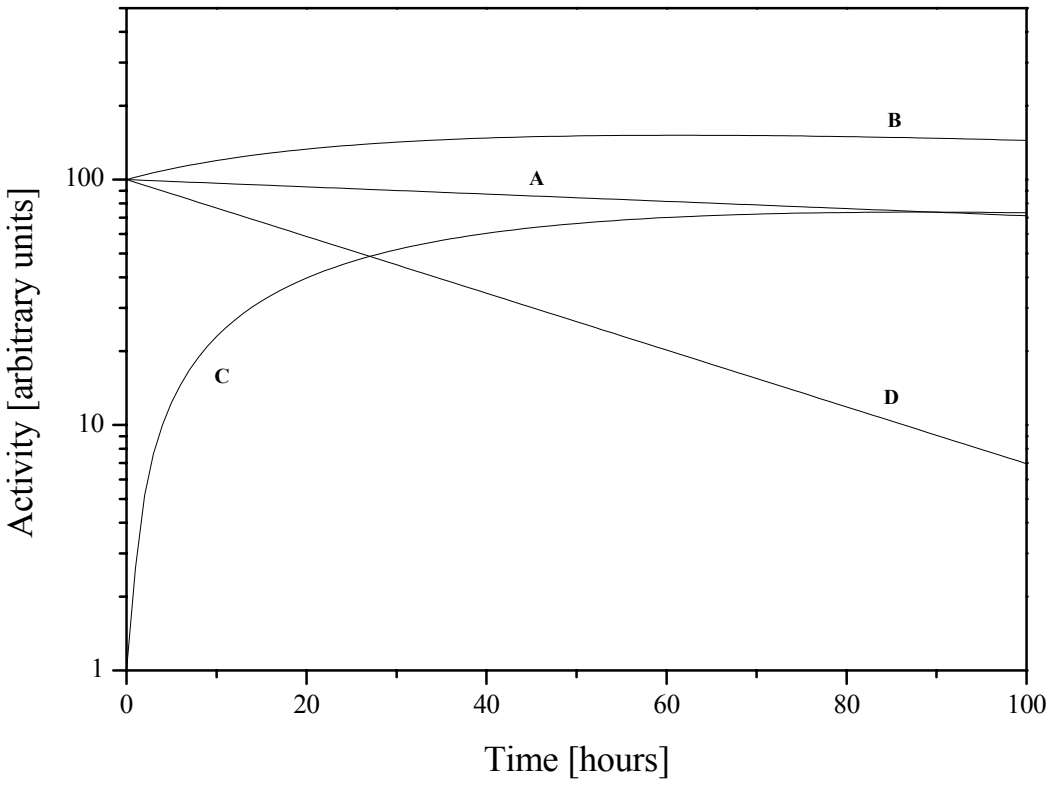

FIGURE 1. Transient radionuclide generator kinetics for the system $^{72}Se/^{72}As$. A - independent activity of the parent isotope; B – growth of cumulative parent and daughter activity in a pure parent fraction; C – growth of daughter activity in a pure parent fraction; D – independent decay of the separated pure daughter fraction at maximum of generated activity

Several $^{72}Se/^{72}As$ generator systems have been proposed previously. Al-Kouraishi and Boswell [7] were able to obtain a 70% elution yield of ^{72}As from a coagulated form of carrier-added ^{72}Se on a Dowex 50 column in 15 ml of water. Due to the amount of selenium carrier, the separation yields were less than 70%. Electrolytic generators with ^{72}Se deposited on Pt electrodes as $Cu^{72}Se$ were reported [8, 9]. Another process using addition of selenium carrier in the form of selenic acid uses the cyclic reduction of selenium to Se° and a separation of ^{72}As by filtration with subsequent oxidative dissolution of Se° using H_2O_2 prior to each separation cycle [5].

The aim of this work was to develop a $^{72}Se/^{72}As$ generator without any addition of selenium carrier. The system should be reliable for the routine separation of ^{72}As to allow investigations on ^{72}As-labelled radiopharmaceuticals.

2. Materials and Methods

Isotope production

^{72}Se was produced at the compact cyclotron CV28 the Forschungszentrum Juelich via the (^{3}He,3n) nuclear reaction on natural germanium. Irradiation was done with 36 MeV ^{3}He-particles at a beam current of 5 μA for 12 h, giving a yield of about 5 mCi. To simulate the behaviour of ^{72}Se, ^{75}Se was used in some experiments, which was produced in a carrier-added (ca) form of specific activity 0.52 GBq/μmol via the (n,γ)-reaction in the nuclear research reactor BERII at the HMI Berlin ($\Phi = 4.0 \times 10^{14}$ n/cm^{2}·s).

Analogously, to simulate the behaviour of no-carrier-added (nca) ^{72}As, ^{77}As was used, which was produced in a nca state via the $^{76}Ge(n,\gamma)^{77}Ge$, $T_{½} = 11.30$ h $\rightarrow$ ^{77}As ($T_{½} = 1.618$ d) reaction on natural germanium at the TRIGA reactor of the Institute of Nuclear Chemistry of the University of Mainz ($\Phi = 4.0 \times 10^{12}$ n/cm^{2}·s).

Radiochemical separation of ^{72}Se

To isolate ^{72}Se from irradiated 100 mg germanium targets, the targets are dissolved in 5 ml aqua regia and transferred to a two-necked flask. $GeCl_4$ is removed from the solution via distillation in an N_2 flow (10 ml/min), while conc. HCl is added continuously (10 drops per minute) at a temperature of 130°C. The distilled $GeCl_4$ is trapped in an ice-cooled flask, filled with 20% H_2SO_4 and precipitates as GeO_2. No-carrier-added ^{72}Se as well as already generated ^{72}As remain in the flask quantitatively. The neutron-irradiated germanium, as well as the neutron irradiated selenium are treated analogously.

Cyclic separation of nca ^{72}As from nca ^{72}Se

For the distillative radionuclide generator system an apparatus was adopted, which has been shown to be versatile and adequate for a variety of thermochromatographic and distillative separations of generator radionuclide pairs. This apparatus, first developed to separate the positron emitter ^{94m}Tc from the irradiated molybdenum oxide within 25 minutes [10], was subsequently improved and used more universally for separations of the systems ^{110}Sn/^{110}In, ^{186}W/^{186}Re, ^{188}W/^{188}Re [11-12]. For a recent review on thermochromatographic separations cf. [13].

The 5 ml HCl solution containing ^{72}Se is transferred to a quartz or glass tube system as shown in Fig. 2, which is inserted vertically into a heated oil-bath. 1.0 g of a chloride salt and 1.0 ml of conc. HCl are added. The following chlorides were tested: KCl, LiCl, NaCl, $AlCl_3$, $CaCl_2$, NH_4Cl, $BaCl_2$ and hydrazine dihydrochloride. As the volume of the loaded generator is a critical parameter, the salts have not been used in equimolar amounts, but with the same mass of 1.0 g. Hydrochloric acid is passed through the inlet into the apparatus with a variable flow rate of 20-120 ml/min. The temperature at the position of the ^{72}Se fraction inside the tube can be raised up to 140°C. The ^{72}As is volatilised as $AsCl_3$ and transported with the stream of hydrochloric acid. It is adsorbed on a cartridge, containing a suitable material (e.g. charcoal). To determine HCl flow rates, the charcoal cartridge was substituted by a 100 ml glass-syringe.

Two types of experimental setups have been used to record the distillation kinetics of nca radioarsenic trichloride ($^{72}AsCl_3$ and $^{77}AsCl_3$). The generator glass tubes were placed at room temperature into the oil bath, which was subsequently heated up to a defined end-temperature [protocol (i)]. The radioarsenic content in the containment was measured on-line via γ–ray spectroscopy. For this purpose, a NaI-detector was integrated into the lead shielding, with the detector head close to the lower end of the generator. Alternatively, the generator glass tubes were placed in a pre-heated oil-bath [protocol (ii)] at an already defined constant temperature and the distillation kinetics were measured analogously to protocol (i).

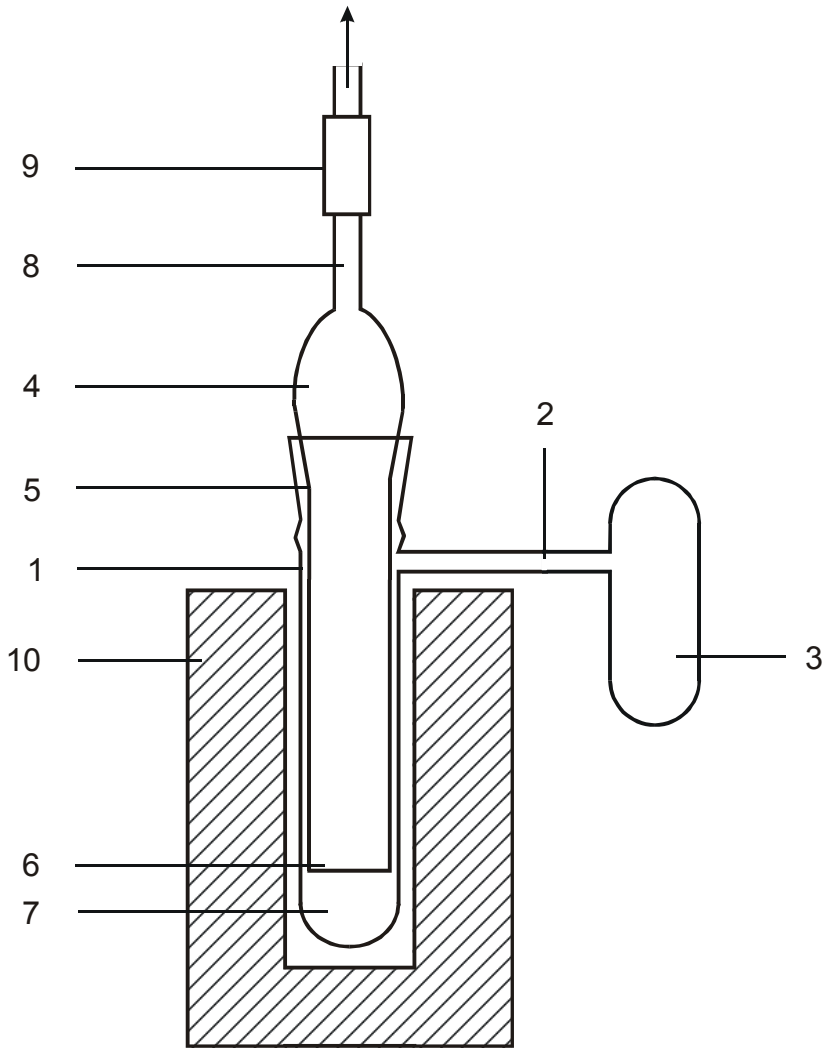

FIGURE 2. Sketch of the $^{72}Se/^{72}As$ radionuclide generator apparatus. 1-outer quartz or glass tube; 2-inlet of HCl; 3-HCl vessel; 4-inner quartz or glass tube; 5-ground joint; 6-open lower end of the inner tube; 7-^{72}Se fraction; 8-upper end of the inner tube; 9-adsorber; 10-heating device, lead shielding

3. Results and Discussion

Separation of ^{72}Se and recovery of macroscopic Ge-targets

The radiochemical procedure used to separate nca ^{72}Se (or nca ^{77}As) from irradiated natural germanium targets is based on the formation of volatile $GeCl_4$ which is distilled at temperatures above 130°C and precipitates in cold 20% H_2SO_4 as GeO_2. During this procedure the arsenic remains in the oxidation state +V as low volatile $AsCl_5$ (bp = 130°C), while the nca radioselenium exists in a non-volatile oxidation state. The overall radiochemical yield of nca ^{72}Se is 90±4 %. The germanium content of the residue is less than 1%. The ^{77}Ge/^{77}As separation was performed analogously with comparable ^{77}As yields.

^{72}Se / ^{72}As generator

The concept of the ^{72}Se/^{72}As isotope generator is based on the high volatility of $AsCl_3$ formed at temperatures above 80°C in the presence of chloride salts and HCl gas ($AsCl_3$ b_p = 130°C), while selenium remains in the residue as a non-volatile complex. The selenium chloride Se_2Cl_2 (b_p = 130°C; decomposition), showing a boiling point similar to $AsCl_3$ is not formed under those experimental conditions. The thermal volatility of $SeCl_4$ (b_b = 191°C; sublimation and almost complete dissociation to lower chlorides and chlorine in the vapour) and of oxochloride $SeOCl_2$ (b_p = 177°C) is low at temperatures below 120°C. However, the stoichiometry of those selenium species might be affected by the chloride salts cations. Hexachloroselenates of type M_2SeCl_6 are known for alkali chloride salts or for other cations and compounds such as $SeCl_4 \cdot AlCl_3$, cf. Fig. 7 [15-18].

Fig. 3 shows the results observed while using the experimental set-up described in protocol (i). The lower group of plots shows the increase of ^{72}As in the absorber at increasing temperatures from 110°C to 140°C. The upper group shows the temperature profiles in the generator flask for the corresponding end temperatures from 110 to 140°C. The highest yield observed is 60% after 30 min at 140°C. At lower temperatures, such as 110°C, only 20% yield of separated ^{72}As is achievable after 40 min. This procedure can be repeated as soon as no-carrier-added ^{72}As is formed again (see also Fig. 1).

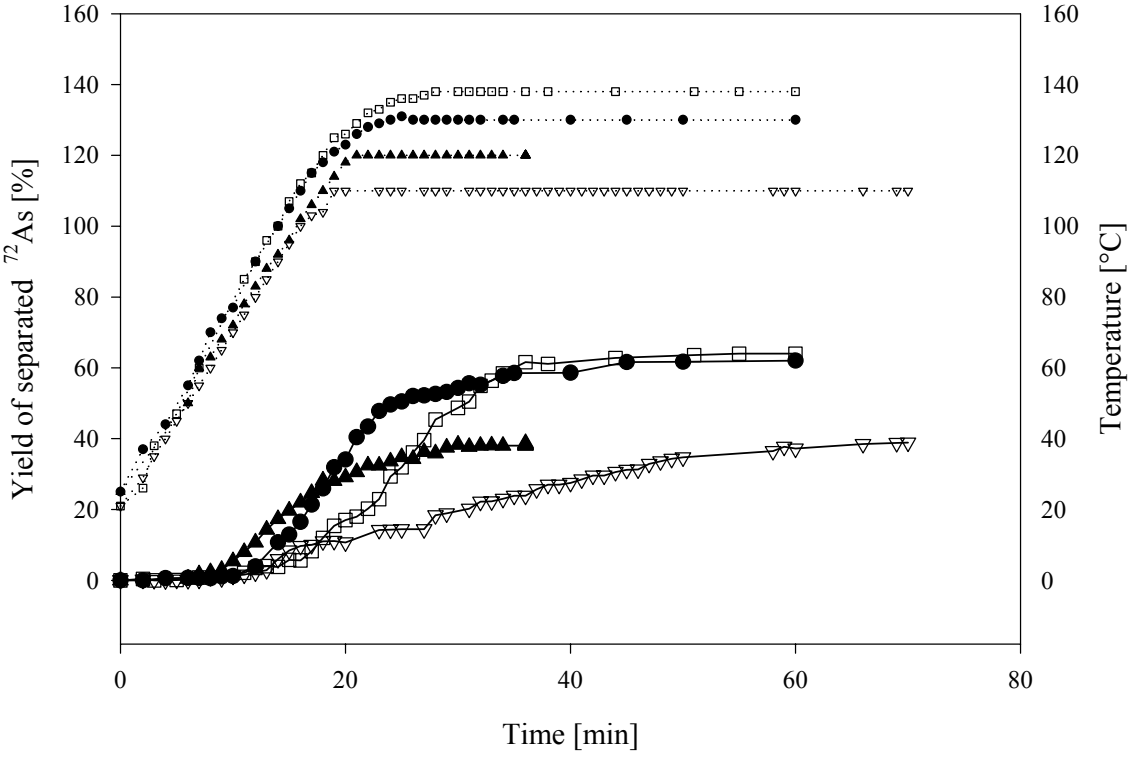

FIGURE 3. Kinetics of distillative ^{72}As separation depending on the temperature; protocol (i). The lower group of graphs shows the increase of ^{72}As in the absorber (9), the upper group shows the temperature profiles in the generator flask.

The advantage of the experimental set-up described in protocol (ii) is a significantly reduced distillation time necessary to separate the nca radioarsenic. Fig. 4 shows the results of the kinetic measurements, performed as described in protocol (ii). At a temperature of 140°C, >98 % yield was already achieved after 7 minutes. In terms of the retention of the nca radioselenium generator charge, it is, however, necessary to compromise between generator running time and temperature. At a temperature of 80°C, the maximum yield of ^{72}As of about 95% was reached after only 17 minutes, and the kinetics obviously are much slower than at higher temperatures. Fig. 5 shows the time needed for 50% and 100% ^{72}As separation yield at different temperatures. A temperature of 105°C seems to be optimum which is the inflection point (zero point in the second derivative) of the graphs shown in Fig. 5.

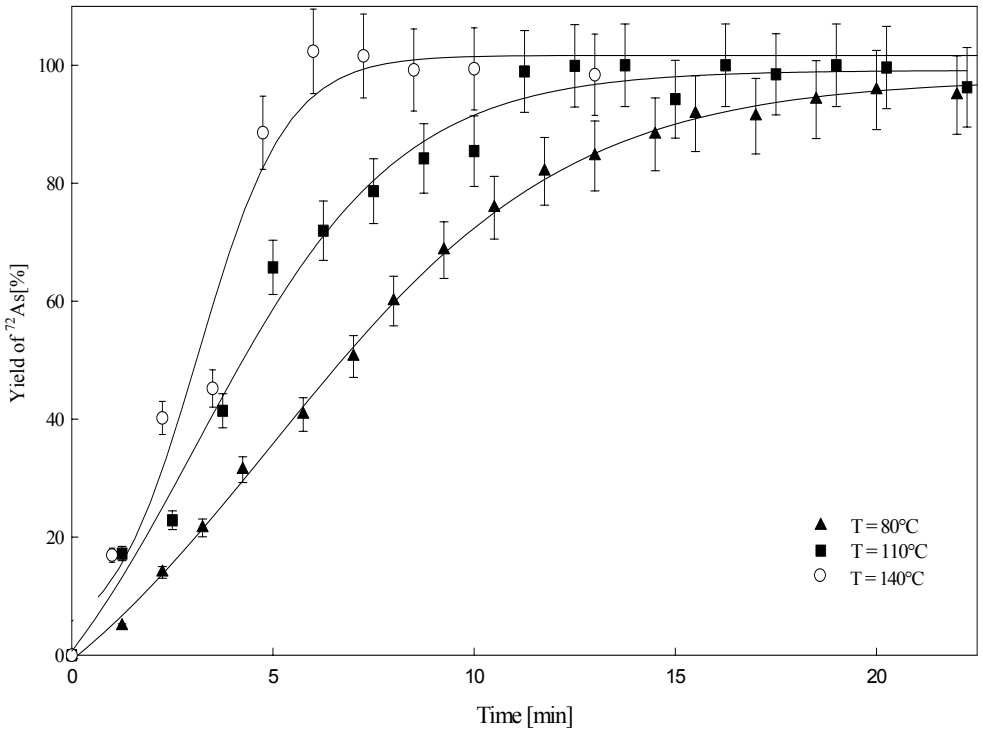

FIGURE 4. Distillation kinetics of $^{77}AsCl_3$; protocol (ii). T = 80, 110 and 140 °C, HCl flow rate = 60 ml/min

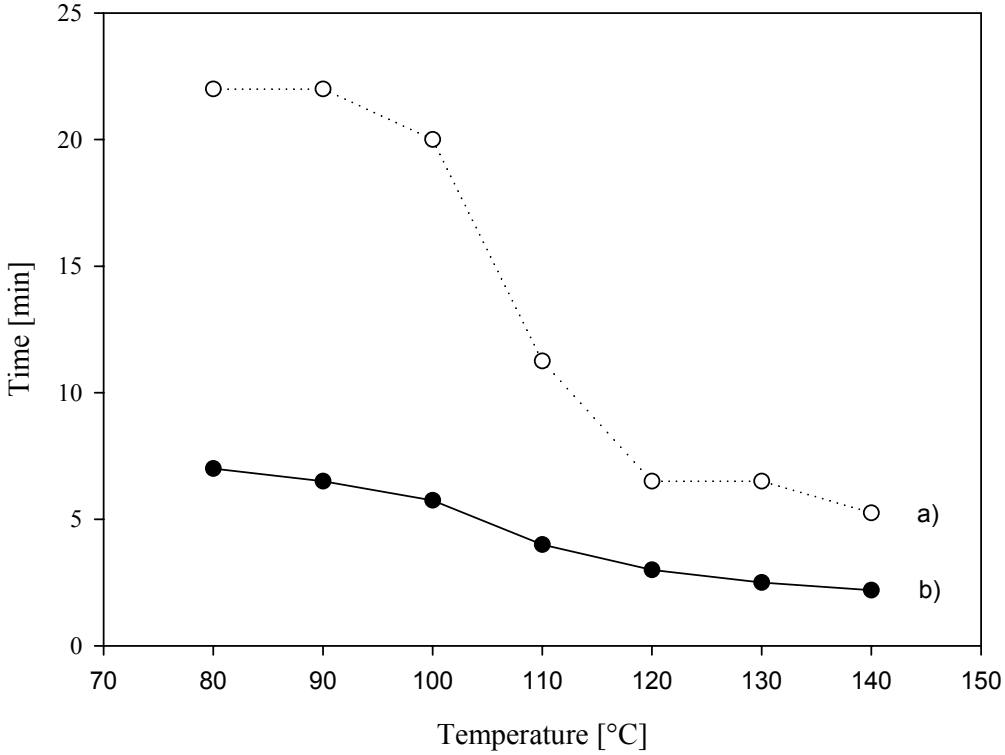

FIGURE 5: Determination of optimum distillation temperature of the $^{72}Se/^{72}As$ radionuclide generator for 100% ^{72}As separation yield (a) and for 50% ^{72}As separation yield (b)

The influence of the HCl flow rate on the distillation kinetics of $^{77}AsCl_3$ was studied in more detail, as illustrated in Fig. 6. A triplication of the HCl flow rate is followed by an approximate triplication in the nca radioarsenic volatilization at t = 10 min. At a lower flow rate of 20 ml/min the ^{72}As separation yield of 100% cannot be achieved. A maximum of 80% yield is achieved after 40 minutes distillation time. Consequently, a constant HCl flow rate of 60 ml/min was adjusted for routine use. This indicates the importance of a reproducible maintenance of the HCl flow. This is, however, a technical problem, because of the fast and severe oxidation of the pressure reducer at the gas cylinder outlet valve.

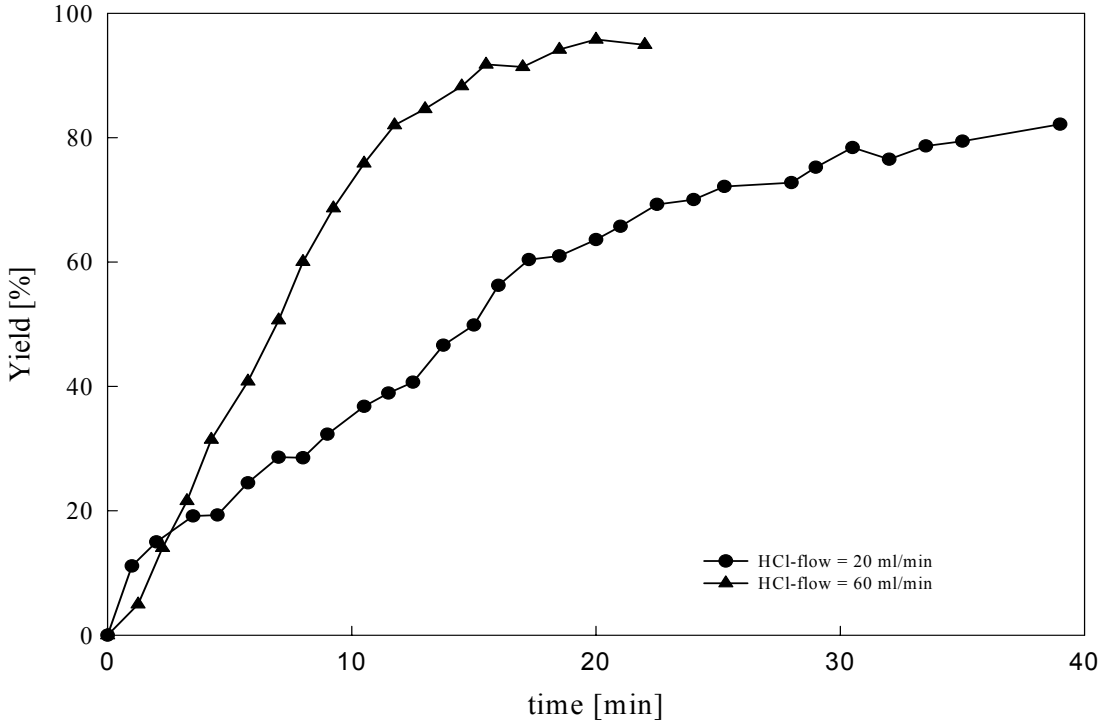

FIGURE 6. Distillation kinetics of $^{77}AsCl_3$ at different HCl flow rates, T = 90°C

The effect of salt additives on the nca separation of ^{72}Se fraction has been systematically studied using the following salts: KCl, NaCl, $AlCl_3$, NH_4Cl, $CaCl_2$, $BaCl_2$ and hydrazine dihydrochloride. The results are illustrated in Fig. 7. Although usage of equimolar amounts of different salts seemed to be quite adequate, this was not possible because of the fixed volume of the generator apparatus, resulting in a constant volume of liquid solution in

which an equimolar amount of salt e.g. $AlCl_3$, would have not been soluble. Therefore, we constantly used equal amounts of 1 g per salt. The different chlorides were used to vary the chlorine ion density in the solution, while hydrazine dihydrochloride was used to observe whether the addition of a reducing agent has an effect on the nca $^{72}AsCl_3$ formation. The amount of chlorine ions per ml generator charge varied from 3.4 mmol for NaCl to 1.0 mmol for $BaCl_2$. Obviously this is not reflected in the measured results, where KCl (2.7 mmol/ml generator charge) showed the best distillation kinetics and NaCl the worst. A possible explanation for this result is the lower solubility of NaCl compared to KCl in hot HCl, which could be visibly observed, but is not described in the literature. For routine use of the generator, KCl is recommended.

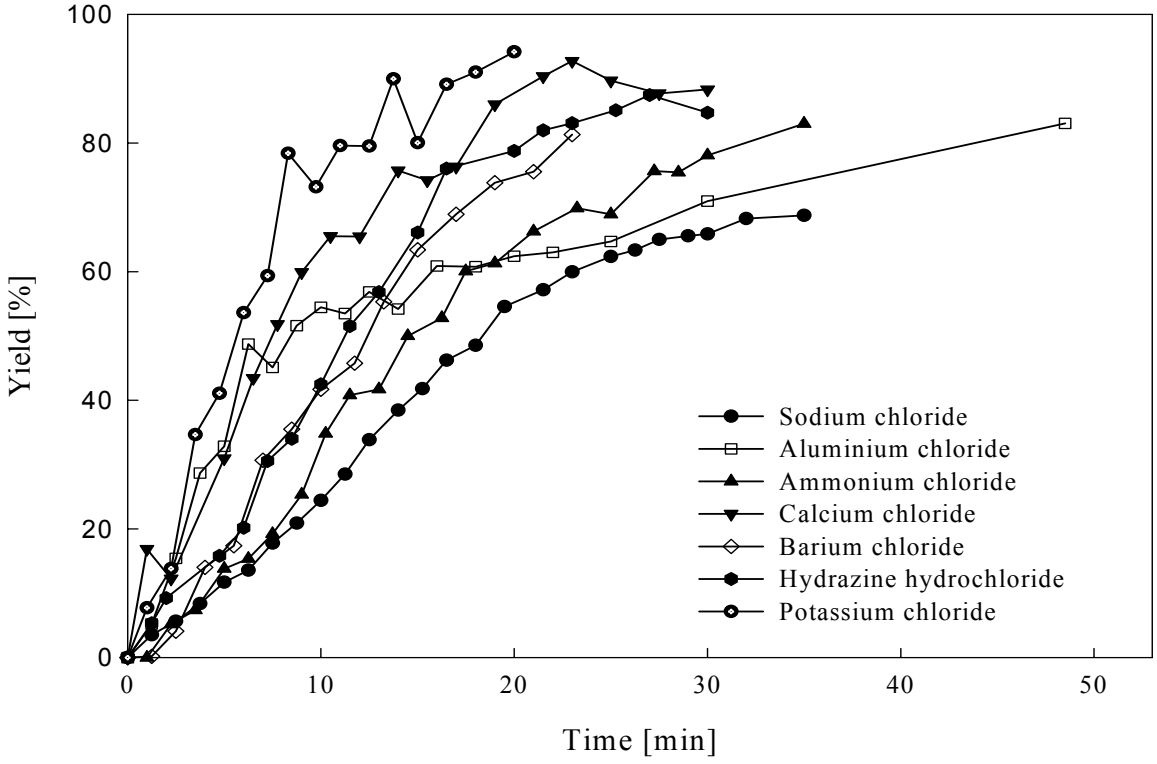

FIGURE 7. Distillation kinetics of $^{72}AsCl_3$ with varying salts in the generator charge, T = 100 °C; HCl flow rate = 60 ml/min

Contrary to nca radioarsenic, which is always present as $AsCl_3$ under these reaction conditions, for selenium different oxidation states seem to be possible, resulting in significant differences in retention in the generator system. Prior to transferring the ca radioselenium ^{75}Se to the generator apparatus, it was completely oxidised via refluxing for 2 h in aqua regia. Fig. 8 shows that the selenium breakthrough is very low within the first hour of the separation process. The procedure is therefore good for the separation of nca radioarsenic. The selenium retention for suggested separation periods of less than 10 minutes is >99.9%.

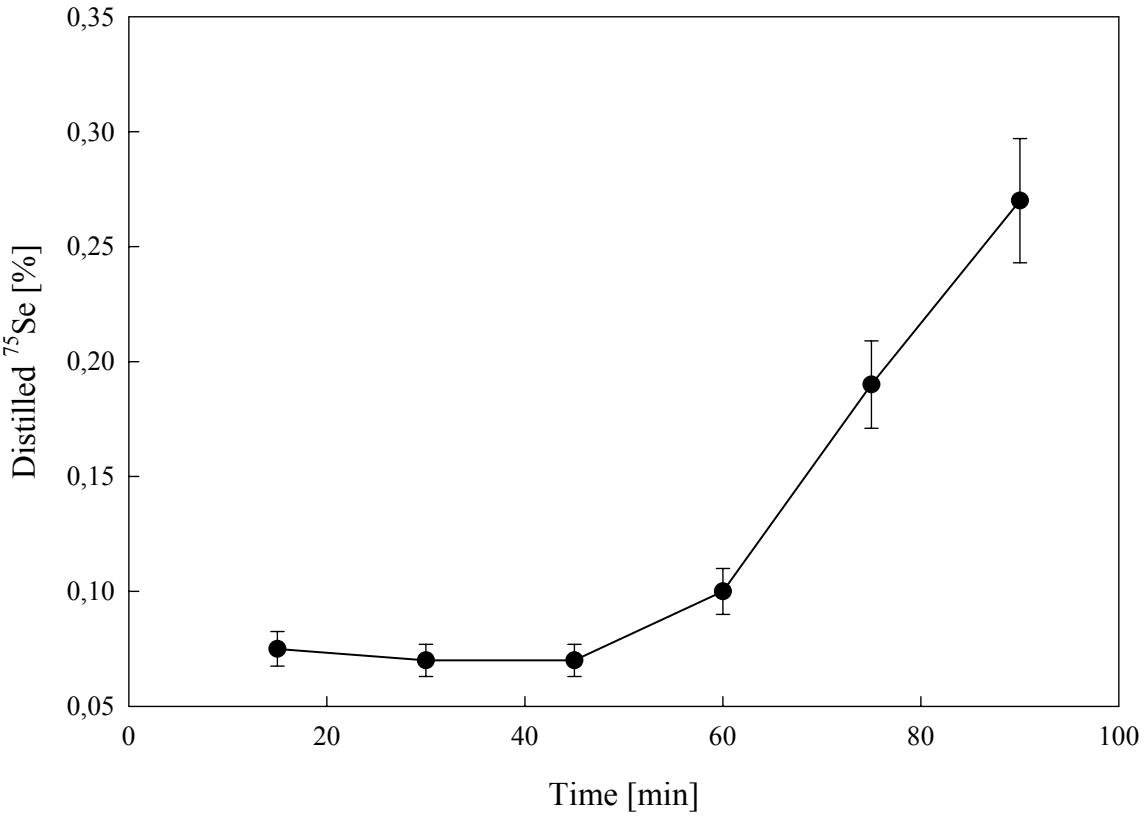

FIGURE 8. Se-retention of the $^{72}Se/^{72}As$ generator after re-oxidation, T = 80 °C; HCl flow rate = 60 ml/min. The result shown here relates to the small amount of ^{75}Se distilled over in a simulation experiment.

A longer separation period will possibly result in the reduction of selenium, yielding volatile radioselenium compounds. This is indicated by an increase of the selenium

breakthrough at t > 60 min (see Fig. 8). Thus, a complete oxidation, in the particular case of nca radioselenium, with aqua regia is recommended prior to subsequent generator utilisation. When the generator was used one day after the previous separation without pre-oxidation, the selenium breakthrough was > 75% at a temperature of 80°C after 20 minutes of the separation process. This could easily be avoided by adding 0.5 ml of concentrated HNO_3 prior to each generator run and heating the system up for 1 hour, before turning on the HCl gas flow.

4. Conclusion

A $^{72}Se/^{72}As$ radionuclide generator utilising a distillation concept has been optimised. It could be automated for future use as a biomedical generator. At an optimum temperature of 105°C, more than 99% of the nca ^{72}As is separated in less than 10 minutes at a nca ^{72}Se contamination level below 0.05%. Systematic chemical investigations on the labelling chemistry of no-carrier-added radioarsenic, however, are required prior to the application of ^{72}As labelled compounds.

Acknowledgement

Financial support by the Deutsche Forschungsgemeinschaft (DFG-Grant Ro 985/9) is gratefully acknowledged.

References

1. Browne, E. and R.B. Firestone, *Table of Radioactive Isotopes*, ed. V.S. Shirley. 1986: John Wiley & Sons, New York
2. Mushtaq, A., S.M. Qaim, and G. Stöcklin: Production of ^{73}Se via (p,3n) and (d,4n) reactions on arsenic. Appl. Radiat. Isot. **39**, 1085-1091 (1988)

3. Mushtaq, A. and S.M. Qaim, Excitation functions of a- and ^{3}He-particle induced nuclear reactions on natural germanium: evaluation of production routes for ^{73}Se. Radiochimica Acta **50,** 27-31 (1990).
4. Nozaki, T., Y. Itoh, and K. Ogawa, Yield of ^{73}Se for various reactions and its chemical processing. Int. J. Appl. Radiat. Isot. **30**, 595-599 (1970)
5. Phillips, D.R., Chemistry and Concept for an Automated ^{72}Se/^{72}As Generator, *United States Patent Nr.: 5,371,372*. 1994: USA.
6. Rösch, F., and Knapp, F.F., Radionuclide Generators, in *Handbook of Nuclear Chemistry* (Eds. Vertés, A., Nagy, S., Klencsár, Z), Kluwer Academic Publishers, Vol.4, Norwell, in press.
7. Al-Kouraishi, S.H. and G. G. J. Boswell: An Isotope Generator for ^{72}As, Int. J. Appl. Radiat. Isot. **29**, 607-609 (1978)
8. Phillips, D.R., Hamilton, V.T., Nix, D.A., Taylor, W.A., Jamariska, D.J., Staroski, R.C., Lopez, R.A., Emran, A.M.: Chemistry and Concept for an Automated ^{72}Se/^{72}As Generator, *New Trends in Radiopharm. Synthesis, QA and Regulatory Control,* 173-181 (1991)
9. Phillips, D.R., Hamilton, V.T., Taylor, M.D., Farnham, J.E., Emran, A.M., Rowe, R.W.: Generator-Produced Arsenic-72 in Positron Emission Tomography, Radioact. Radiochem. **3,** 53-58 (1992)
10. Rösch, F., Novgorodov, A. F., Qaim, S. M.: Thermochromatographic separation of ^{94m}Tc from enriched molybdenum targets and its large scale production for nuclear medical application, Radiochim. Acta **64**, 113 (1994).
11. Ying-Ming Tsai, Rösch, F., Novgorodov, A.F., Qaim, S.M.: Production of the positron-emitting indium isotope ^{110g}In via the ^{110}Cd(^{3}He,3n)^{110}Sn$\rightarrow$^{110g}In-process, Appl. Radiat. Isot., **48**, 19 (1997)
12. Novgorodov, A.F., Bruchertseifer, F., Brockmann, J., Lebedev, N.A., Rösch, F.,: Thermochromatographic separation of no-carrier-added ^{186}Re or ^{188}Re from tungsten targets relevant to nuclear medical applications, Radiochim. Acta **88**, 163 (2000).
13. Novgorodov, A. F., Rösch, F., Korolev, N. A.: Radiochemical separations by thermochromatography, in *Handbook of Nuclear Chemistry* (Eds. Vertés, A., Nagy, S., Klencsár, Z.), Vol. 5. Kluwer Academic Publishers, Norwell, in press.

14. Gmelin, Handbuch der anorganischen Chemie, 8. Auflage, Arsen, ELEM As, Verlag Chemie, Weinheim, 383 (1953)
15. Gmelin, Handbuch der anorganischen Chemie, 8. Auflage, Selen, ELEM Se, Verlag Chemie, Weinheim, 383 (1953)

II.

A no-carrier-added ^{72}Se/^{72}As radionuclide generator based on solid phase extraction

A no-carrier-added $^{72}Se/^{72}As$ radionuclide generator based on solid phase extraction

by M. Jennewein[1], S.M. Qaim[2], P.V. Kulkarni[3], R.P. Mason[3], A. Hermanne[4] and F. Rösch[1]

[1]Institute of Nuclear Chemistry, Johannes Gutenberg University of Mainz, Fritz-Strassmann-Weg 2, 55128 Mainz, Germany

[2]Institute of Nuclear Chemistry, Forschungszentrum Juelich, Leo-Brandt-Strasse, 52428 Juelich, Germany

3Department of Radiology, University of Texas Southwestern Medical Center at Dallas, 5323 Harry Hines Blvd, Dallas, Texas 75390-9058, USA

[4]Cyclotron Department, Vrije Universiteit Brussel, Laarbeeklaan 103, 1090 Brussels, Belgium

Key Words:

As-72, Se-72, radionuclide generator, solid-phase extraction

Summary

^{72}As-labelled radiopharmaceuticals could be a valuable resource for Positron Emission Tomography (PET). In particular, the long half-life ($T_{1/2}$= 26 h) facilitates the observation of long term physiologic or metabolic processes, like the enrichment and distribution of antibodies in tumor tissue. This work describes the primary no-carrier-added (nca) radiochemical separation of ^{72}Se from cyclotron irradiated germanium targets and the development of a polystyrene based solid-phase extraction based ^{72}Se/^{72}As radionuclide generator, avoiding the addition of any selenium carrier. The irradiated germanium target is dissolved in $HF_{conc.}$ and the induced radio-selenium is reduced with hydrazinium dihydrochloride. The nca $^{72}Se^{(0)}$ is then adsorbed on a solid-phase extraction cartridge, representing the generator column. The daughter product ^{72}As is eluted using various aqueous solvents with a 40-60 % yield and < 0.1 % ^{72}Se content within 5 minutes. To enable a radiopharmaceutical arsenic chemistry, subsequent chemical modification of the nca ^{72}As eluate to nca [^{72}As]AsI_3 provides a versatile radioarsenic labelling synthon.

1. Introduction

The recent increasing interest in the element arsenic in environmental sciences [1], toxicology and carcinogenesis [2] and medicine [3, 4], stimulates a need to develop convenient and reproducible methods to trace this element and its compounds in subtoxic and subpharmaceutical concentrations. Arsenic provides several isotopes of interest for medical or environmental application (cf. Table 1).

	^{72}As	^{73}As	^{74}As	^{76}As	^{77}As
$T_{1/2}$ [d]	1.1	80.3	17.8	1.1	1.6
Mode of decay	100 % EC β^+ (87.8 %)	100 % EC	66 % EC β^+ (29.0 %)	100 % β^-	100 % β^-
Most abundant γ-lines [keV]	834.0 (79.5 %) 629.9 (7.9 %)	53.4 (10.0 %)	595.8 (59.0 %)	559.1 (45.0 %) 657.1 (6.2 %)	239.0 (1.6 %)
Positron-energy [MeV]	Mean: 1.17, Max: 1.53		Mean: 0.44, Max: 0.70		

TABLE 1. Nuclear data for the most relevant arsenic isotopes [24]

A number of approaches to develop an easy and practical system to separate these isotopes from cyclotron or reactor irradiated germanium or germanium oxide targets have been described [5-8]. In parallel, a ^{72}Se/^{72}As radionuclide generator has been studied [9-15]. Strategies towards a versatile radioarsenic labelling chemistry were developed to generate arsenic isotopes in chemical forms suitable for future application in labelling chemistry, radiopharmacy and, ultimately, for molecular imaging using Positron Emission Tomography (PET). Recent advances in using ^{74}As labelled antibodies directed against the apoptotic marker phophatidylserine (PS) in a Dunning R3327 AT1 prostate cancer model [16], clearly demonstrate the potential of those radioarsenic isotopes. This strengthens the motivation to develop adequate and reliable radiochemical separations.

^{72}As is a positron emitting arsenic isotope, with properties suitable for possible application in ^{72}As-labelled PET-radiopharmaceuticals. It has a positron emission rate of 88% with $E_{\beta+max}$ = 2.5 MeV and $E_{\beta+mean}$ = 1.0 MeV [17]. Although the positron emission is accompanied by the emission of photons of 834 keV (79.5%), 630 keV (7.9%), 1461 keV (1.1%) and others (< 0.5%), the long physical half-life of 26 hours may render ^{72}As as a PET radionuclide of choice for the quantitative imaging of biochemical and physiological processes with longer biological half-lives, e.g. immunoimaging and receptor mapping. In these cases, the half-life of ^{72}As is commensurate with the radiopharmacological requirements resulting from the slower localization kinetics of the labelled species. These advantages are comparable to what can be expected from ^{124}I ($T_{1/2}$= 4.18 d), but note that this radio-isotope has a β^+-branching of only 24%. On the other hand, compared to established radiohalogenation strategies, development of a versatile chemistry of arsenic is required to permit the radiolabelling of a broad spectrum of potentially valuable pharmaceuticals.

In addition to direct production routes, the radionuclide ^{72}As can be obtained as a daughter radionuclide of the relatively long-lived ^{72}Se ($T_{1/2}$ = 8.5 d). Various methods for the production of ^{72}Se have been described but mainly in the context of ^{73}Se production [18-22]. Both deuteron- and proton-induced reactions on arsenic, and α- and ^{3}He-induced reactions on germanium have been investigated. Alternatively, ^{72}Se can be obtained via proton induced spallation, which was proven on RbBr [11].

Radionuclide generator systems play a key role in providing both diagnostic and therapeutic radioisotopes for various applications in nuclear medicine, oncology and interventional cardiology. In particular, centers lacking a cyclotron to produce the necessary radionuclides on site might benefit substantially from the availability of biomedical PET radionuclide generators [15]. Several ^{72}Se/^{72}As generator systems have been proposed previously. Al-Kouraishi and Boswell [9] eluted ^{72}As from a coagulated form of carrier-added ^{72}Se on a Dowex 50 column in 15 ml of water. Electrolytic generators with ^{72}Se deposited on Pt electrodes as Cu^{72}Se were reported [12, 13]. Another process using addition of selenium carrier in the form of selenic acid uses the cyclic reduction of selenium to $Se^{(0)}$ and a separation of ^{72}As by filtration with subsequent oxidative dissolution of $Se^{(0)}$ using H_2O_2 prior to each separation cycle [11]. As published recently, our group developed a no-carrier-added generator based on distillation [10].

Following $^{nat}Ge(^{3}He,3n)^{72}Se$ reactions, the irradiated Ge was dissolved in aqua regia and germanium was removed via distillation as $GeCl_4$. The remaining solution of ^{72}Se in conc. HCl was transferred to a vertical quartz tube device. In the presence of various chloride salts in the ^{72}Se solution no-carrier-added ^{72}As was nearly quantitatively released within 10 min at temperatures of 100°C in an HCl gas flow.

The aim of the present work was to develop a $^{72}Se/^{72}As$ generator, still without any addition of selenium carrier, but which should be more practical and convenient compared to previously published systems. Moreover, the transfer of the separated and purified ^{72}As fraction to a chemical form (synthon), optimal for future labelling chemistry should represent an important feature of the radionuclide generator system to allow investigations of ^{72}As-labelled radiopharmaceuticals. The system should be reliable for the routine separation of ^{72}As, and finally, the handling time should be reduced to a minimum.

2. Materials and Methods

Isotope production

^{72}Se was produced at the compact cyclotron CV28 at the Forschungszentrum Juelich via the ^{nat}Ge ($^{3}He,3n$) nuclear reaction. Irradiation was done with 36 MeV ^{3}He-particles at a beam current of 5 μA for 12 h, giving a yield of about 185 MBq (3.1 MBq/μAh). ^{72}Se was also produced at the cyclotron of the Vrije Universiteit Brussel via the $^{70}Ge(\alpha,2n)^{72}Se$ reaction with a bombarding energy of 36.5 MeV. The beam current was 4.5 μA and irradiations of 5 h resulted in an activity of about 185 MBq (8.2 MBq/μAh). All nuclear reactions were performed on natural or isotopically enriched germanium or on natural germanium oxide.

Radiochemical separation of ^{72}Se and generator setup

To isolate ^{72}Se from the irradiated germanium targets, 100 mg of irradiated metallic germanium are dissolved in 5 ml HF_{conc} and 500 μl HNO_{3conc} at room temperature within 3 hours. The amount of HNO_{3conc} necessary could be reduced with a prolonged dissolution

period, e.g. to 50 µl, if the target is stirred overnight in 5 ml HF_{conc} prior to adding the oxidizing acid. Germanium oxide targets can be dissolved directly in 5 ml HF_{conc} without addition of HNO_3. The subsequent procedures are identical for metallic and oxide targets. In order to reduce $Se^{(VI)}$ to $Se^{(0)}$, 10 mg of hydrazine dihydrochloride or SO_2 are added to the solution.

A polystyrene based (Varian ENV, 500 µl bed volume) solid phase extraction cartridge is preconditioned with 5 ml of CH_3OH, 5 ml H_2O and 5 ml HF_{conc}. before the mixture containing reduced Se is transferred to the cartridge. $^{72}Se^{(0)}$ is adsorbed on the solid phase, while macroscopic Ge is eluted with the mobile phase as $[GeF_6]^{2-}$. After this first setup of the generator column, the remaining HF is removed with N_2 and the cartridge is stored in a sealed container in N_2 atmosphere for the next elution.

Elution of nca ^{72}As from the nca ^{72}Se loaded generator cartridge

The generated daughter ^{72}As can be eluted subsequently using various aqueous solvents. In this work, HF, aqua regia, pure H_2O, 0.1 and 1.0 molar NaOH and MeOH/H_2O gradients have been used to find optimal elution conditions. The effect of various liquids and/or gases under which the generator is stored between two successive elutions was studied. The generators were eluted daily and every 48 h. Fractions of 100 µl were collected and ^{72}As and ^{72}Se content were determined using γ-spectroscopy.

Reaction to $^{72}AsI_3$

The combined eluate fractions (V = 2 ml) are diluted with 3 ml HF_{conc}. at room temperature in a Teflon flask containing 10 mg of KI. The solution is stirred for 10-15 minutes, until it develops a slight yellowish colour. The mixture is then transferred to a second identical ENV-solid phase extraction cartridge preconditioned with 5 ml of MeOH, 5 ml H_2O and 5 ml HF_{conc}. containing potassium iodide at a concentration of 1 mg/ml. The nca $[^{72}As]AsI_3$ is absorbed on that cartridge. Subsequently, it can be eluted with ethanol or other organic solvents. Some following chemistry may require a water-free environment. In this case, the nca $[^{72}As]AsI_3$ can be eluted with chloroform and dried with $CaCl_2$ before further reactions.

Determination of radionuclidic purity and radiochemical separation yields

Radionuclide purity and radiochemical separation yields have been analysed using γ-ray spectroscopy. Aliquots of the dissolved target were measured and quantitatively compared to γ-ray spectra of the loaded generator, eluates and waste-solutions. All γ-ray spectroscopy was performed using an Ortec high-purity germanium detector system and the GammaVision 5.0 software by Ortec for analysis.

Materials

Metallic germanium (99.9999 % grade) and germanium(IV)oxide (99.9999 % grade, PURA TREM) were purchased from Strem Chemicals Inc.. Concentrated hydrofluoric acid (48 %) and potassium iodide were purchased from Aldrich. BOND ELUT ENV solid phase extraction cartridges with a bed volume of 500 µl were purchased from Varian. Isotopically enriched germanium was purchased from Campro Scientific with 96.4% ^{72}Ge content.

3. Results and Discussion

Separation of ^{72}Se

The radiochemical procedure used to separate nca ^{72}Se from irradiated germanium targets (natural or isotopically enriched) is based on the formation of soluble [GeF_6^{2-}] in concentrated hydrofluoric acid and the reduction of ^{72}Se to $^{72}Se^{(0)}$ by hydrazine. This reduction is a standard reaction for the gravimetric estimation of macroscopic selenium (IV) and (VI) in aqueous solutions, cf. e.g. [23].

$$H_2SeO_3 + N_2H_4 \longrightarrow Se + 3\ H_2O + N_2$$

Other reducing agents described are sulphur dioxide or tin(II) chloride [23]. As we wanted to avoid the addition of other metals, we evaluated sulphur dioxide and hydrazinium dihydrochloride only. Both approaches gave comparable separation yields of 98 ± 2% nca ^{72}Se. However, SO_2 causes a significant loss (> 30 %) of ^{72}Se-activity, due to volatilization together with excess sulphur dioxide, which was not observed using hydrazinium dihydrochloride as reducing agent.

The oxidation state of the target material is also pertinent.. The use of the GeO_2 is preferable, since macroscopic Ge is already in the oxidation state +IV. However, to date isotopically enriched germanium as target material is only available as metal. In the case of metallic germanium as target material, small amounts of HNO_3 have to be added to oxidise $Ge^{(0)}$ to $Ge^{(IV)}$ and to dissolve the target. Heating of the target accelerates the dissolution significantly, but results also in a loss of selenium, as under these conditions the volatile SeF_4 is formed. The formation of SeF_4 (T_b=106°C; [23]) is negligible at room temperature. Comparing γ-spectroscopically measured ^{72}Se contents of the target solution before and after reduction and before and after solid-phase extraction indicate separation yields > 95% for ^{72}Se using hydrazinium dihydrochloride. The amount of Ge separated from the initial cartridge is > 99.9 %.

^{72}Se / ^{72}As radionuclide generator

For the transient radionuclide generator kinetics, the time the daughter activity reaches maximum can be calculated to be 88.6 h. However, after 48 h, i.e. every second day, it is theoretically possible to elute about 75% of the maximum daughter activity (~ 40 % to elute every 24 h) [10]. Fig. 1 shows a γ-ray spectrum of the loaded generator at equilibrium in linear scale. The characteristic γ-lines of ^{72}As besides the 511 keV annihilation are 834.0 keV (79.5 %) and 629.9 keV (7.92 %). ^{72}Se can only be identified by its emission at 46.0 keV (58.0%).

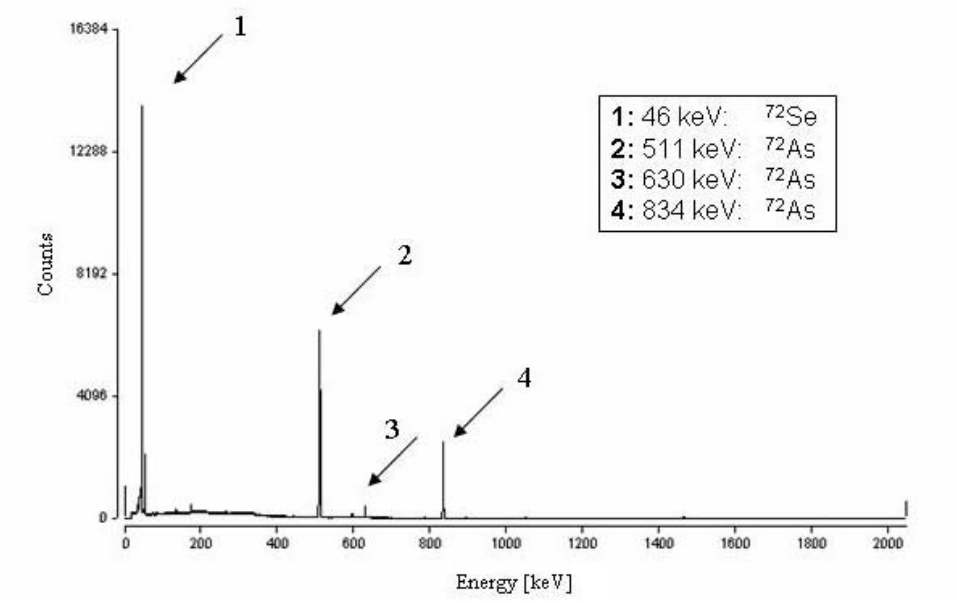

FIGURE 1. γ-spectrum of a 100 µCi ^{72}Se/^{72}As radionuclide generator before elution

The radiochemical separation yields were evaluated in function of different solvents for the elution of the daughter activity over a wide pH range. From the individual γ-ray spectra of aliquot, peak areas for ^{72}As (834 keV) and ^{72}Se (46 keV) were determined prior and after each separation step. Table 2 shows ^{72}As yields and ^{72}Se breakthrough for 4 eluents.

Eluent	^{72}As-yield	^{72}Se-breakthrough
$HF_{conc.}$	50 ± 5 %	< 0.1 %
H_2O	60 ± 5 %	1.9 %
NH_3, 1.3 %, pH=11.5	30 ± 5 %	0.4 %
Phosphoric acid, 1.3 %, pH=0.5	30 ± 5 %	1.2 %

TABLE 2. ^{72}As yields and ^{72}Se breakthroughs for 4 eluents (V = 2 ml)

Deionized water as eluent gives highest radiochemical ^{72}As separation yields of 60%. The breakthrough of the mother radionuclide is minimal when eluting with $HF_{conc.}$, however the ^{72}As yields are with 50 % significantly lower compared to deionized water. A change of pH using NH_3 or phosphoric acid as eluents does not increase the ^{72}As elution yields. To keep the eluate volume small, the generator was eluted with a volume of 1 ml independent of the solvent. Higher yields could be possible with larger volume (compare to the volume of 15 ml Al-Kourashi and Boswell used in [9]), but a higher volume could result in difficulties for a subsequent labelling chemistry.

The initial content of ^{72}Se in the generator eluate is relevant for possible medical application. However, there are two further process steps to consider, namely (a) formation of [^{72}As]AsI_3 including an ENV cartridge separation process, and (b) final labelling with [^{72}As]AsI_3 of the biomolecules of interest. Both processes will further reduce the level of ^{72}Se in the final ^{72}As fractions. This further discrimination is 5fold for process (a), as selenium generally does not react with iodides [23].

Thus, the ^{72}Se breaktrough appears to be more relevant in terms of the overall ^{72}Se/^{72}As generator activity. However, the generator load losses caused by an average breakthrough of 1% are negligible compared to the loss by the decay of ^{72}Se. Therefore, we suggest choosing the eluent based on the solvent-requirements for the following experiments with.

Fig. 3 shows a typical elution profile of a 100 µCi ^{72}Se/^{72}As isotope generator (eluted with HF_{conc}). The daughter activity concentration has its maximum after 200 µl and it is possible to elute the whole activity in 500 µl.

The radiochemical purity of the eluted ^{72}As was determined using γ-ray spectroscopy of the daughter fraction after elution with $HF_{conc.}$ with the generator stored dry under nitrogen (Fig. 3a-c). Fig. 3a is in linear scale and Fig. 3b in logarithmic scale. Fig. 3c has enlarged logarithmic scale, clearly demonstrating that ^{72}Se (e.g. at 46 KeV) is not detectable after an 1 h measurement. Using these spectroscopic data, the ^{72}Se-breakthough was calculated to be less than 0.1%.

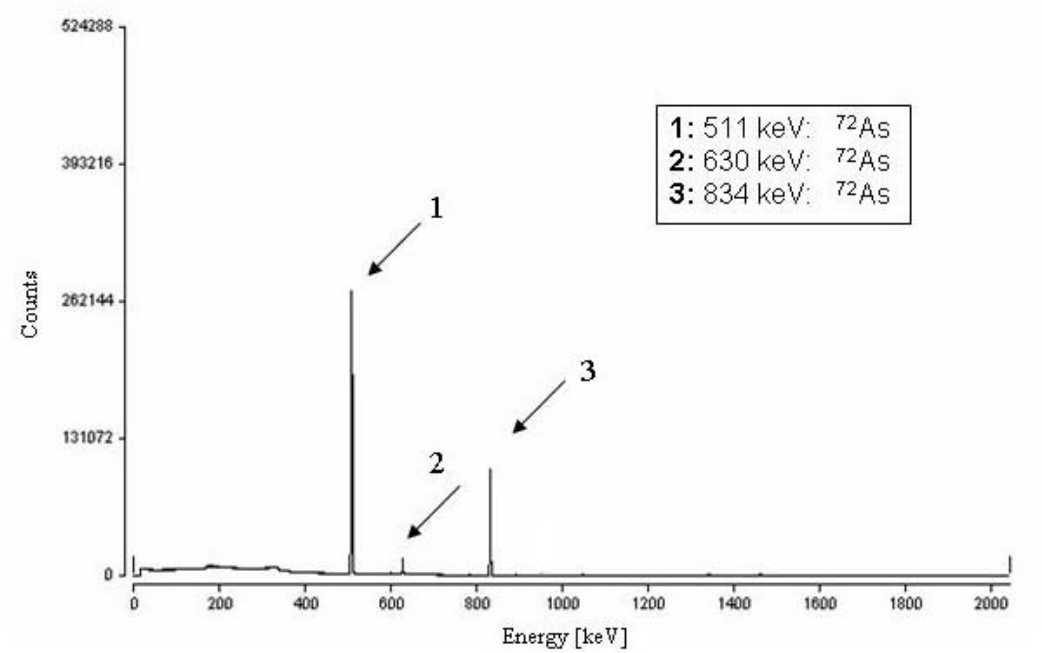

FIGURE 3a. γ-spectrum of the eluted ^{72}As, linear scale

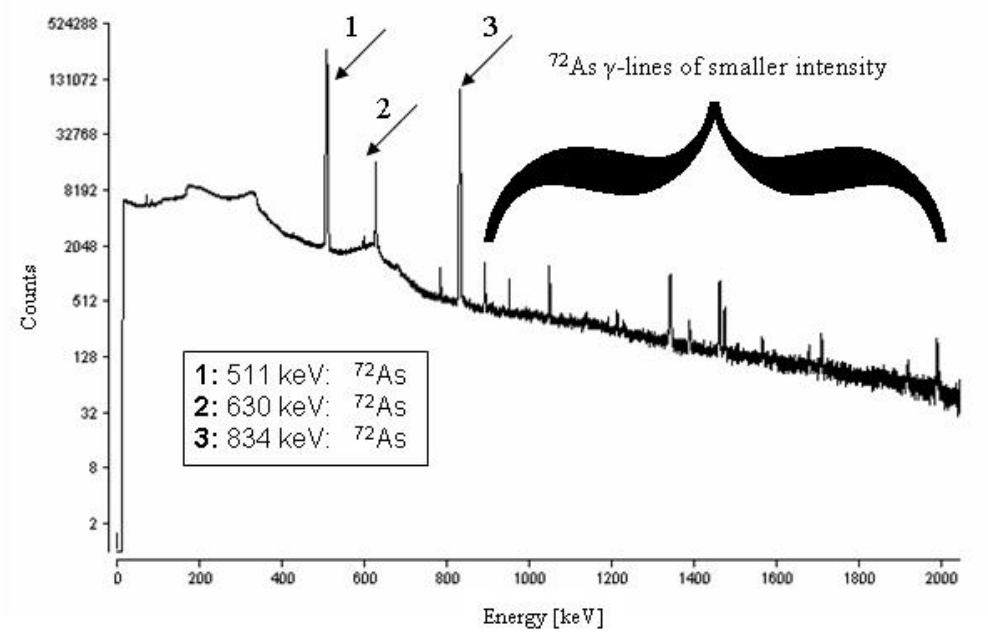

FIGURE 3b. γ-spectrum of the eluted ^{72}As, logarithmic scale

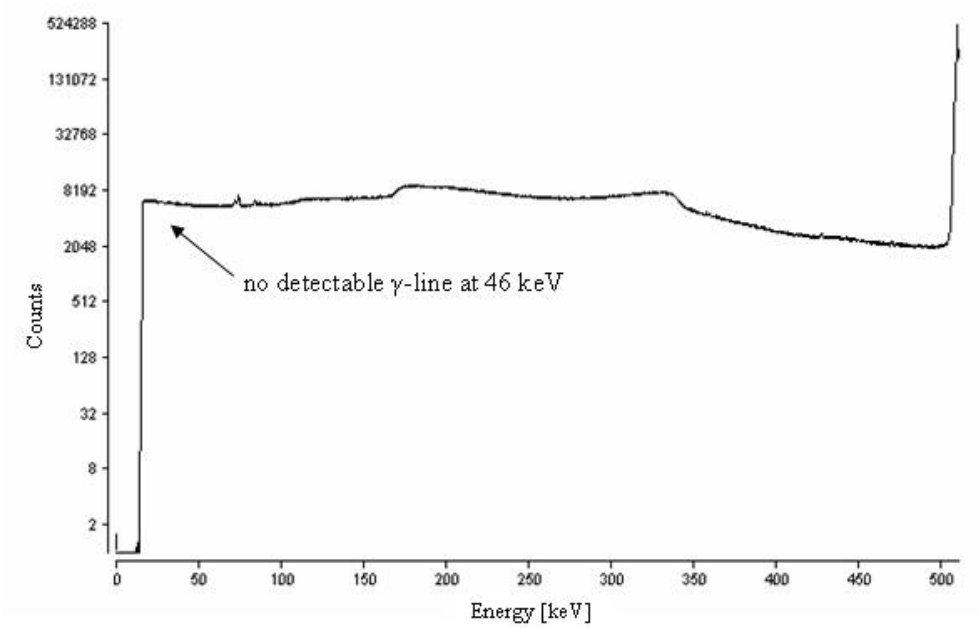

FIGURE 3c. γ-spectrum of the eluted daughter ^{72}As, enlarged logarithmic scale

The radiochemical purity is very much dependent on the storage conditions of the generator between subsequent elutions. The reduced $Se^{(0)}$ on the cartridge is sensitive to oxidation. If the generator is stored under $HF_{conc.,}$ but under air instead of nitrogen for 2 days without elution, up to 10% of the ^{72}Se load breaks through. This can be avoided by removing excessive $HF_{conc.}$ with nitrogen after elution and storing the generator in a sealed nitrogen-filled container. Another option is to store the generator column under reducing conditions filled with 0.1 M hydrazinium dihydrochloride containing $HF_{conc.}$ solution. While this option works well for the development of radiochemical processes, hydrazinium dihydrochloride might interfere when the eluted activity is used for subsequent chemical reactions.

[^{72}As]AsI_3

The eluted ^{72}As activity reacts to [^{72}As]AsI_3 after the addition of potassium iodide. This process also can be observed when adding macroscopic amounts of As_2O_3 and KI to a HF solution. The bright orange AsI_3 precipitates immediately. The yield for the cold reaction is

>95%. Elution with HF has the advantage that [^{72}As]AsI_3 is soluble in organic solvents and can easily be separated from the $HF_{conc.}$ solution by liquid-liquid or solid phase extraction. The formation of [^{72}As]AsI_3 transforms the generator eluate to a definite chemical form and its solubility in organic solvents makes [^{72}As]AsI_3 a very useful synthon for a possibly following labelling chemistry.

Apparatus

A schematic representation of the ^{72}Se/^{72}As radionuclide generator system is shown in Fig. 4. It consists of two Teflon reactors and the two corresponding polystyrene based ENV solid phase extraction cartridges. The first cartridge represents the generator column and the second one is used for the solid phase extraction based separation of nca [^{72}As]AsI_3 from the radionuclide generator eluate. Reservoirs are there for all solutions necessary as described and the apparatus can be flushed with nitrogen. This system is well suited for future automation.

1. Nitrogen
2. Methanol
3. Water
4. HF with KI
5. HF with hydrazinium hydrochloride
6. Chloroforme
7. Target
8. Reactor I
9. Reactor II
10. Generator cartridge
11. cartridge for separation of [^{72}As]AsI_3
12. Drying cartridge
13. Waste
14. Product, nca [^{72}As]AsI_3

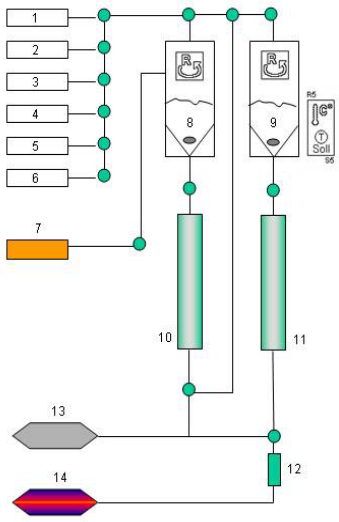

FIGURE 4. Scheme of a ^{72}Se/^{72}As-Isotope generator based on solid phase extraction

4. Conclusion

Following radiochemical separation of ^{72}Se from irradiated Ge or GeO_2 targets, nca ^{72}Se was used to design a convenient solid phase extraction radionuclide generator. After initial reduction of radioselenium, nca $Se^{(0)}$ is fixed on a polysterene based soild phase extraction column. Macroscopic Ge is separated as $[GeF_6]^{2-}$. Depending on the eluent, ^{72}As can be obtained with yields > 60% and a selenium contamination of less then 0.1%.

In addition to radionuclide generator performance, two other aspects are important. Compared to previously described $^{72}Se/^{72}As$ radionuclide generator designs, the method presented here (A) allows an efficient route to ^{72}As labelling of molecules relevant to biochemistry and medicine via the labelling synthon $[^{72}As]AsI_3$ and (B) represents a convenient technological realisation with rather low operation costs and easy to automate for routine use. Systematic chemical investigations on the labelling chemistry of no-carrier-added radioarsenic, however, are required prior to the application of ^{72}As labelled compounds.

Acknowledgement

Financial support was provided by the Deutsche Forschungsgemeinschaft (DFG-Grant Ro 985/9 and 985/17), an NCI P2O PRE-ICMIC (CA086334), the NMFZ of the University of Mainz, and by the Boehringer Ingelheim Fonds for Basic Medicinal Research, represented by Dr. H. Fröhlich.

References:

1. *The U.S. Geological Survey Workshop on arsenic in the environment, available at wwwbrr.cr.usgs.gov/Arsenic/*. 2004.
2. Evans, C.D., K. LaDow, B.L. Schumann, R.E. Savage, Jr., J. Caruso, A. Vonderheide, P. Succop, and G. Talaska, *Effect of arsenic on benzo[a]pyrene DNA adduct levels in mouse skin and lung.* Carcinogenesis, 2004. **25**(4): p. 493-7.

3. Ravandi, F., *Arsenic trioxide: expanding roles for an ancient drug?* Leukemia, 2004. **18**(9): p. 1457-9.
4. Miller, W.H., Jr., H.M. Schipper, J.S. Lee, J. Singer, and S. Waxman, *Mechanisms of action of arsenic trioxide.* Cancer Res, 2002. **62**(14): p. 3893-903.
5. Basile, D., C. Birattari, M. Bonardi, L. Goetz, E. Sabbioni, and A. Salomone, *Excitation functions and production of arsenic radioisotopes for environmental toxicology and biomedical purposes.* Int J Appl Radiat Isot, 1981. **32**(6): p. 403-10.
6. Byrne, A.R., *Simple production of ^{77}As from reactor irradiated germanium.* Int Conf on Nuc Radiochem, 1984: p. 239.
7. Mausner, L.F., S.O. Kurczak, and D.J. Jamriska, *Production of 73As by irradiation of Ge target.* J Nucl Med, 2004. **45**(5S): p. 471P.
8. Ward, T.E., D.L. Swindle, R.J. Wright, and P.K. Kuroda, *Radiochemical procedure for arsenic and germanium.* Radiochimica Acta, 1970. **14**(2): p. 70-72.
9. Al-Kourashi, S.H. and G.G.J. Boswell, *An Isotope Generator for ^{72}As.* Int J Appl Radiat Isot, 1978. **29**: p. 607-609.
10. Jennewein, M., A. Schmidt, A.F. Novgorodov, S.M. Qaim, and F. Rösch, *A no-carrier-added 72Se/72As radionuclide generator based on distillation.* Radiochimica Acta, 2004. **92**: p. 245-249.
11. Phillips, D.R., *Chemistry and Concept for an Automated ^{72}Se/^{72}As Generator*. 1994: Patent No. 5,371,372, United States.
12. Phillips, D.R., V.T. Hamilton, D.A. Nix, W.A. Taylor, D.J. Jamriska, R.C. Staroski, R.A. Lopez, and A.M. Emran, *Chemistry and Concept for an Automated ^{72}Se/^{72}As Generator.* New Trends in Radiopharm. Synthesis, QA and Regulatory Control, 1991: p. 173-181.
13. Phillips, D.R., V.T. Hamilton, M.D. Taylor, A.M. Farnham, A.M. Emran, R.W. Rowe, and D. Pattel, *Generator-Produced Arsenic-72 in Positron Emission Tomography.* Radioact Radiochem, 1992. **3**: p. 53-58.
14. Rösch, F., A.F. Novgorodov, and J. Brockmann, *Offenlegungsschrift DE 100 28 056 A 1*, in *Deutsches Patent- und Markenamt*. 2002: Deutschland.
15. Rösch, F. and F.F. Knapp, *Radionuclide generators*, in *Handbook of Nuclear Chemistry*, A. Vertés, et al., Editors. 2003, Kluwer Academic Publishers. p. 81-118.
16. Jennewein, M., A. Constantinescu, O. Bergner, M. Lewis, D. Zhao, S. Seliouine, N. Slavine, S. O'Kelly, S. Maus, S.M. Qaim, E. Tsyganov, P.P. Antich, F. Rösch, R.P.

Mason, and P.E. Thorpe, *Molecular Imaging of the Vascular Targeting Antibody Vatuximab® in Rat Prostate Cancer, Eur. J. Nuc. Med. Mol. Im. 31 (2004) 259.* Eur J Nuc Med Mol Im, 2004. **31**: p. 259.

17. Browne, E. and R.B. Firestone, *Table of Radioactive Isotopes*, ed. V.S. Shirley. 1986, New York: John Wiley & Sons.
18. Mushtaq, A., S.M. Qaim, and G. Stöcklin, *Production of 73Se via (p,3n) and (d,4n) reactions on arsenic.* Appl Radiat Isot, 1988. **39**(10): p. 1085-1091.
19. Mushtaq, A. and S.M. Qaim, *Excitation functions of α- and ^{3}He-particle induced nuclear reactions on natural germanium: evaluation of production routes for ^{73}Se.* Radiochimica Acta, 1990. **50**: p. 27-31.
20. Nozaki, T., Y. Itoh, and K. Ogawa, *Yield of 73Se vor various reactions and its chemical processing.* Int J Appl Radiat Isot, 1979. **30**: p. 595-599.
21. Hara, T., R.S. Tilbury, B.R. Freed, H.Q. Woodard, and J.S. Laughlin, *Production of 73 Se in cyclotron and its uptake in tumors of mice.* Int J Appl Radiat Isot, 1973. **24**(7): p. 377-84.
22. Guillaume, M., R.M. Lambrecht, and A.P. Wolf, *Cyclotron isotopes and radiopharmaceuticals - XXVII. ^{73}Se.* Int J Appl Radiat Isot, 1978. **29**: p. 411-417.
23. Bagnall, K.W., *Selenium, Tellurium and Polonium*, in *Comprehensive Inorganic Chemistry*, J.C. Bailar, et al., Editors. 1973, Pergamon Press Ltd.: New York. p. 935-1009.
24. *National Nuclear Data Center, Brookhaven National Laboratory*. 2004, http://www.nndc.bnl.gov/nudat2/index.jsp.

III.

A New Method for Radiochemical Separation of Arsenic from Reactor and Cyclotron Irradiated Germanium Oxide

A New Method for Radiochemical Separation of Arsenic from Irradiated Germanium Oxide

M. Jennewein[1,2], S.M. Qaim[3], A. Hermanne[4], M. Jahn[1], E. Tsyganov[2], S. Seliounine[2], N. Slavine[2], P.P. Antich[2], P.V. Kulkarni[2], P.E. Thorpe[5], R.P. Mason[2] and F. Rösch[1,*]

[1]Institute of Nuclear Chemistry, Johannes Gutenberg University of Mainz, Fritz-Strassmann-Weg 2, 55128 Mainz, Germany
[2]Department of Radiology, University of Texas Southwestern Medical Center at Dallas, 5323 Harry Hines Blvd, Dallas, Texas 75390-9058, USA
[3]Institut fuer Nuklearchemie, Forschungszentrum Juelich, 52428 Juelich, Germany
[4]Cyclotron Department, Vrije Universiteit Brussel, Laarbeeklaan 103, 1090 Brussels, Belgium
[5]Department of Pharmacology and Simmons and Hamon Cancer Centers, University of Texas Southwestern Medical Center at Dallas, Dallas, Texas, USA

Key Words:

As-71, As-72, As-73, As-74, As-77, radiochemical separation, solid-phase extraction

Abstract

Radioarsenic labelled radiopharmaceuticals could be a valuable asset to Positron Emission Tomography (PET). In particular, the long half-lives of ^{72}As ($T_{1/2}$= 26 h) and ^{74}As ($T_{1/2}$= 17.8 d) allow the investigation of slow physiological or metabolical processes, like the enrichment and distribution of antibodies in tumor tissue. This work describes the direct production of no-carrier-added (nca) arsenic isotope *As, with * = 71, 72, 73, 74 or 77, to [*As]AsI_3 and its radiochemical separation from the irradiated solid germanium oxide via polystyrene-based solid-phase extraction. The germanium oxide target, irradiated at a cyclotron or a nuclear reactor, is dissolved in concentrated HF and Ge is separated almost quantitatively (99.97 %) as $[GeF_6]^{2-}$. [*As]AsI_3 is formed by addition of potassium iodide. The radiochemical separation yield for arsenic is > 90%. [*As]AsI_3 is a versatile radioarsenic labelling synthon.

1. Introduction

The recent increasing interest in the element arsenic in environmental sciences [1], toxicology and carcinogenesis (Evans et al., 2004) and medicine, particularly in the treatment of promyelocytic leukaemia (Ravandi, 2004; Miller et al., 2002; Zhu et al., 2002; Zhu et al., 2003; Zhu et al., 2001; Zhu et al., 1997; Chen et al., 1997; Shen et al., 1997; Chen et al., 1996; Wang, 2001), stimulates a need to develop convenient and reproducible methods to trace this element and its compounds in subtoxic and subpharmaceutical concentrations. Arsenic has several radioisotopes of interest for molecular/medical or environmental application (cf. Table 1).

Property	^{71}As	^{72}As	^{73}As	^{74}As	^{76}As	^{77}As
$T_{1/2}$ [d]	2.7	1.1	80.3	17.8	1.1	1.6
Mode of decay (%)	EC (70) β^+ (30)	EC (12.2) β^+ (87.8)	EC (100)	EC (66) β^+ (29)	β^- (100)	β^- (100)
Most abundant γ-lines [keV]	175.0 (82.0 %)	834.0 (79.5 %) 629.9 (7.9 %)	53.4 (10.0 %)	595.8 (59.0 %) 634.8 (15.4 %)	559.1 (45.0 %) 657.1 (6.2 %)	239.0 (1.6 %) 520.6 (0.5 %)
Positron-energy [keV]	Mean: 350	Mean: 1117		Mean: 440		

TABLE 1. Decay data of the most relevant arsenic isotopes (National Nuclear Data Center, 2004)

Several approaches to develop an easy and practical system to separate these isotopes from cyclotron or reactor irradiated germanium or germanium oxide targets have been described in the past (Basile et al., 1981; Byrne, 1984; Mausner et al., 2004; Ward et al., 1970). In addition, strategies towards a versatile radioarsenic labelling chemistry were developed to generate arsenic isotopes in chemical forms suitable for future application in labelling chemistry, radiopharmacy and, ultimately, for molecular imaging using Positron Emission Tomography (PET). Recent advances in using ^{74}As labelled antibodies directed against the

apoptotic marker phophatidylserine (PS) in a Dunning R2337 AT1 prostate cancer model (Jennewein et al., 2004) clearly demonstrate the potential of these radioarsenic isotopes. This strengthens the motivation to develop adequate and reliable radiochemical separations.

The decay properties of radioactive arsenic isotopes are summarized in Table 1.

^{71}As has a half-life of 65 h. It decays by 70% through electron capture and has a positron emission rate of 30% with E_{β^+mean} = 350 keV. It can be produced by the ^{70}Ge(d,n)^{71}As reaction (Beard, 1960) and by Ge(p,xn)^{71}As processes (Basile et al., 1981).

^{72}As is a positron emitting arsenic isotope, with properties suitable for application in ^{72}As-labelled PET-radiopharmaceuticals. It has a positron emission rate of 88% with E_{β^+mean} = 1117 keV. Although the positron emission is accompanied by the emission of photons of 834 keV (79.5%), 630 keV (7.9%), 1461 keV (1.1%) and others (< 0.5%), the long physical half-life of 26 hours may render ^{72}As a PET radionuclide of choice for the quantitative imaging of biochemical and physiological processes with longer biological half-lives, *e.g.* immunoimaging and receptor mapping. In these cases, the half-life of ^{72}As is commensurate with the radiopharmacological requirements resulting from the relatively slow localization kinetics of the labelled species. These virtues are comparable to those of ^{124}I ($T_{1/2}$= 4.18 d), but note that this radioisotope has a β^+-branching of only 22%. In addition to production from a generator following the reaction ^{70}Ge(α,2n)^{72}Se → ^{72}As (Al-Kourashi et al., 1978; Jennewein et al., 2004; Philipps, 1994; Philipps et al., 1991; Philipps et al. 1992; Rösch et al., 2002; Rösch et al., 2003; Jennewein et al., 2005), it can be produced directly in high yields, e.g. via the ^{72}Ge(p,n)^{72}As reaction using small-sized cyclotrons (Basile et al., 1981).

^{73}As has a half-life of 80.3 d and decays exclusively via electron capture, emitting only γ-ray of 53.4 keV. Because of the long half-life, it is mainly applied as a tracer for environmental sciences. It is currently produced via the Ge(p,xn)^{73}As reaction with subsequent distillation and purification on a cation exchange column (Mausner, et al., 2004).

^{74}As is also a positron emitter, but has a much longer half-life ($T_{1/2}$= 17.8 d) than ^{72}As. It thus represents one of the longest living positron emitters with sufficient β^+ branching. It

has a positron emission rate of 29 % with a low positron energy of E_{β^+mean} = 440 keV and an electron emission rate of 34.2 % and E_{β^-mean} = 137 keV. The low positron energy provides a high local resolution, comparable to that of ^{18}F, when measured via PET, as shown in Fig. 1. The spatial resolution dependency on positron energy was measured using the Small Animal PET of the University of Texas Southwestern Medical Center at Dallas for point sources (Ø = 1 mm) of ^{72}As, ^{74}As, ^{124}I , ^{18}F and ^{22}Na.

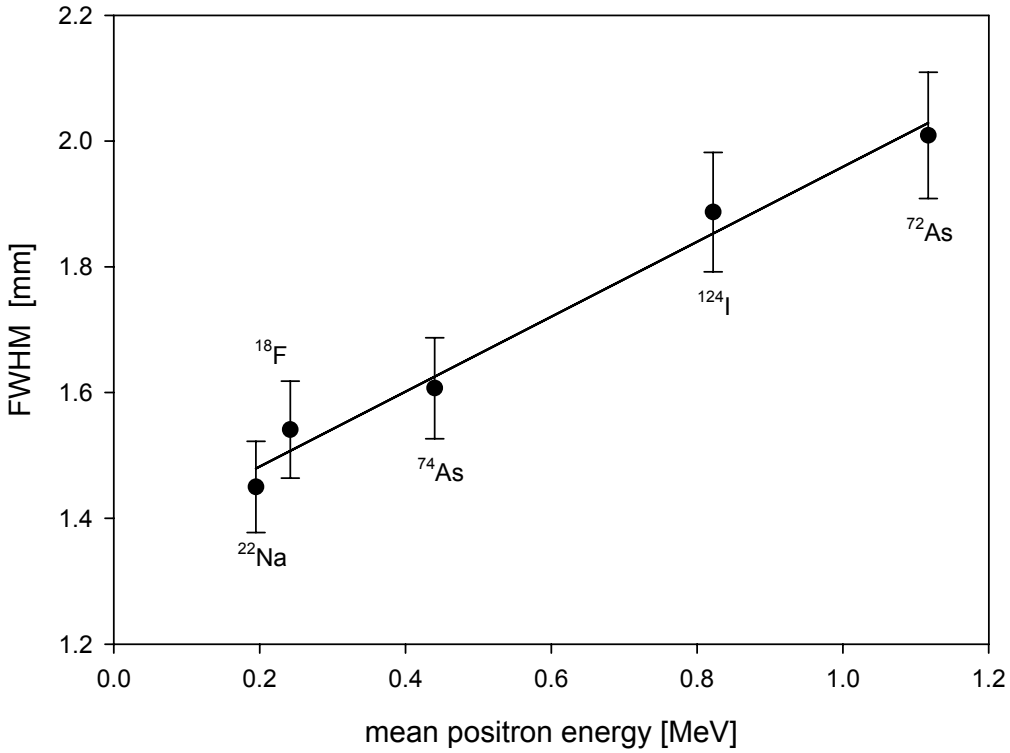

FIGURE 1. Spatial resolution for different positron emitting isotopes versus their positron energy. Measurements were done at the Small Animal PET of the UTSW Medical Center at Dallas using equal-sized point sources, Ø = 1 mm.

^{74}As was one of the first isotopes used in the very preliminary stages of PET in the 1950s and 1960s (Sweet et al., 1955; Leicester et al., 1966; Mealy, 1963; Wilcke, 1965; Wilcke, 1965; Wilcke et al., 1965) called positrocephalography at that time. Due to its long half-life, it is more appropriate for animal use than human use, but could also provide a useful

tool for the study of long-lasting metabolic processes, like antibody-antigen interactions or, in general, long term pharmacokinetics of developmental drugs. ^{74}As can be produced best by the ^{74}Ge(p,n)^{74}As or ^{73}Ge(d,n)^{74}As reaction at a small-sized cyclotron. Excitation functions and target yields were described in detail previously (Basile et al., 1981).

^{77}As is a 100 % electron emitting isotope with a half-life of 1.6 d and $E_{\beta^- mean}$ = 226 keV. This isotope could be of future use in arsenic based endoradiotherapeutics. ^{77}As can be produced at nuclear reactors via the ^{nat}Ge(n,γ)^{77}Ge reaction, ^{77}Ge decaying to ^{77}As with a half-life of 11.3 h. In addition, also deuteron induced reactions on enriched ^{76}Ge targets could provide pathways for direct or indirect production of ^{77}As.

Separations

All the production routes mentioned both at accelerators and nuclear reactors share the radiochemical separation of nca radioarsenic from macroscopic germanium targets. The radiochemical procedures for germanium are described in detail by Mirzadeh (Mirzadeh et al., 1986; Mirzadeh et al., 1981; Mirazdeh et al., 1996). Only a few alternative radiochemical separations for radioactive arsenic isotopes have been reported to date. Schindewolf and Irvine (Schindewolf et al., 1958) and Basile (Basile et al., 1981) dissolved the irradiated germanium target in conc. HF and used an anion exchange column to separate As(III) from Ge(IV) which is retained by the resin as hexafluorocomplex. A second anion exchange column with HF/HCl gradients was required for purification. Mukhopadhyay (Mukhopadhyay et al., 2002) produced nca radionuclides of arsenic and selenium in an ^{16}O irradiated cobalt target matrix. The initial products, formed by ^{59}Co(^{16}O,*x*n)$^{70\text{-}73}$Br reactions, decayed promptly to arsenic and selenium radionuclides, which were subsequently separated by liquid-liquid extraction (LLX) using di-(2-ethylhexyl) phosphoric acid (HDEHP) and trioctylamine (TOA) as liquid ion exchangers. The radiochemical separation of ^{77}As from ^{77}Ge using thin-layer chromatographic and electrophoretic methods is described by Halpern (Halpern et al., 1964) and Maki and Murakami (Maki et al., 1974). Other radiochemical separations of As from Ge used an oxidative distillation followed by a reductive distillation (Beard, 1960). The major drawback of all the previous methods, however, was that they lacked the option of using the separated nca radioactive arsenic isotopes for a following labelling chemistry of biomolecules.

The aim of the present work was to develop a more convenient radiochemical separation method for radioactive arsenic isotopes from reactor or cyclotron irradiated germanium oxide targets with optimized radiochemical yields, separation efficiencies and radiochemical product purity. Moreover, the transfer of the separated and purified radioarsenic fractions to a chemical form (synthon), optimum for future labelling chemistry, should represent an important feature of the separation to allow investigations and application of radioarsenic-labelled radiopharmaceuticals. The system should be reliable for the routine separation of various arsenic isotopes, and finally, the handling time should be reduced to a minimum.

A radiochemical procedure based on the formation of soluble [GeF_6^{2-}] in concentrated hydrofluoric acid and the reaction to [*As]AsI_3 through addition of KI is described to separate nca *As (* = 71,72,73,74,77) from irradiated germanium oxide targets

2. Materials and Methods

Isotope production

^{74}As was produced by the ^{nat}Ge(p,x)^{74}As reaction [E_p= 20 MeV] on 100 mg GeO_2 pellets (850 μm equivalent Ge thickness) pressed at 10 t and placed in watercooled stainless steel target holders and covered by a thin pure Al-foil. To avoid excessive burning of the target material by the energy deposition of the 16 MeV incident proton beam, the particle current was limited to 8 μA in a homogeneous beam. The thick target yield under these conditions is 2.5 MBq/μA·h (at EOB) for production of ^{74}As with high levels of ^{72}As contamination.

^{77}As was produced in nca state via the ^{76}Ge(n,γ)^{77}Ge $\rightarrow \beta^-$ $T_{½}$ = 11.30 h $\rightarrow$ ^{77}As processes at the TRIGA reactor of the Institute of Nuclear Chemistry of the University of Mainz (Φ = 4.0 x 10^{12} n/cm^2s). All irradiations were performed using 100 mg of $^{nat}GeO_2$.

Materials

Germanium(IV)oxide (99.9999 % pure, PURA TREM) was purchased from Strem Chemicals Inc. Concentrated hydrofluoric acid (48 %) and potassium iodide were

purchased from Aldrich. BOND ELUT ENV solid phase extraction cartridges with a sorbent mass of 50 mg and a volume of 1 ml were purchased from Varian.

Radiochemical separation

Irradiated germanium oxide targets were dissolved in 5 ml conc. HF at room temperature for 1 h. Subsequently, potassium iodide was added and stirred for 10 minutes. The amount of KI was varied between 0.1 and 10 mg/ml HF. The mixture was transferred to an ENV-solid phase extraction cartridge. The cartridge-holder and fittings to standard size syringes were made in the machine-shop of the Institute of Nuclear Chemistry, University of Mainz. The ENV cartridge was preconditioned with 5 ml of MeOH, 5 ml H_2O and 5 ml conc. HF containing potassium (1 mg/ml). The nca [*As]AsI_3 was fixed to the solid phase, while the macroscopic $[GeF_6]^{2-}$ was eluted quantitatively with the mobile phase. After the fixation of [*As]AsI_3, excess the HF was removed with a nitrogen-flow over the cartridge for 5 min. The elution of [*As]AsI_3 was performed with 500-1000 µl of various organic solvents (toluene, chloroform, dichloromethane, hexane, cyclohexane and ethanol). If the subsequent labeling chemistry requires anhydrous solvent conditions, a $CaCl_2$ drying cartridge could be used.

Determination of radionuclidic purity and radiochemical separation yields

The radionuclidic purity and radiochemical separation yields were determined using γ-ray spectroscopy. Aliquots of the dissolved target were measured and quantitatively compared with the γ-ray spectra of the solid phase extraction cartridges, eluates and waste-solutions. The γ-ray spectroscopy was performed using an Ortec HPGe detector system, and the GammaVision 5.0 software by Ortec was used for peak area analysis.

3. Results and Discussion

Target dissolution

For optimum target dissolution, it is important to use precipitated germanium oxide and not burned germanium oxide as target material, as the latter is not soluble at room temperature. Higher temperatures should be avoided, since an increased temperature leads to the formation of arsine (AsH_3) and thus to significant volatilization of activity (>60 %, $T_b(AsH_3)$= -62.5 °C (Smith, 1973)). Low temperatures, fast target dissolution and the quantitative formation of nca [*As]AsI_3 minimize the formation of arsine and loss of activity due to volatilization. The use of metallic germanium was also evaluated, but GeO_2 is preferable, since the macroscopic Ge is already in the oxidation state +IV. However, to date isotopically enriched germanium is only available as metal. If metallic germanium is used as target material, small amounts of HNO_3 must be added to the HF solution to oxidise $Ge^{(0)}$ to $Ge^{(IV)}$ and thus to dissolve the target. Heating of the target accelerates the dissolution process significantly, but leads also to a loss of arsenic activity, due to the formation of *AsH_3, as described above. *AsH_3 formation and volatilization was not observed at room temperature. However, the oxidizing conditions after addition of HNO_3 in the target solution lead to the formation of free iodine when adding potassium iodide in an exothermic reaction. The procedures described in this article therefore are not applicable to metallic germanium targets. If isotopically enriched target material is used, an oxidation prior to irradiation is crucial.

Following both p- and n-irradiation of 100 mg $^{nat}GeO_2$ targets, the optimum dissolution was achieved at room temperature after 20 minutes.

A comparison of γ-spectroscopically measured As contents of the target solution before and after the solid-phase extraction gives separation yields > 90% for *As, independent of the produced arsenic isotope. The amount of Ge separated from the cartridge is > 99.97%.

*Formation and fixation of [*As]AsI_3*

Macroscopic AsI_3 is dark orange, the melting point is 140.4°C and the boiling point 371°C (Smith, 1973). Its solubility in polar solvents is limited and therefore it is slightly soluble in water, but well soluble in organic solvents, like CS_2, benzene, toluene, xylene and

chloroform (Zingaro, 1994). The formation of macroscopic AsI_3 under these conditions was observed when adding equimolar amounts of KI and macroscopic As_2O_3 to conc. HF. The dark orange AsI_3 precipitated immediately and quantitatively. AsF_3 can also be formed in conc. HF from As_2O_3, but not without the addition of concentrated H_2SO_4 (Shriver, 1997).

The amount of KI necessary for quantitative formation of nca [*As]AsI_3 was evaluated (cf. Fig. 2). After the addition of 2 mg/ml HF solution (12 µmol/ml), the yield was 95±5 % and did not change with the increase in the KI concentration.

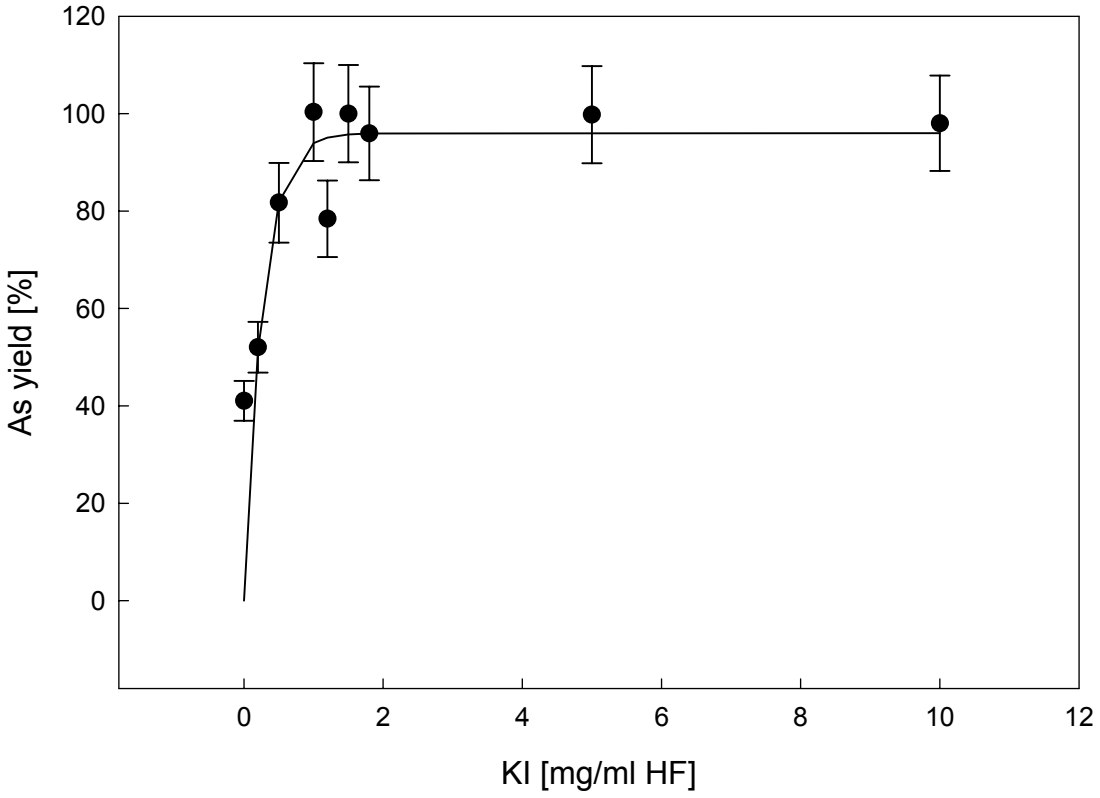

FIGURE 2. Yield of nca [*As]AsI_3 versus the potassium iodide content in conc. HF. Nca [*As]AsI_3 was eluted with chloroform after fixation on an ENV solid phase extraction cartridge.

Bond Elut ENV, a high purity styrene divinyl benzene (SDVB) polymer has been optimized for the extraction of polar organic residues, such as herbicide metabolites and explosives from large volume water samples. Although primarily developed for environmental applications, it can also be used for clinical purposes such as the extraction of metabolites from human fluids. Bond Elut ENV features a 125 µm highly cross-linked spherical polymer with a surface area of 500 m^2/g and a pore volume of 1.3 ml/g. The absence of secondary interactions on the polymer surface eases the elution of a wide range of molecular species. The cartridges are resistant to concentrated hydrofluoric acid. Using these cartridges, > 90 % of the nca [*As]AsI_3 could be fixed.

Elution

Various organic solvents were studied to elute the fixed [*As]AsI_3 activity. We observed similar elution yields, independent of polarity and lipophilicity of the tested solvents (toluene, chloroform, dichloromethane, hexane, cyclohexane and ethanol). Yields were > 95 % in a volume of 1000 µl for all solvents, with > 80 % of the eluted [*As]AsI_3 obtained in the first 500 µl (Fig. 3). Thus, the solvent for the elution should be chosen based on the requirements of the intended subsequent labelling chemistry. In an antibody labelling study, prior to studies *in vitro* and *in vivo* (Jennewein et al., 2004), the elution was performed with ethanol. The solution could be concentrated to 50 µl after elution at 50°C and a slow nitrogen flow in 20 minutes to keep the antibody from precipitating and to reduce the ethanol burden, which was injected in animals. If the nca [*As]AsI_3 should be used later in a nonaqueous labeling environment, *e.g.* for synthesis of organometallic compounds (Jennewein et al., 2003 (a); Jennewein et al., 2003 (b)), it can be eluted with chloroform and dried with chemically inert $CaCl_2$ before further reaction. The use of sodium thiosulfate as drying reagent was also evaluated, but the high affinity of arsenic for sulfur leads to a loss of arsenic activity (> 80 %) and therefore has to be avoided. A typical elution profile for ^{77}As is given in Fig. 3.

The radionuclidic purity of the eluted ^{77}As was determined using γ-ray spectroscopy analysing the fractions eluted with ethanol. The spectrum obtained was compared with that of an aliquot of the target solution (Fig. 4a-b). Whereas in the target sample the γ-rays of ^{77}Ge, e.g. at 211 keV (29.2 %) and 216 keV (27.1 %) could clearly be observed, these lines are not detectable in the separated ^{77}As fractions, as demonstrated in the expanded part of

the spectrum (note the longer measurement time for the ^{77}As spectrum of 10 h compared to 1 h for the target spectrum). Integrating the spectroscopic data for the 211 and 216 kev γ-ray lines, the amount of Ge remaining in the ^{77}As fraction was calculated to be lower than 0.0002 %, which is < 2 μg for a 100 mg GeO_2 target.

At 264 keV a small γ-ray line is visible in the enlarged view of the spectrum of the separated ^{77}As fraction, which also is part of the ^{77}Ge γ-emissions. However, this γ-ray line also represents radioselenium impurities. ^{74}Se has only a 0.89 % natural abundance, but a high (n,γ) cross section of 46 barn. As the (n,γ) reaction to ^{77}Ge has a cross section of only 0.06 barn, even small impurities of selenium could have a measurable effect, as the 264.7 keV line is the highest intensity γ-ray line of ^{75}Se with 58.9 % abundance. Therefore the 264 keV γ-ray line was not used for the determination of the radiochemical purity of the separated ^{77}As.

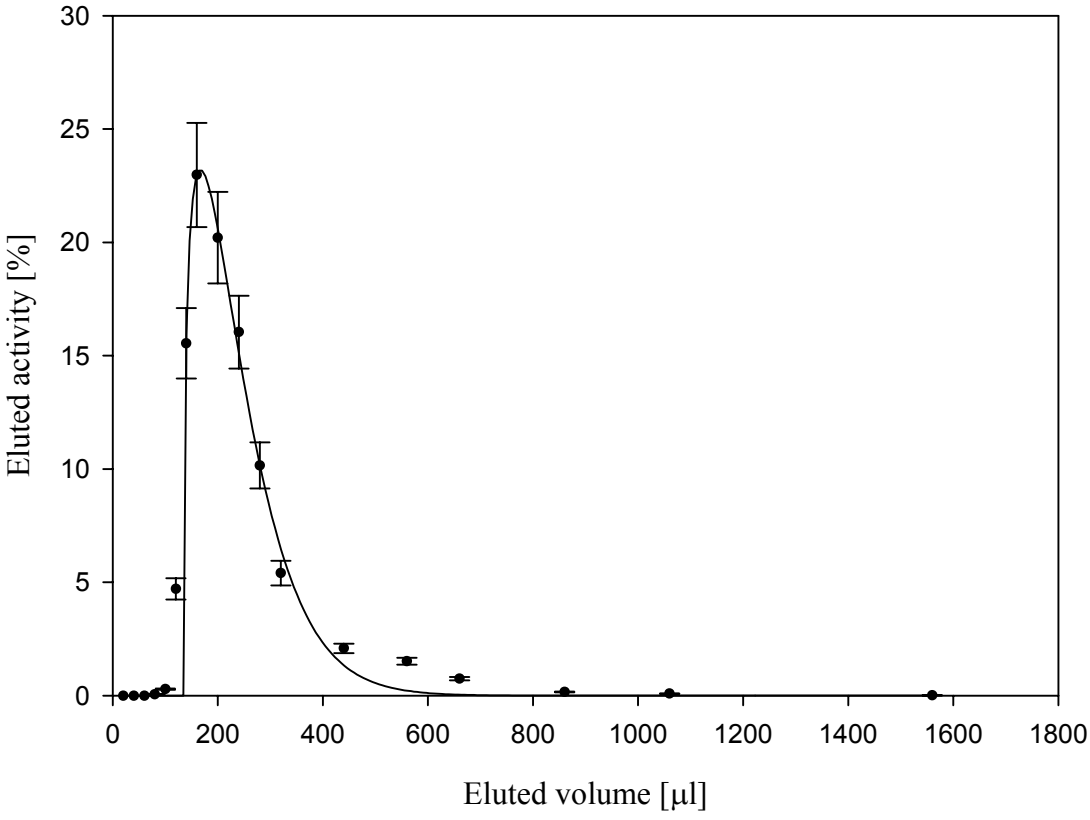

FIGURE 3. Typical elution profile of a nca $^{77}AsI_3$ loaded polystyrene ENV cartridge (eluted with ethanol, percentage of eluted activity based on the activity-balance of all the fractions, total elution volume 1.8 ml)

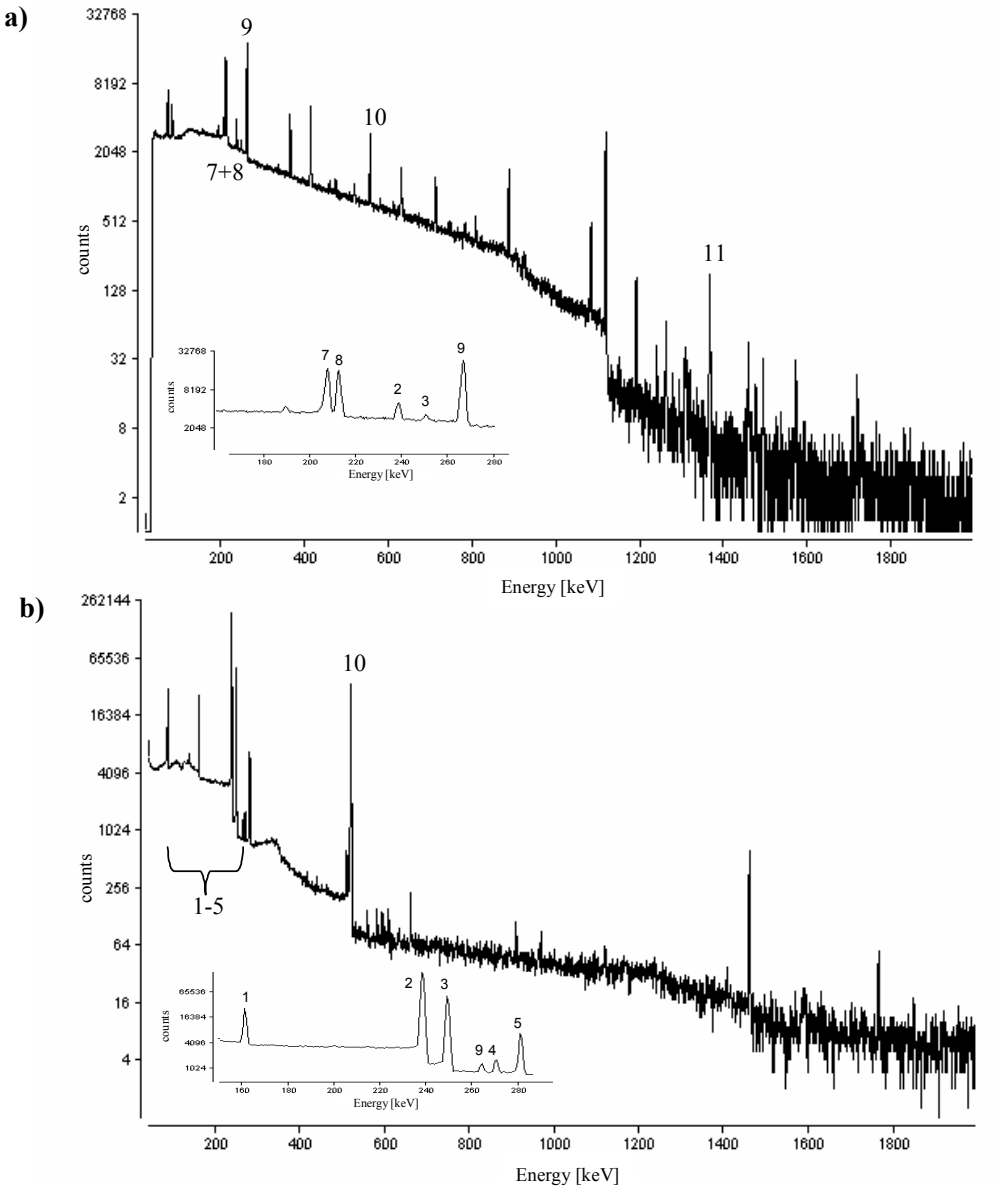

^{77}As: 1) 162 keV, 2) 239 keV, 3) 249 keV, 4) 271 keV, 5) 281 keV, 6) 521 keV
^{77}Ge: 7) 211 keV, 8) 216 keV, 9) 264 keV, 10) 558 keV, 11) 1368 keV

FIGURE 4. Radiochemical purity of the separated nca $^{77}AsI_3$ in ethanol: a) γ-ray spectrum of the target after dissolution in conc. HF; measurement time = 1 h; b) γ-ray spectrum of ^{77}As; measurement time = 10 h;

Apparatus

A schematic representation of the separation system is shown in Fig. 5. It essentially comprises a temperature controlled Teflon reactor with a stirrer and a polystyrene based ENV solid phase extraction cartridge. All parts are resistant to concentrated hydrofluoric acid and organic solvents. Reservoirs are available for all solutions necessary and the apparatus can be flushed with nitrogen. This system is well suited for future automation.

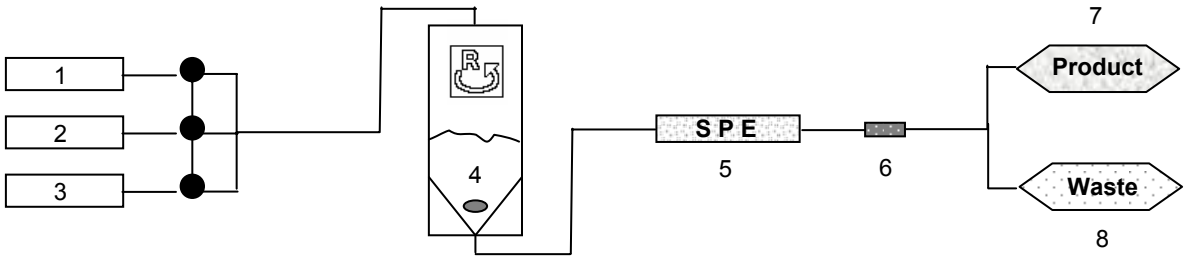

1. Nitrogen
2. HF with KI
3. Organic solvent
4. Reactor with target
5. cartridge for separation of [^{72}As]AsI_3
6. Drying cartridge
7. Product, nca [^{72}As]AsI_3
8. Waste

FIGURE 5. Scheme of the described extraction system for the separation of nca radioactive arsenic isotopes from reactor or cyclotron irradiated germanium oxide targets

The separation method introduced here was exemplified by ^{77}As and ^{74}As, but the main impact may lie in the separation of ^{72}As. In previous work of our group, the radionuclide generator system ^{72}Se/^{72}As was described (Jennewein et al., 2004; Jennewein et al., 2005). The idea of a generator seems to be very appealing in a clinical environment without a

cyclotron. However, the production yields of ^{72}Se (Basile et al., 1981; Horiguchi et al., 1983; Dmitriev, 1986) are rather low from the viewpoint of preparing generators for a sufficient supply of ^{72}As. In contrast the production yields in the direct production of ^{72}As via the ^{72}Ge(p,n)^{72}As reaction would be relatively high. From the systematics, the maximum of the excitation function is expected to be between 9 and 15 MeV, which is covered by small-sized medical cyclotrons. A batch yield of several GBq of ^{72}As could be obtained, which would be sufficient for systematic medical applications. Even commercial distribution seems to be feasible.

4. Conclusion

A new method was developed to separate radioactive arsenic isotopes from reactor or cyclotron irradiated germanium oxide targets. Following initial target dissolution, the arsenic reacts on addition of KI to form [*As]AsI_3. This nca radioarsenic triiodide is fixed on a polystyrene based solid phase extraction column. Macroscopic Ge is separated as $[GeF_6]^{2-}$. Nca [*As]AsI_3 can be obtained in yields > 85% with a contamination from germanium of less than 0.01%. This approach suggests a convenient technological realisation with rather low operation costs, and would be easy to automate for routine use. Compared to previously described radioarsenic separations from macroscopic germanium, the method allows an efficient route to *As labelling of molecules relevant to biochemistry and medicine via the labelling synthon [*As]AsI_3. This approach might be in particular relevant to the large-scale production of ^{72}As following ^{72}Ge(p,n)^{72}As reaction on highly enriched $^{72}GeO_2$.

Acknowledgement

Financial support was provided by the Deutsche Forschungsgemeinschaft (DFG-Grant Ro 985/9 and 985/17), an NCI P2O pre-ICMIC (CA086334), the NMFZ of the University of Mainz, and by the Boehringer Ingelheim Fonds for Basic Medicinal Research, represented by Dr. H. Fröhlich.

References:

Al-Kourashi, S. H., and Boswell, G. G. J. (1978). An Isotope Generator for ^{72}As. Int J Appl Radiat Isot *29*, 607-609.

Basile, D., Birattari, C., Bonardi, M., Goetz, L., Sabbioni, E., and Salomone, A. (1981). Excitation functions and production of arsenic radioisotopes for environmental toxicology and biomedical purposes. Int J Appl Radiat Isot *32*, 403-410.

Beard, H. C. (1960). The radiochemistry of arsenic (Washington, National Academy of Sciences).

Byrne, A. R. (1984). Simple production of ^{77}As from reactor irradiated germanium. Int Conf on Nuc Radiochem, 239.

Chen, G. Q., Shi, X. G., Tang, W., Xiong, S. M., Zhu, J., Cai, X., Han, Z. G., Ni, J. H., Shi, G. Y., Jia, P. M.*, et al.* (1997). Use of arsenic trioxide (As_2O_3) in the treatment of acute promyelocytic leukemia (APL): I. As_2O_3 exerts dose-dependent dual effects on APL cells. Blood *89*, 3345-3353.

Chen, G. Q., Zhu, J., Shi, X. G., Ni, J. H., Zhong, H. J., Si, G. Y., Jin, X. L., Tang, W., Li, X. S., Xong, S. M.*, et al.* (1996). In vitro studies on cellular and molecular mechanisms of arsenic trioxide (As2O3) in the treatment of acute promyelocytic leukemia: As2O3 induces NB4 cell apoptosis with downregulation of Bcl-2 expression and modulation of PML-RAR alpha/PML proteins. Blood *88*, 1052-1061.

Dmitriev, P. P. (1986). Radionuclide Yield in Reactions with protons, deuterons, α-particles and ^{3}He (Moskau, Energo Atom ISDAT).

Evans, C. D., LaDow, K., Schumann, B. L., Savage, R. E., Jr., Caruso, J., Vonderheide, A., Succop, P., and Talaska, G. (2004). Effect of arsenic on benzo[a]pyrene DNA adduct levels in mouse skin and lung. Carcinogenesis *25*, 493-497.

Halpern, A., Siekierska, K. E., and Siuda, A. (1964). The Chemical Forms of Radioarsenic Activated in β^- Decay of $^{77}GeCl_4$ and in the $^{75}AsCl_3$ (n,γ) Reaction in Benzene. Radiochimica Acta *3*, 40-44.

Horiguchi, T., Kumahora, H., Inoue, H., and Yoshizawa, Y. (1983). Excitation Functions of Ge(p,xnpy) Reactions and Production of ^{68}Ge. Int J Appl Radiat Isot *34*, 1531-1535.

Jennewein, M., Constantinescu, A., Bergner, O., Lewis, M., Zhao, D., Seliouine, S., Slavine, N., O'Kelly, S., Maus, S., Qaim, S. M.*, et al.* (2004). Molecular Imaging of the Vascular Targeting Antibody Vatuximab® in Rat Prostate Cancer. Eur J Nuc Med Mol Im *31*, 259.

Jennewein, M., Qaim, S. M., Kulkarni, P. V., Mason, R. P., Hermanne, A., and Roesch, F. (2005). A no-carrier-added $^{72}Se/^{72}As$ radionuclide generator based on solid phase extraction. submitted to Radiochimica Acta.

Jennewein, M., Schirrmacher, R., Maus, S., and Rösch, F. (2003)(a). Macroscopic synthesis of arsenoorganic precursors and first no-carrier-added radioarsenic labelling. J Lab Comp Radiopharm *46*, 42.

Jennewein, M., Schirrmacher, R., Maus, S., and Rösch, F. (2003)(b). Synthesis of 1,3-dimercaptopropyl arsenic-BOC-cysteine-O-BZL and diphenyl arsenic-BOC-cysteine-O-Bzl and first radioarsenic labelling. J Lab Comp Radiopharm *46*, 283.

Jennewein, M., Schmidt, A., Novgorodov, A. F., Qaim, S. M., and Rösch, F. (2004). A no-carrier-added $^{72}Se/^{72}As$ radionuclide generator based on distillation. Radiochimica Acta *92*, 245-249.

Leicester, J., and Vanderfield, G. K. (1966). The detection of cerebral lesions by the newer forms of encephalography: positron scanning and echoencephalography. Med J Aust *2*, 680-683.

Maki, Y., and Murakami, Y. (1974). The Separation of Arsenic-77 in a Carrier-Free State from the Parent Nuclide Germanium-77 by a Thin-Layer Chromatographic Method. J Radioanal Chem *22*, 5-12.

Mausner, L. F., Kurczak, S. O., and Jamriska, D. J. (2004). Production of ^{73}As by irradiation of Ge target. J Nucl Med *45*, 471P.

Mealey, J., Jr. (1963). Radioisotopic Localization in Subdural Hematomas. An Experimental Study with Arsenic-74 and Radioiodinated Human Serum Albumin in Dogs. J Neurosurg *20*, 770-776.

Miller, W. H., Jr., Schipper, H. M., Lee, J. S., Singer, J., and Waxman, S. (2002). Mechanisms of action of arsenic trioxide. Cancer Res *62*, 3893-3903.

Mirzadeh, S., and Kahn, M. (1986). Studies of the Chemical Behavior of Carrier-Free ^{68}Ge: III. Adsorptive Properties. Radiochimica Acta *39*, 189-194.

Mirzadeh, S., and Lambrecht, R. M. (1996). Radiochemistry of Germanium. J Radioanal Nuc Chem *202*, 7-102.

Mirzadeh, S., Kahn, M., Grant, P. M., and O'Brien, H. A. (1981). Studies of the Chemical Behavior of Carrier-Free ^{68}Ge: I. Purification by Distillation from Acidic Chloride Solutions. Radiochimica Acta *28*, 47-49.

Mukhopadhyay, K., Nayak, D., and Lahiri, S. (2002). Separation of no-carrier-added As and Se produced in ^{16}O irradiated cobalt target. J Radioanal Nuc Chem *251*, 159-162.

National Nuclear Data Center, Brookhaven National Laboratory (http://www.nndc.bnl.gov/nudat2/index.jsp).

Phillips, D. R. (1994). Chemistry and Concept for an Automated ^{72}Se/^{72}As Generator (Patent No. 5,371,372, United States).

Phillips, D. R., Hamilton, V. T., Nix, D. A., Taylor, W. A., Jamriska, D. J., Staroski, R. C., Lopez, R. A., and Emran, A. M. (1991). Chemistry and Concept for an Automated $^{72}Se/^{72}As$ Generator. New Trends in Radiopharm Synthesis, QA and Regulatory Control, 173-181.

Phillips, D. R., Hamilton, V. T., Taylor, M. D., Farnham, A. M., Emran, A. M., Rowe, R. W., and Pattel, D. (1992). Generator-Produced Arsenic-72 in Positron Emission Tomography. Radioact Radiochem *3*, 53-58.

Ravandi, F. (2004). Arsenic trioxide: expanding roles for an ancient drug? Leukemia *18*, 1457-1459.

Rösch, F., and Knapp, F. F. (2003). Radionuclide generators. In Handbook of Nuclear Chemistry, A. Vertés, S. Nagy, Z. Klencsár, and F. Rösch, eds. (Kluwer Academic Publishers), pp. 81-118.

Rösch, F., Novgorodov, A. F., and Brockmann, J. (2002). Offenlegungsschrift DE 100 28 056 A 1. In Deutsches Patent- und Markenamt (Deutschland).

Schindewolf, U., and Irvine, J. W. (1958). Preparation of carrier-free Vanadium, Scandium and Arsenic Activities from Cyclotron Targets by ion exchange. Anal Chem *30*, 906-907.

Shen, Z. X., Chen, G. Q., Ni, J. H., Li, X. S., Xiong, S. M., Qiu, Q. Y., Zhu, J., Tang, W., Sun, G. L., Yang, K. Q.*, et al.* (1997). Use of arsenic trioxide (As2O3) in the treatment of acute promyelocytic leukemia (APL): II. Clinical efficacy and pharmacokinetics in relapsed patients. Blood *89*, 3354-3360.

Shriver, D. F., Atkins, P. W., and Langford, C. H. (1997). Inorganic Chemistry (Weinheim; New York, Wiley-VCH).

Smith, J. D. (1973). Arsenic, Antimony and Bismuth. In Comprehensive Inorganic Chemistry, Trotman-Dickenson, ed. (New York, Compendium Publishers).

Sweet, W. H., and Brownell, G. L. (1955). Localization of intracranial lesions by scanning with positron-emitting arsenic. J Am Med Assoc *157*, 1183-1188.

The U.S. Geological Survey Workshop on arsenic in the environment (2004), available at wwwbrr.cr.usgs.gov/Arsenic/

Wang, Z. Y. (2001). Arsenic compounds as anticancer agents. Cancer Chemother Pharmacol *48 Suppl 1*, S72-76.

Ward, T. E., Swindle, D. L., Wright, R. J., and Kuroda, P. K. (1970). Radiochemical procedure for arsenic and germanium. Radiochimica Acta *14*, 70-72.

Wilcke, O. (1965). [Scintigraphy of brain tumors]. Radiologe *5*, 393-400.

Wilcke, O. (1965). [The diagnosis of brain tumors using isotopes]. Nervenarzt *36*, 508-514.

Wilcke, O., and Brock, M. (1965). [Positrocephalography. Results in 1,400 cases. Comparative study with angiography, pneumoencephalography and electroencephalography]. Arq Neuropsiquiatr *23*, 261-270.

Zhu, J., Chen, Z., Lallemand-Breitenbach, V., and de The, H. (2002). How acute promyelocytic leukaemia revived arsenic. Nat Rev Cancer *2*, 705-713.

Zhu, J., Koken, M. H., Quignon, F., Chelbi-Alix, M. K., Degos, L., Wang, Z. Y., Chen, Z., and de The, H. (1997). Arsenic-induced PML targeting onto nuclear bodies: implications for the treatment of acute promyelocytic leukemia. Proc Natl Acad Sci U S A *94*, 3978-3983.

Zhu, J., Lallemand-Breitenbach, V., and de The, H. (2001). Pathways of retinoic acid- or arsenic trioxide-induced PML/RARalpha catabolism, role of oncogene degradation in disease remission. Oncogene *20*, 7257-7265.

Zhu, J., Okumura, H., Ohtake, S., Nakamura, S., and Nakao, S. (2003). Arsenic trioxide induces apoptosis in leukemia/lymphoma cell lines via the CD95/CD95L system. Oncol Rep *10*, 705-709.

Zingaro, R. A. (1994). Arsenic: Inorganic and Organoarsenic Chemistry. In Encyclopedia of Inorganic Chemistry, R. B. King, ed. (John Wiley&Sons), pp. 192-219.

IV.

Macroscopic Syntheses of Arsenoorganic Precursors and first no-carrier-added Radioarsenic Labelling

Conference Proceeding of the 15th International Conference of Radiopharmaceutical Chemistry, Sydney, Australia.

Macroscopic Syntheses of arsenoorganic Precursors and first no-carrier-added radioarsenic labelling

M. Jennewein, R. Schirrmacher, S. Maus, F. Rösch

Institute of Nuclear Chemistry, University of Mainz, D-55128 Mainz, Germany.

Keywords: arsenic, precursor, mercaptanes

The long-lived ^{72}As represents an interesting positron emitter with potential for PET. A new $^{72}Se/^{72}As$-generator based on solid phase extraction techniques delivers no-carrier-added (nca) AsI_3 [1,2]. The subsequent step for the future labelling of biomolecules with radioactive arsenic isotopes is to synthesize a small precursor molecule based on AsI_3 by inhibiting binding sites of two of the arsenic in oxidation state +III with a very stable compound while one binding site remains for coupling to a biomolecule, e.g. via nucleophilic substitution. This work describes the macroscopic and nca syntheses of dimercapto arsenic iodides and diphenyl arsenic iodides.

To simulate the behaviour of ^{72}As, ^{77}As was used as produced at the TRIGA reactor at the University of Mainz via following reaction:

$$^{nat}Ge(n,\gamma)^{77}Ge(T_{1/2}=11.3\ h) \xrightarrow{\beta^-} {}^{77}As(T_{1/2}=38.8\ h).$$

Synthesis of dimercapto arsenic iodides:

147.90 mg AsI_3 (0.325 mmol) are dissolved in 5 ml anhydrous dichloromethane. The mixture is stirred under argon, cooled with liquid nitrogen and protected against light. An equimolar amount of a dimercapto compound and 51.3 µl pyridine (0.65 mmol) are added. The mixture is then allowed to warm up and stirred for 1 hour at room temperature. Formed pyridinium salts are removed via filtration. FD-MS is performed directly with this solution. To isolate the solid yellow products, the solvent is removed in an Ar-stream.

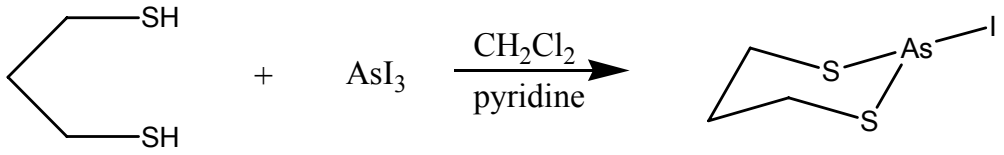

FIGURE 1. Reaction scheme for the synthesis of 1,3-dimercaptopropyl arsenic iodide

Synthesis of diphenyl arsenic iodide:

1 g diphenyl mercury (2.82 mmol) is dissolved in 15 ml toluene and is heated up to 60°C under stirring. 1.28 g arsenic triiodide (2.82 mmol) are suspended in 15 ml toluene and added dropwise. The mixture is refluxed for 1 h at 130°C. FD-MS is performed directly with this solution. To further prove their existence they have been derivatized to stable compounds.

The nca synthesis of dimercapto arsenic and diphenyl arsenic iodides was performed according to the procedures above, using nca $^{77}AsI_3$. The radiochemical yield of the nca synthesis is above 99%. Thus, two types of arsenoorganic precursors could be synthesized for future labelling experiments. As instable reactive intermediates, they could only be analyzed by FD-MS.

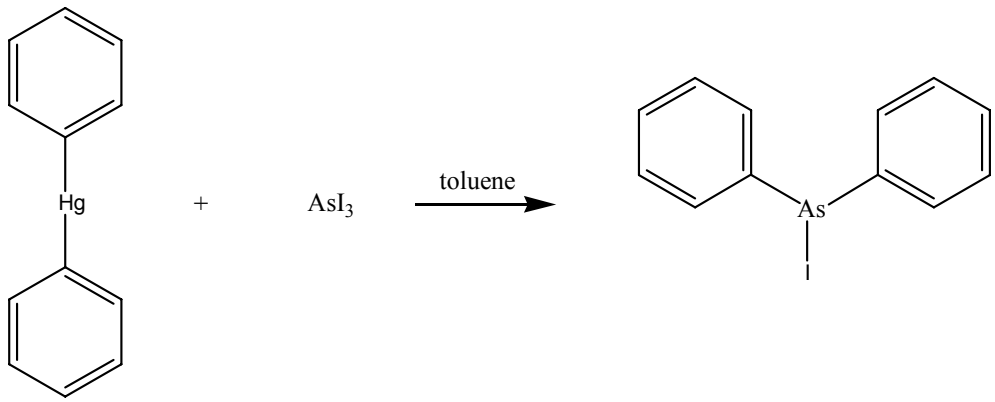

FIGURE 2. Reaction scheme for the synthesis of diphenyl arsenic iodide

References:

[1] Novgorodov AF, Schmidt A, Brockmann J, Qaim SM, Rösch F, *J Lab Comp Radiopharm* Supplement 1, 2001; 44: 778-780

[2] Phillips DR, Hamilton VT, Taylor MD, Farnham AM, Emran AM, Rowe RW, Pattel D, *Radioact Radiochem* 1992; 3: 53-58

[3] Blicke FF et al., *J Am Soc* 1929; 51: 3479-3481

Financial support of the Boehringer Ingelheim Foundation is gratefully acknowledged.

V.

Synthesis of 1,3-Dimercaptopropyl arsenic-Boc-Cysteine-O-Bzl and Diphenyl arsenic-Boc-Cysteine-O-Bzl and first labelling experiences

Conference Proceeding of the 15th International Conference of Radiopharmaceutical Chemistry, Sydney, Australia.

Synthesis of 1,3-Dimercaptopropyl arsenic-Boc-Cysteine-O-Bzl and Diphenyl arsenic-Boc-Cysteine-O-Bzl and first radioarsenic labelling

M. Jennewein, R. Schirrmacher, S. Maus, F. Rösch

Institute of Nuclear Chemistry, University of Mainz, D-55128 Mainz, Germany.

Keywords: arsenic, cysteine, mercaptanes

The long-lived ^{72}As represents an interesting positron emitter with potential for PET. The amino acid cysteine was chosen as a first molecule, suitable for labelling with no-carrier-added (nca) arsenic isotopes as delivered from a new ^{72}Se/^{72}As-generator-system, based on solid-phase extraction [1]. Because cysteine is SH-functionalized, a high affinity to arsenic and formation of stable covalent bonds is expected. The amino acid cysteine is involved in peptide biosynthesis. The protein synthesis rate increases in tumor growth, and hence, it should be possible to use either ^{72}As-cysteine for the diagnosis of tumor processes with long biological half-lives via PET, or ^{77}As-cysteine for therapeutic treatment of some tumor sorts.

To simulate the behaviour of nca ^{72}As, nca ^{77}As was used as produced at the TRIGA reactor at the University of Mainz via following reaction:

$$^{nat}Ge(n,\gamma)^{77}Ge(T_{1/2}=11.3\ h) \xrightarrow{\beta^-} {}^{77}As(T_{1/2}=38.8\ h)$$

S-1,3-dimercaptopropylarsenic-N-tert-butyloxycarbonyl cysteine benzyl ester:

100 mg (0.32 mmol) 1,3-dimercaptopropylarsenic iodide are synthesized according to [1] and without further purification 95 mg (0.32 mmol) of N-tert-butyloxycarbonyl cysteine benzyl ester and 25 µl pyridine (0.32 mmol) are added at T= 0°C. The mixture is stirred for 30 min at room temperature and is then washed with water to give a pale yellow liquid after filtration. Solvent is removed in vacuo giving 47 mg of oily product (30% yield).

Diphenylarsenic-N-tert-butyloxycarbonyl cysteine benzyl ester:

330 mg (0.94 mmol) diphenylarsenic iodide are synthesized according to [1] and without further purification 293 mg (0.94 mmol) N-tert-butyloxycarbonyl cysteine benzyl ester and 75 µl pyridine are added at T=0°C. The mixture is stirred vigorously for 10 min and is then allowed to warm up to room temperature. Ice is added and after phase separation, the organic layer is 3 times extracted with water. Solvent is removed in vacuo giving 340.5 mg of oily product (69% yield).

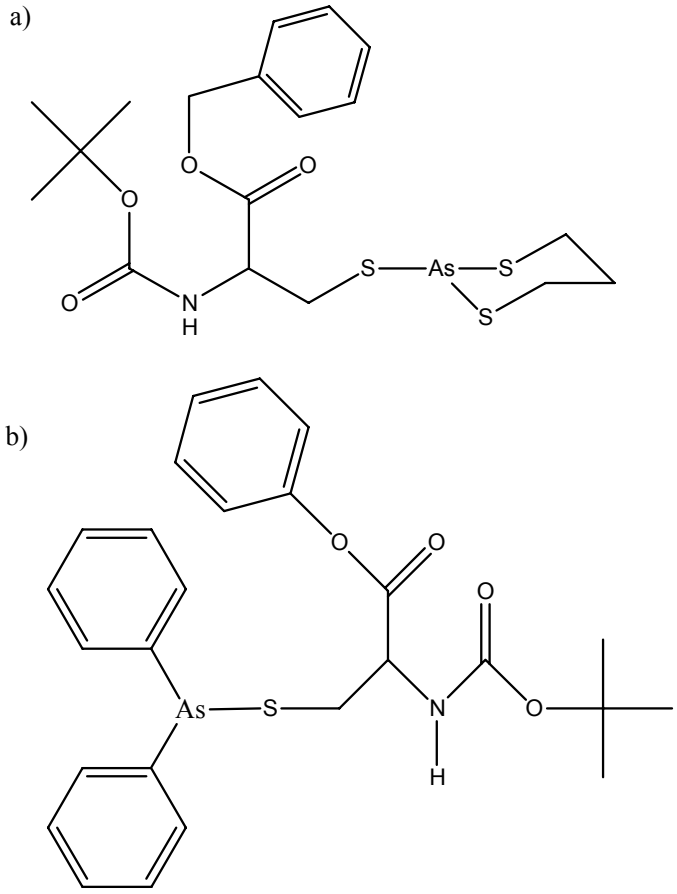

FIGURE 1. a) S-1,3dimercaptopropylarsenic-N-tert-butyloxycarbonylcysteine benzyl ester b) Diphenylarsenic-N-tert-butyloxycarbonyl cysteine benzyl ester

The products could be analyzed via FD-MS, ^{1}H- and ^{13}C-NMR. The synthesis of nca dimercapto arsenic and diphenyl arsenic cysteines was performed according to the procedures above, using nca $^{77}AsI_3$ giving radiochemical yields more then 60 % each.

References:

[1] Jennewein M, Maus S, Qaim SM, Brockmann J, Rösch F, *Annual Report 2002*, Institute of Nuclear Chemistry, University of Mainz, Germany

Financial support of the Boehringer Ingelheim Foundation is gratefully acknowledged.

VI.

Vascular imaging of solid tumors in rats with a radioactive arsenic-labeled antibody that binds anionic phospholipids

Vascular imaging of solid tumors in rats with a radioactive arsenic-labeled antibody that binds anionic phospholipids

[1,2]Marc Jennewein, [2]Matthew Lewis, [2]Dawen Zhao, [2]Vikram Kodibagkar, [2]Edward Tsyganov, [2]Nikolai Slavine, [2]Serguei Seliounine, [4]Alex Hermanne, [2]Ralph P. Mason, [1]Frank Rösch, [5]Jin He and [5]Philip E. Thorpe

[1]Institute of Nuclear Chemistry, Johannes Gutenberg-University of Mainz, Fritz-Strassmann-Weg 2, 55128 Mainz, Germany
[2]Department of Radiology, University of Texas Southwestern Medical Center at Dallas, Dallas, Texas, USA
[4]VUB Cyclotron, University of Brussels, Laarbeeklaan 103, 1090 Brussels, Belgium
[5]Department of Pharmacology and Simmons and Hamon Cancer Centers, University of Texas Southwestern Medical Center at Dallas, Dallas, Texas, USA

Running title:
Targeting anionic phospholipids on tumor vessels

Key words:
tumor microcirculation and microenvironment, new targets, phosphatidylserine, radioactive arsenic, PET

This work was conducted with the support of a grant from the Gillson-Longenbaugh Foundation, a SPORE grant in lung cancer research, a sponsored research agreement with Peregrine Pharmaceuticals Inc (Tustin, CA), the Boehringer Ingelheim Fonds for Basic

Research in Biomedicine, the Deutsche Forschungsgemeinschaft (DFG-Grant Ro 985/17) and the NCI P2O PRE-ICMIC CA086334.

Address correspondence to:
Philip E. Thorpe, Department of Pharmacology and Simmons and Hamon Cancer Centers, University of Texas Southwestern Medical Center at Dallas, 2201 Inwood Road NC7.304, Dallas, Texas 75390-8594, USA. Phone: (214) 648-1268; Fax: (214) 648-1613; E-mail: Philip.Thorpe@utsouthwestern.edu

Nonstandard abbreviations used:
PS, phosphatidylserine; PI, phosphatidylinositol; PA, phosphatidic acid; CL, cardiolipin; PE, phosphatidylethanolamine; PC, phosphatidylcholine; SM, sphingomyelin; HRP, horseradish peroxidase; i.p., intraperitoneal(ly); s.c., subcutaneous(ly); APTT, activated partial thromboplastin time; PT, prothrombin time; TGF-β, transforming growth factor-β; VEGF, vascular endothelial cell growth factor; APS, anti-phospholipid syndrome.

Abstract

Purpose: We recently reported that anionic phospholipids, principally phosphatidylserine, become exposed on the external surface of viable vascular endothelial cells in tumors, possibly in response to oxidative stresses present in the tumor microenvironment. In the present study, we tested the hypothesis that a monoclonal antibody directed against anionic phospholipids and labeled with radioactive arsenic isotopes can be used for the vascular targeting and molecular imaging of solid tumors in rats *in vivo*.

Experimental design: A new chimeric IgG_3 monoclonal antibody, ch3G4 (Tarvacin®), directed against anionic phospholipids was raised. A method for the labeling of antibodies with radioactive arsenic isotopes was developed and the radioarsenic labeled antibody was tested for its ability in terms of localization to tumor vessels and imaging qualities.

Results: The mab ch3G4 recognized anionic phospholipids on the external membrane of Dunning prostate R3327 solid tumors in male Copenhagen rats. The tumors could be imaged with planar scintigraphy techniques and with Positron Emission Tomography *in vivo*, showing excellent and antigen-specific localization. In addition, the experiments proved the concept of the radiochemical separations applied and the developed labeling chemistry and demonstrated the potential benefits of the use of arsenic radioisotopes for molecular imaging of antibodies.

Conclusion: The mab ch3G4 localized specifically to anionic phospholipids on the surface of vascular endothelial cells in Dunning prostate tumors in rats. The biomedical use of radioactive arsenic isotopes was exemplified for the first time in a multi-modality molecular imaging approach *in vivo*.

1. Introduction

Vascular targeting agents (VTAs) for the treatment of cancer are designed to cause selective shutdown of pre-existing tumor blood vessels [1]. VTAs can result in tumor cell death by indirect means ("starving" the tumor cells of their blood supply) and may therefore be effective against tumors which are resistant to conventional anti-proliferative chemotherapy [2, 3]. This is in contrast with antiangiogenic drugs that are designed to inhibit the formation of new vessels, but have no effect on the existing tumor vasculature. VTAs may show enhanced therapeutic benefit when combined with chemotherapeutic agents, radiation or hyperthermia [1, 4].

We have developed a new type of VTA that represents an unconjugated, or 'naked', monoclonal antibody directed against anionic phospholipids, principally phosphatidylserine (PS). PS, which is the most abundant anionic phospholipid of the plasma membrane, is tightly segregated to the internal surface of the plasma membrane in most cell types, including the vascular endothelium [5, 6]. Phosphatidylinositol (PI), another major anionic phospholipid, is also situated predominantly on the internal surface of the plasma membrane [7]. The minor anionic phospholipid, phosphatidic acid (PA), has been examined in very few cell types but also appears to be expressed predominantly intracellulary [8]. PS asymmetry is maintained by an ATP-dependent aminophospholipid translocase (a Mg^{2+} - ATPase) that catalyzes the transport of aminophospholipids from the external to the internal leaflet of the plasma membrane[9]. Loss of PS asymmetry occurs during apoptosis [10], necrosis [11], cell activation [12] and transformation [13], resulting in the exposure of PS on the external surface of the cells. PS exposure occurs when the aminophospholipid translocase becomes inhibited [14] or when transporters such as scramblase [15] and the ABC-1 floppase [16] become activated by Ca^{2+} fluxes into the cytosol [17].

We previously demonstrated that anionic phospholipids become exposed on the vascular endothelium of blood vessels in mice bearing various types of solid tumors [18, 19]. This was shown by generating a rat IgM monoclonal antibody, 9D2, directed against anionic phospholipids and administering it i.v. to the mice. 9D2 localized specifically to 15 – 40% of blood vessels in various tumors. The distribution of 9D2 was indistinguishable from that of Annexin A5, which also binds to PS [19]. Since the vascular endothelium in normal tissues did not stain, PS is considered to be a specific marker of the tumor vasculature. PS-expressing tumor endothelial cells appear to be viable. Those cells lack

markers of apoptosis (active caspase-3, TUNEL), are morphologically intact and metabolically active, and the vessels are functional at transporting blood and solutes [19]. Hypoxia/reoxygenation, acidity, thrombin, inflammatory cytokines and reactive oxygen species all induced PS exposure on vascular endothelial cells *in vitro*, suggesting that stress conditions in the tumor microenvironment may be responsible for inducing PS exposure on viable endothelium [19]. Stress conditions may generate Ca^{2+} fluxes in the tumor vascular endothelium that activate scramblase or ABC-1 floppase or inhibit aminophospholipid translocase [20]. Alternatively, sphingomyelinase might be activated to generate ceramide, which facilitates transbilayer lipid translocation [21].

These answers to the question on what the molecular basis and mechanisms of binding of specific mabs to PS are stimulate a new question: Might those mab be modified in terms of potential molecular imaging *in vivo*? Among the molecular imaging modalities relevant to this aim, quantitative PET might be an excellent choice. Smith-Jones et al. [22] already demonstrated the use of PET for the molecular imaging of small antibody fragments. However, because of the long-term metabolism of the whole antibody, their concept of labeling the mab with ^{68}Ga ($T_{1/2}$ = 68 min) is not feasible in our case.

Arsenic provides several radioisotopes of interest for medical or environmental application, including the positron emitters ^{72}As and ^{74}As, which are excellent candidates for the imaging of longer lasting biological processes (cf. Table 1).

Property	^{71}As	^{72}As	^{73}As	^{74}As	^{76}As	^{77}As
$T_{1/2}$ [d]	2.7	1.1	80.3	17.8	1.1	1.6
Mode of decay (%)	EC (70) β^+ (30)	EC (12.2) β^+ (87.8)	EC (100)	EC (66) β^+ (29)	β^- (100)	β^- (100)
Most abundant γ-lines [keV]	175.0 (82.0 %)	834.0 (79.5 %) 629.9 (7.9 %)	53.4 (10.0 %)	595.8 (59.0 %) 634.8 (15.4 %)	559.1 (45.0 %) 657.1 (6.2 %)	239.0 (1.6 %) 520.6 (0.5 %)
Positron-energy [keV]	Mean: 350	Mean: 1117		Mean: 440		

TABLE 1. Decay data of the most relevant arsenic isotopes [69]

In addition, the recent increasing interest in the element arsenic in environmental sciences [23], toxicology [24] and carcinogenesis [25, 26] and medicine [27-35], stimulates a need to develop convenient and reproducible methods to trace this element and its compounds in subtoxic and subpharmaceutical concentrations.

A number of approaches to develop an easy and practical system to separate these isotopes from cyclotron or reactor irradiated germanium or germanium oxide targets have been described [36-40]. In addition, we previously developed strategies towards a versatile radioarsenic labelling chemistry to generate arsenic isotopes in chemical forms suitable for future application in labelling chemistry, radiopharmacy and, ultimately, for molecular imaging using Positron Emission Tomography (PET).

In the present study, we tested the hypothesis that a monoclonal antibody directed against anionic phospholipids and labeled with radioactive arsenic isotopes can be used for charesteristic vascular targeting in vitro and ex vivo and for the molecular imaging of solid tumors in rats *in vivo*. For this purpose, a chimeric IgG_3 monoclonal antibody, ch3G4, against anionic phospholipids was raised and labeled with radioactive arsenic isotopes. Radioarsenic labeled ch3G4 localizes to tumor vessels specifically and demonstrates the first use of radioactive arsenic isotopes for molecular imaging *in vivo*.

2. Materials and Methods

Animal care

Experiments were carried out under a protocol approved by the UTSW Institutional Animal Care and Use Committee and followed institutional guidelines for the proper and human use of animals in research.

Materials

Germanium(IV)oxide (99.9999 % grade, PURA TREM) was purchased from Strem Chemicals Inc.. Concentrated hydrofluoric acid (48 %) and potassium iodide were purchased from Aldrich. BOND ELUT ENV solid phase extraction cartridges with a sorbent mass of 50 mg and a volume of 1 ml were purchased from Varian.

Antibodies

Hamster anti-mouse CD31, rat anti-mouse CD31, rat anti-mouse Ly-6G (Gr-1), hamster anti-mouse Ly-49C, F, H and I, rat anti-mouse CD11b (M1/70, Mac-1, integrin α_M-chain, complement receptor CR3), hamster anti-mouse CD11c (integrin α_x-chain) and rat anti-mouse FcγIII/II receptor (CD16/CD32) monoclonal antibodies were from BD Pharmingen (San Diego, CA). Monoclonal rat anti-mouse F4/80 was from Serotec Inc., (Raleigh, NC). All secondary mabs were from Jackson Immunoresearch Labs (West Grove, PA). A hybridoma secreting monoclonal mouse IgG_3, κ antibody (23.8.34.24; HB-10113) against a Babesia bovis antigen was obtained from the American Type Culture Collection (Rockville, MD) and this monoclonal antibody is referred to herein as BBG3. Rituximab (MabThera®, CD20) was purchased from Roche.

Isotopes

^{74}As is a positron emitting isotope with a long half-life of $T_{1/2}$= 17.8 d. It has a positron emission rate of 29 % with an extreme low positron energy of E_{β^+mean} = 128 keV, providing high local resolution when measured via PET and an electron emission rate of 34.2 % and E_{β^-mean} = 137 keV [41]. It was one of the first isotopes used for very preliminary forms of PET in the 1950s and 1960s [42-47] called positrocephalography in

those times. Due to its half-life it will be more appropriate for animal use than human use, but as well could provide a useful tool for the study of long lasting metabolic processes, like antibody-antigen interaction or in general long term pharmacokinetics of developmental drugs. ^{74}As can be produced best by the ^{74}Ge(p,n)^{74}As or ^{73}Ge(d,n)^{74}As reaction at a small-sized cyclotron. Excitation functions and target yields are described in detail in [36]. ^{74}As was produced by the ^{nat}Ge(p,x)^{74}As reaction [E_p= 20 MeV, 3 h irradiation at 15 µA] giving a yield of about 370 MBq at the VUB Cyclotron at the University of Brussels, Belgium.

^{77}As is an 100% electron emitting isotope with a half-life of $T_{1/2}$= 1.6 d and $E_{\beta^- mean}$ = 226 keV. This isotope could be of future use for an endoradiotherapeutic arsenic based radiopharmaceutical. ^{77}As can be produced at nuclear reactors via the ^{nat}Ge(n,γ)^{77}Ge reaction. ^{77}Ge decays to ^{77}As with a half-life of 11.3 h. It was produced in nca state via the ^{76}Ge(n,γ)^{77}Ge, $T_{½}$ = 11.30 h → β^- → ^{77}As processes at the TRIGA reactor of the Nuclear Engineering Teaching Laboratory of the University of Texas at Austin (Φ = 4.0 x 10^{13} n/cm^2·s).

All nuclear reactions were performed on 100 mg of $^{nat}GeO_2$.

Radiochemical Separations

Irradiated germanium oxide targets were dissolved in 5 ml $HF_{conc.}$ at room temperature for 1 h. Subsequently, potassium iodide was added up to 10 mg/ml $HF_{conc.}$ and stirred for 10 minutes. The mixture was transferred to an ENV-solid phase extraction cartridge. Cartridge-holder and fittings to standard size syringes were homemade in the machine-shop of the Institute of Nuclear Chemistry, University of Mainz. The ENV cartridge was preconditioned with 5 ml of MeOH, 5 ml H_2O and 5 ml $HF_{conc.}$ containing sodium iodide in the concentration of 1 mg/ml. Nca [*As]AsI_3 was fixed to the solid phase, while macroscopic $[GeF_6]^{2-}$ was eluted quantitatively with the mobile phase. After the fixation of [*As]AsI_3, excessive $HF_{conc.}$ was removed with a high pressure nitrogen-flow over the cartridge for 5 min. The elution was performed with 500 µl ethanol. The solution was concentrated to 50 µl under a slight N_2-flow at T = 70 °C immediately before the subsequent labeling procedure.

Antibody Conjugation and Testing

Antibodys were SATA-modified according to the protocol of Pierce Endogen [48, 49]. The deprotection of the sulfhydryl groups of the mab was performed directly before the labelling. 100 µg of the SATA-modified antibody in 3 ml PBS at pH=7.5 then were combined with the nca [*As]AsI_3 solution at 37°C for 30 minutes. Quality control was performed by HPLC, using an Agilent 1100 Series HPLC system, with an LDC/Milton Roy UV-Monitor III at 254 nm and a 'Gabi' NaI-radiation Monitor from Raytest. The HPLC column was a Bio-Silect Sec 250-5, 300x7.8 mm and PBS + 0.01M NaN_3 was used as solvent.

***In vitro* Stability**

In vitro stability of the radioarsenic labeled ch3G4 was tested via incubation in fetal bovine serum (FBS) and HPLC measurements at various timepoints up to 72 h. 10 µg of radioarsenic labeled ch3G4 in 50 µl PBS were combined with 500 µl FBS and incubated at T= 37 °C. Aliquots of 50 µl were taken at t=30 min, 24, 48, and 72 h, diluted with 200 µl water and 20 µl were taken for HPLC under the conditions described above.
The Immunoreactivity was tested with an ELISA of ^{77}As[SATA]ch3G4, using unlabelled and unmodified ch3G4 as positive control and ^{77}As[SATA]Rituxan as negative control.

Growth of tumors

For subcutaneous tumor studies, 2×10^7 Dunning prostate R3327 cancer cells [50, 51] were injected s.c. into the right flank of male Copenhagen rats (Charles River, Wilmington, MA) to create a donor animal. To induce tumors in following animals, small tumor pieces, excised from the donor animal, were implanted subcutaneously in the right thigh of the rat and allowed to grow to the size of 9-13 mm diameter.

Biodistribution studies

Tumor bearing rats were injected, via the lateral tail vein, with either 185 kBq of ^{74}As[SATA]ch3G4 or ^{74}As[SATA]Rituxan in 500 µl of PBS (pH 7.4, 1 mMol EDTA).

Groups of animals were sacrificed by exsanguination and perfusion via cardiac puncture under general anaesthesia, after 48 h or 72 h post injection and major organs and tumors were collected. These samples were weighed and counted, with appropriate standards, in an automatic NaI(Tl) counter. These relative-activity data (c.p.m.) are background corrected and expressed as a percentage of the injected dose per gram (% ID/g).

In addition, tumors were cut in 1 mm slices and used for planar imaging.

Imaging

Planar imaging studies

3 animals were injected with 5 MBq of ^{74}As[SATA]ch3G4 in 500 µl of PBS (ph 7.4, 1 mMol EDTA) in the tail vein. The animals were sedated using Isoflurane (Baxter Healthcare) and imaged planar on a 25.2x30.3 cm Fuji CR ST-VN Imaging Plate (Fuji Photo Film, Tokyo) with 15 min exposure time at 24 h, 30 min at 48 h and 1 h at 72 h. The photostimulable plates were read on a Molecular Dynamics Storm (Amersham Biosciences) scanner and ROIs drawn around the tumors and major other areas for quantification.

In a second study, 4 animals were injected with 1 MBq of each ^{77}As[SATA]ch3G4 and ^{77}As[SATA] Rituxan and imaged as described above.

In a third study, 1 mm slices of tumors from the other studies were imaged with an exposure time of 12 h, as described above.

PET studies

The PET studies were performed on a self-developed Small Animal Imaging (SAI) PET system built in the Advanced Radiological Sciences Division of the University of Texas Southwestern Medical Center at Dallas, which allows images in sub-millimeter spatial resolution. Four animals were injected with 10 MBq of ^{74}As[SATA]ch3G4 in 500 µl of PBS (pH 7.4, 1 mMol EDTA) in the tail vein. The animals were sedated using Isoflurane (Baxter Healthcare) and imaged with the Small Animal PET camera at 24, 48 and 72 h after injection. Coincident data were collected for the 511 keV gamma rays with a 250-750 keV window for 2 h. The SAI comprises two plastic fiber scintillator detectors, the position

sensitive photo multiplier tube (PSPMT) light sensors, PET coincidence trigger electronics, and a custom-built FADC crate to digitize detector signals. The images were reconstructed using the maximum Likelihood - Expectation Maximization (ML-EM) algorithm [52] for 3D reconstruction algorithm and the animals were sacrificed by exsanguination and perfusion via cardiac puncture under general anaesthesia and major organs and tumors were collected and counted in a gamma counter with a known sample of the %ID.

MRI studies

T1 weighed spin- echo MR images were obtained to show the underlying anatomy. The images were acquired with a TR/TE = 450/14 ms. The acquisition matrix was 128X256 zero-filled to 512X1024. The field of view was 10 cm X 20 cm with a slice thickness of 1mm. MRI was performed on rats with simultaneously implanted tumors with same size, weight and tumor size and tumor in the same position and orientation as in the PET or planar scintigraphy imaging studies.

Reactivity of ch3G4 antibody with plastic-immobilized phospholipids

Phospholipids were dissolved in *n*-hexane to a concentration of 50 μg/ml. 100 μl of this solution was added to wells of 96-well microtiter plates. After evaporation of the solvent in air, the plates were blocked for 2 h with 1% BSA diluted in PBS (binding buffer). 3G4 antibody was diluted in the binding buffer at an initial concentration of 33 nM. Serial two-fold dilutions were prepared in the plates (100 μl per well). The plates were then incubated for 1 h at room temperature. After washing with PBS, HRP goat anti-human IgG (diluted 1:2000) was used to detect ch3G4. Secondary reagents were detected by using chromogenic substrate OPD followed by reading plates at 490 nm using a microplate reader (Molecular Devices, Palo Alto, CA).

Detection of localized ch3G4 in tumor bearing rats *in vivo*

Groups of two male Copenhagen rats (200 gram weight) bearing s.q. AT1 tumors (1 cm diameter) were injected i.v. with 1 mg ch3G4 or control antibody (Rituxan®). 24h later, rats were anesthetized and their blood circulation was perfused with heparinized saline to clear it of free antibody as previously described. Organs and tumors were removed and

snap-frozen for preparation of cryosections. Sections were fixed with 4% paraformaldehyde/PBS and blocked with PBS containing 1% bovine serum albumin. To prevent loss of phospholipids during slide processing, detergents and organic solvents were omitted from blocking and washing buffers. Chimeric IgG was detected using biotinylated goat anti-human IgG followed by Cy2-streptavidin. Vascular endothelium was detected by mouse anti-rat CD31 antibody followed by Cy3-goat anti-mouse antibody (minimally reactive with rat serum). Tumor sections derived from rat injected with Rituxan® of irrelevant specificity served as negative controls. Single images, taken with appropriate filters for Cy2 (green) and Cy3 (red) fluorescence, respectively, were captured by digital camera and transferred to a computer. Images of 10 random fields (0.317 mm^2/field) were merged with the aid of Metaview software. When ch3G4 was bound to tumor endothelium, the green and red fluorescence often merged to give a yellow color. The percentage of vessels with localized ch3G4 was calculated.

3. Results

Labeling

As described previously in [53], nca *AsI_3 (* = 71, 72, 73, 74, 76, 77) could be ideal as a versatile labeling synthon for the coupling of radioactive arsenic isotopes to biomolecules. In this work, a new method for the labeling of monoclonal antibodies with radioactive arsenic isotopes via this labeling synthon was developed. Arsenic has a high affinity to sulphur and AsI_3 is able to bind covalently to sulfhydryl groups which could be shown on reference substances like cysteine and glutathione [54, 55]. In antibodies, sulphur is mainly bound to dithiol-bridges. To increase the number of free thiols, the antibodies were modified with SATA (N-succinimidyl S-acetylthioacetate). The amount of free thiol-groups per antibody-molecule was calculated to be 3.5 using Ellmann's reagent and cysteine based standards. To keep the thiols from forming disulfide bridges, all solutions used contained 1 mM EDTA. The coupling of nca *AsI_3 to the introduced free SH is illustrated in Fig. 1.

The quality control of the labeling was done using radio-HPLC using a size-exclusion column. No free *As was detectable. Labelling yields after 30 min labeling time in general were above 99.9 %.

The *in vitro* stability of the radioarsenic label was evaluated by incubating the radioarsenic labelled mab in serum, followed by HPLC characterization. No release of radioarsenic from the labelled mab and no formation of antibody fragments was observed for incubation times up to 72 h.

The immunoreactivity of the labelled ch3G4 could be demonstrated using ELISA. No inhibition of immunoreactivity following SATA-modification and subsequent labelling with nca *AsI_3 could be observed.

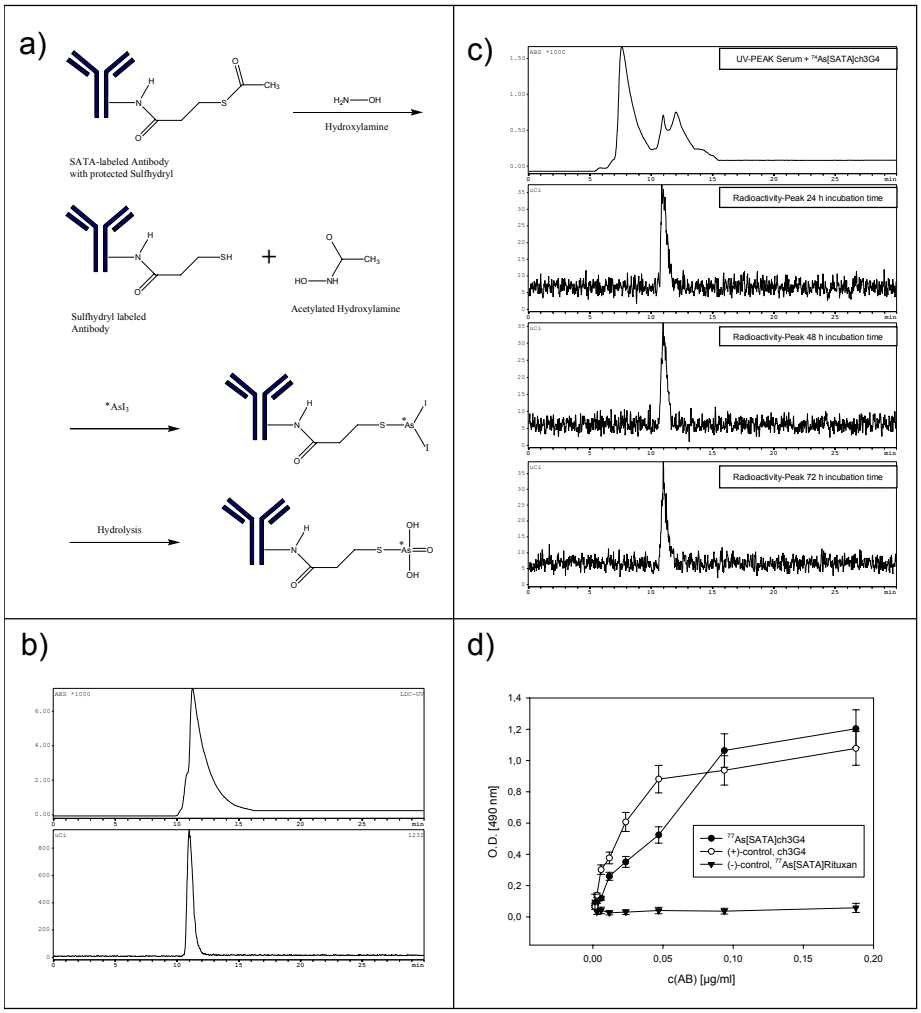

FIGURE 1.

a) Reaction scheme for the labelling of SATA-modified antibodies with radioactive arsenic isotopes. After deprotection of the sulfhydryl of the SATA-modified AB, the labeling is directly performed with nca *AsI_3 as labeling synthon. The *AsI_3 couples to one SH under elimination of HI, which can be catched by salts in the buffer solution. The 2 iodines remaining at the arsenic are hydrolysed and As appears to be oxidized to +V.

b) Quality Control of the labeling of ch3G4 with radioactive arsenic isotopes. After a labeling time of 30 min, an aliquot of 20 µl of the ^{74}As[SATA]ch3G4-solution was given over a size-exclusion column for radio-HPLC. The upper graph shows the UV-spectrum, the lower the corresponding radioactivity-progression. No free ^{74}As was detectable. Labelling yield is > 99.9 %.

c) *in vitro* stability of [^{74}As]SATA-ch3G4. *In vitro* stability was tested through incubation in serum following radio-HPLC of diluted aliquots after 24, 48 and 72 h. The upper graph shows the UV spectrum. Because of the low concentration of AB versus serum-proteins, we see a typical serum profile. The lower graph shows the corresponding radioactivity-progression. The radioactivity peak remains unchanged in position and peak area. The arsenic label stays stable for up to 72 h at the molecular mass of the AB.

d) Immunoreactivity. Immunoreactivity was tested with an ELISA of ^{77}As[SATA]ch3G4, using unlabelled and unmodified ch3G4 as positive control and ^{77}As[SATA]Rituxan as negative control. No reduction of immunoreactivity through the applied SATA-modification with subsequent radioarsenic labeling was detectable.

Biodistribution

Biodistribution studies were performed to confirm imaging results. Animals were perfused to clear the vasculature of blood and to be able to observate the targeting of tumor vascular endothelium. Whole body biodistribution was performed 48 and 72 h post injection and tumor/muscle and tumor/liver ratios were determined to reflect imaging qualities. Tumor uptake and tumor/background ratios were highest 72 h p.i. which is consistent with the imaging results. However, we observed a very high spleen uptake compared to liver uptake. It might be, that due to the SATA-modification of the antibody, inter-molecular disulphide bridges were formed during the labelling procedure, although this should have been prevented by the addition of EDTA to the labelling solutions. Conglomerates of a higher molecular mass than 150.000 g/mol for the AB are usually metabolized in the spleen.

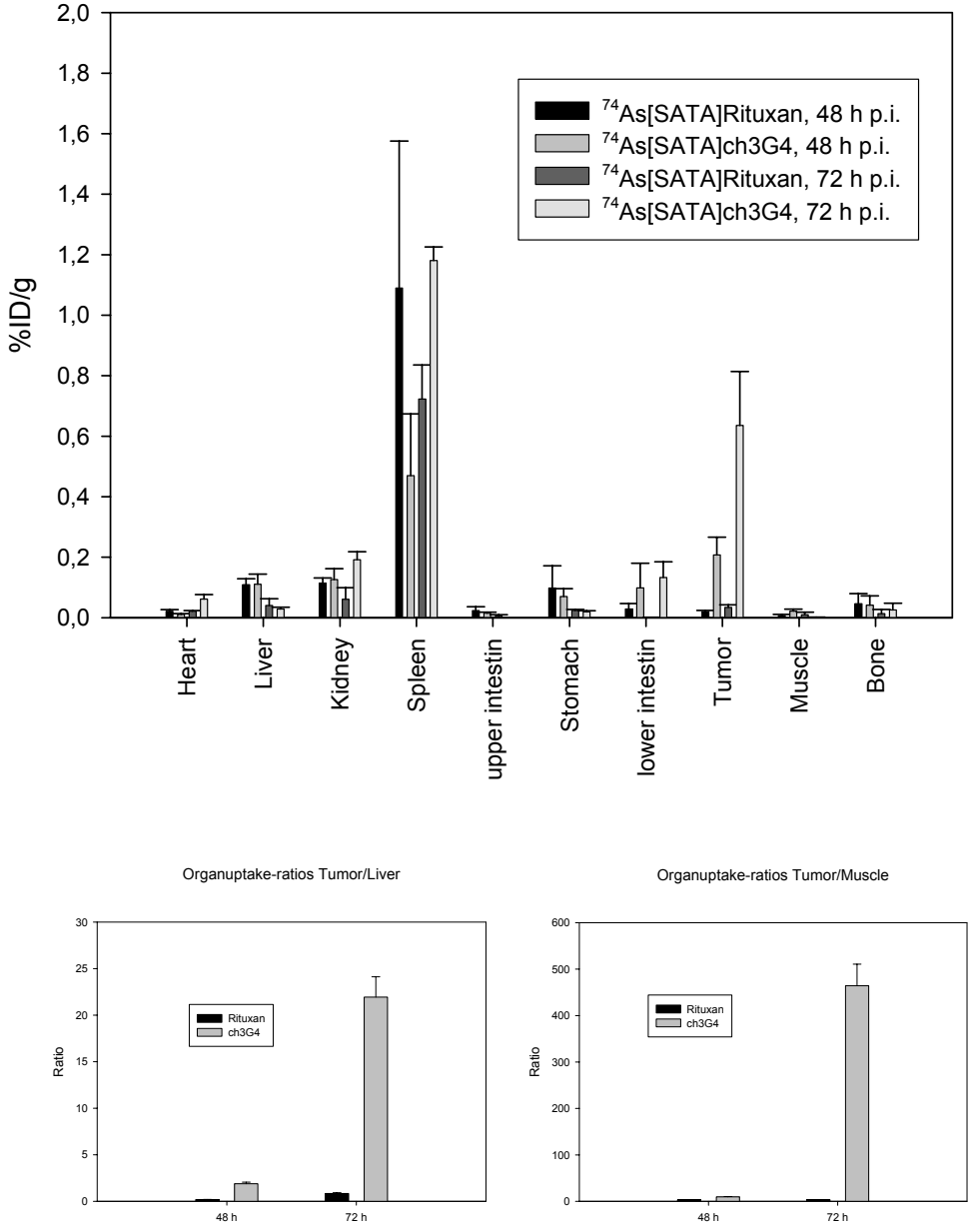

FIGURE 2.

Biodistribution

Tumor bearing rats were injected, via the lateral tail vein, with either 185 kBq of ^{74}As[SATA]ch3G4 or ^{74}As[SATA]Rituxan in 500 µl of PBS (pH 7.4, 1 mMol EDTA).

Groups of animals were sacrificed by exsanguination and perfusion via cardiac puncture under general anaesthesia, after 48 h or 72 h post injection. All major organs and tumors were collected. These samples were weighed and counted, with appropriate standards, in an automatic NaI(Tl) counter. These relative-activity data (c.p.m.) are background corrected and expressed as a percentage of the injected dose per gram (% ID/g).

Planar Imaging

The *in vivo* imaging of animals on photostimulable plates which can be read in standard molecular biology phosphor imaging scanners is certainly limited to processes close to the animal skin, such as subcutaneous tumors, as imaging quality and resolution decreases strongly with the distance from the plate. Nevertheless, for subcutaneously implanted tumors this technique could provide a useful qualitative high-troughput imaging tool. Fig. 3 shows images of a rat injected with 5 MBq of ^{74}As[SATA]ch3G4. The rat was imaged for 3 days every 24 h and the images were overlayed on MRI images of a rat with a matched tumor, for better visualization. At 24 h, the tumor is hardly distinguishable because of the high whole-body background. At 48 h, the mAb is clearly localized to the tumor, but also some blood pool in liver, heart, and other upper organs is visible. At 72 h the labeled mab has cleared from the blood and only the antigen-specific binding at the tumor is visible. It is also possible to see some heterogeneity in distribution inside of the tumor. This might be due to heterogeneity in vasculature, which is discussed in detail with the PET pictures. The imaging results presented are consistent with the *ex vivo* biodistribution data.

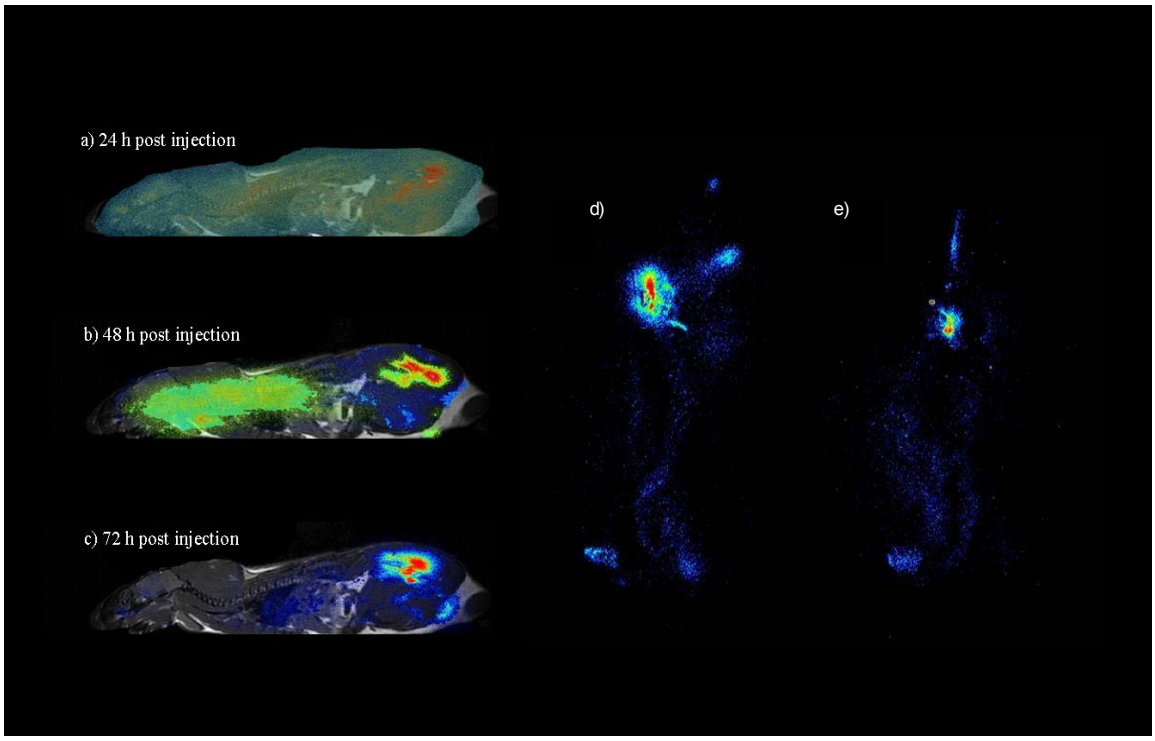

FIGURE 3.

Whole-Body Planar Scintigraphy.

a-c: Dunning prostate R3327 AT1 tumor bearing rats were injected with 5 MBq of ^{74}As[SATA]ch3G4 in 500 µl of PBS (pH 7.4, 1 mMol EDTA) in the tail vein and imaged planar on a 25.2x30.3 cm Fuji CR ST-VN Imaging Plate with 15 min exposure time at 24 h, 30 min at 48 h and 1 h at 72 h. The photostimulable plates were read on a Molecular Dynamics Storm (Amersham Biosciences) scanner and overlayed with representative Small Animal MRIs for better orientation. Whereas at 24 h p.i. no reasonable contrast to image the tumor could be achieved, due to the pharmacokinetics of mabs, at 48 h the tumor becomes clearly distinguishable. At 72 h, the tumor to background ratio is best, as almost all not antigen-bound ^{74}As[SATA]ch3G4 has cleared from the blood.

d-e: One series of Dunning prostate R3327 AT1 tumor bearing rats was injected with 3 MBq of ^{77}As[SATA]ch3G4 in 500 µl of PBS (pH 7.4, 1 mMol EDTA) and a second series with ^{77}As[SATA]Rituxan in 500 µl of PBS (ph 7.4, 1 mMol EDTA) as negative control in the tail vein and imaged planar on a 25.2x30.3 cm Fuji CR ST-VN Imaging Plate with 120 min exposition time at 72 h. Based on ROIs and integrating the ratio between antigen specific antibody and ch3G4 could determined to be > 8:1.

PET

10 MBq of ^{74}As[SATA]ch3G4 were injected in Dunning prostate R3327 AT1 tumor bearing rats. Fig. 4a-c shows representative images obtained with a Small Animal PET camera 48 h after injection in frontal, sagittal, and transversal orientation. The PET images were overlayed with Small Animal MRI Images of rats with same animal size and weight, tumor size, tumor localization and orientation after 3D reconstruction for better visualization. Fig. 4.d shows 1 mm slices through the AT1 tumor capsule after injection of 10 MBq of ^{74}As[SATA]ch3G4 48 h post injection and imaged with PET. The resolution reveals the heterogeneity of activity and therefore ch3G4 distribution in the tumor tissue, with less activity in the center of the tumor and more in the periphery. This reflects the histological structure of the tumor capsule, with viable tissue and dense vasculature in the circumferential tumor area and a core which is less well perfused and partly necrotic. After imaging, rats were sacrificed and tracer uptake was quantified by gamma-counting. The imaging results obtained by PET reflect very well the biodistribution and the data confirms the accuracy of PET imaging to noninvasively determine tumor tissue accumulation of ^{74}As-labelled PS-selective antibodies in the Dunning prostate R3327 tumor model.

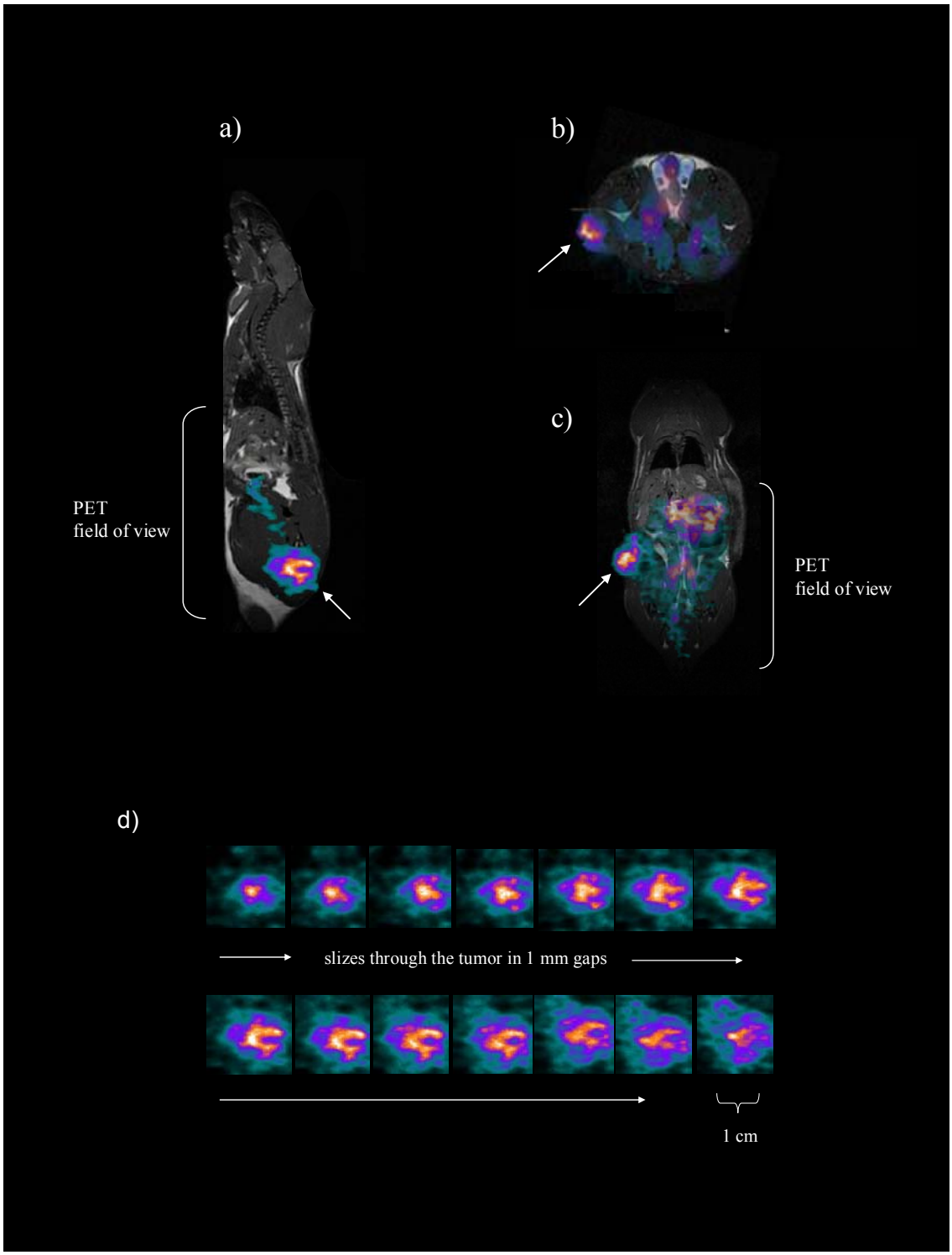

FIGURE 4.

Small Animal PET

a-c: Dunning prostate R3227 AT1 tumor bearing rats were injected with 10 MBq of ^{74}As[SATA]ch3G4 in 500 µl of PBS (ph 7.4, 1 mMol EDTA) in the tail vein. The graphic

shows representative images obtained with a Small Animal PET camera 48 h p.i. in frontal sagittal, and transversal orientation. The PET images were overlayed with Small Animal MRI Images of rats with same animal size and weight, tumor size, tumor localization and orientation after 3D reconstruction for better visualization.

d: The graphic shows 1 mm slices through a AT1 tumor capsule after injection of 10 MBq of ^{74}As[SATA]ch3G4 48 h post injection. The resolution allows to observe the heterogeneity of activity and therefore ch3G4 distribution in the tumor tissue, with less activity in the center of the tumor, but enrichment in the periphery. This reflects the histological structure of the tumor capsule, with viable tissue and dense vasculature in the circumferential tumor area and a core which is partly necrotic.

Selective localization of ch3G4 to tumor blood vessels in subcutaneous AT1 rat prostate tumors.

The ability of ch3G4 to localize selectively to tumor blood vessels in vivo was determined by injecting the antibody i.v. and exsanguinating the rats 24h later. Frozen sections of tumor and normal tissues were stained for the presence of human immunoglobulin. Sections were counterstained with anti-rat CD31 to detect vascular endothelium. The images were merged. Coincidence of staining between localized ch3G4 and CD31 was taken as evidence of specific localization. Coincident staining appeared yellow, unless dominated by a particularly intense green or red fluorescence in that region. The antigen specificity of vessel localization was confirmed by the lack of endothelial staining in tumors from rats injected with the isotype-matched control antibodies, Rituxan®.

ch3G4 localized to an average of 40 ± 10% of tumor blood vessels after i.v. injection into rats bearing s.q. AT1 prostate tumors. Labeled vessels were visible in all regions of the tumors, but were particularly abundant in and around regions of necrosis. Larger vessels sometimes had regions where the vascular endothelium was positive for localized ch3G4 and other regions where it was not, showing heterogeneity of PS exposure within a single vessel. Regions where ch3G4 had leaked into the tumor interstitium were also visible around the endothelium of some vessels.

Localization of ch3G4 to vascular endothelium in normal tissues was not observed in rats. Normal tissues examined were: heart, lung, liver, pancreas, kidney, spleen, brain and testis.

4. Discussion

The major findings to emerge from the present study are that a chimaeric monoclonal antibody, ch3G4, directed against anionic phospholipids localizes specifically to vascular endothelial cells in tumors in rats which could be shown via small animal PET of an radioarsenic labelled ch3G4.

ch3G4 localized specifically to tumor vessels and to tumor cells in and around necrotic regions of tumors after injection into rats bearing Dunning prostate R3327 AT1 tumors. An average of 40 ± 10% of vessels were bound by ch3G4. Staining patterns were similar to those found previously using 9D2 and annexin A5 [18]. Vascular endothelium in normal tissues was unstained. In this regard, ch3G4 differs from other antibodies that recognize tumor vessel markers. Most tumor vessel markers are present on vessels in the ovary, a site of physiological angiogenesis, or in the kidney and pancreatic islets where vessels have high permeability [1]. PS is likely to be the anionic phospholipid primarily detected by ch3G4. PS is the most abundant anionic phospholipid and the one whose exposure is best known to be regulated by environmental conditions or injury [6, 20]. However, we cannot exclude the possibility that other anionic phospholipids (PI, PA) contribute to the ch3G4 effects that we observe. As noted in our earlier study [18], the PS-positive tumor vessels in untreated mice appear to be intact and functional. They transport blood and are perfusible. The vascular endothelium of PS-positive vessels does not display markers of advanced apoptosis (active caspase 3, TUNEL), is morphologically intact and is metabolically active, as judged by co-expression of the rapidly turned over protein, VCAM-1. Prior evidence suggests that stress factors in the tumor microenvironment (hypoxia/reoxygenation, inflammatory cytokines, low pH) may induce PS exposure on viable tumor endothelium [18]. It is possible that reactive oxygen species (ROS) generated by tumor cells and neutrophils cause PS exposure [56-58]. The ROS may oxidize phospholipids or ion transporters and induce Ca^{2+} fluxes into the cytosol that cause externalization of PS. Indeed, peroxides have been shown to induce PS-exposure on viable endothelial cells *in vitro* by a mechanism that relates to glutathione oxidation and/or lipid peroxidation, not apoptosis [59].

FIGURE 5a.

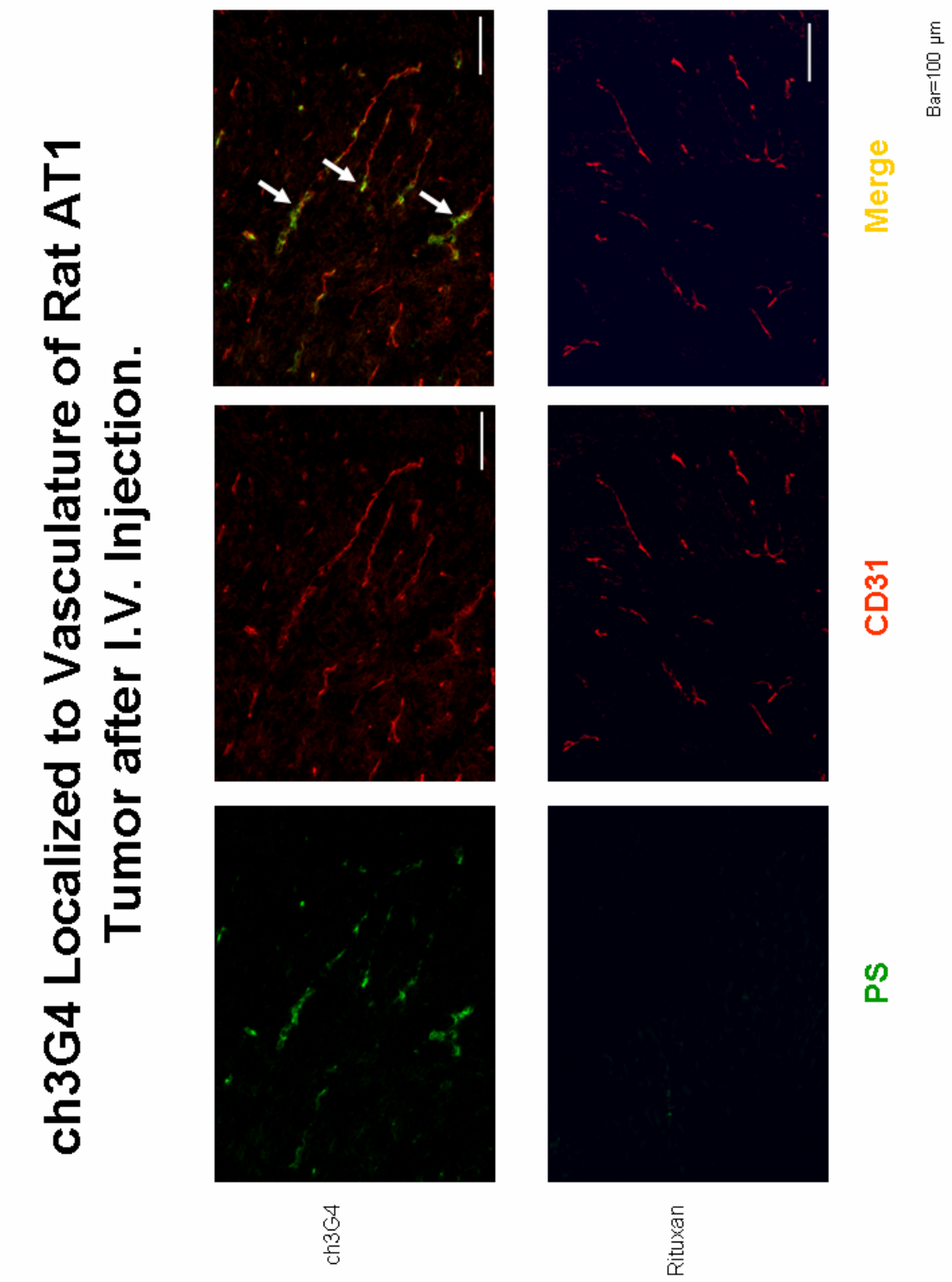
ch3G4 Localized to Vasculature of Rat AT1
Tumor after I.V. Injection.
PS
CD31
Merge
ch3G4
Rituxan
Bar=100 µm

FIGURE 5b.

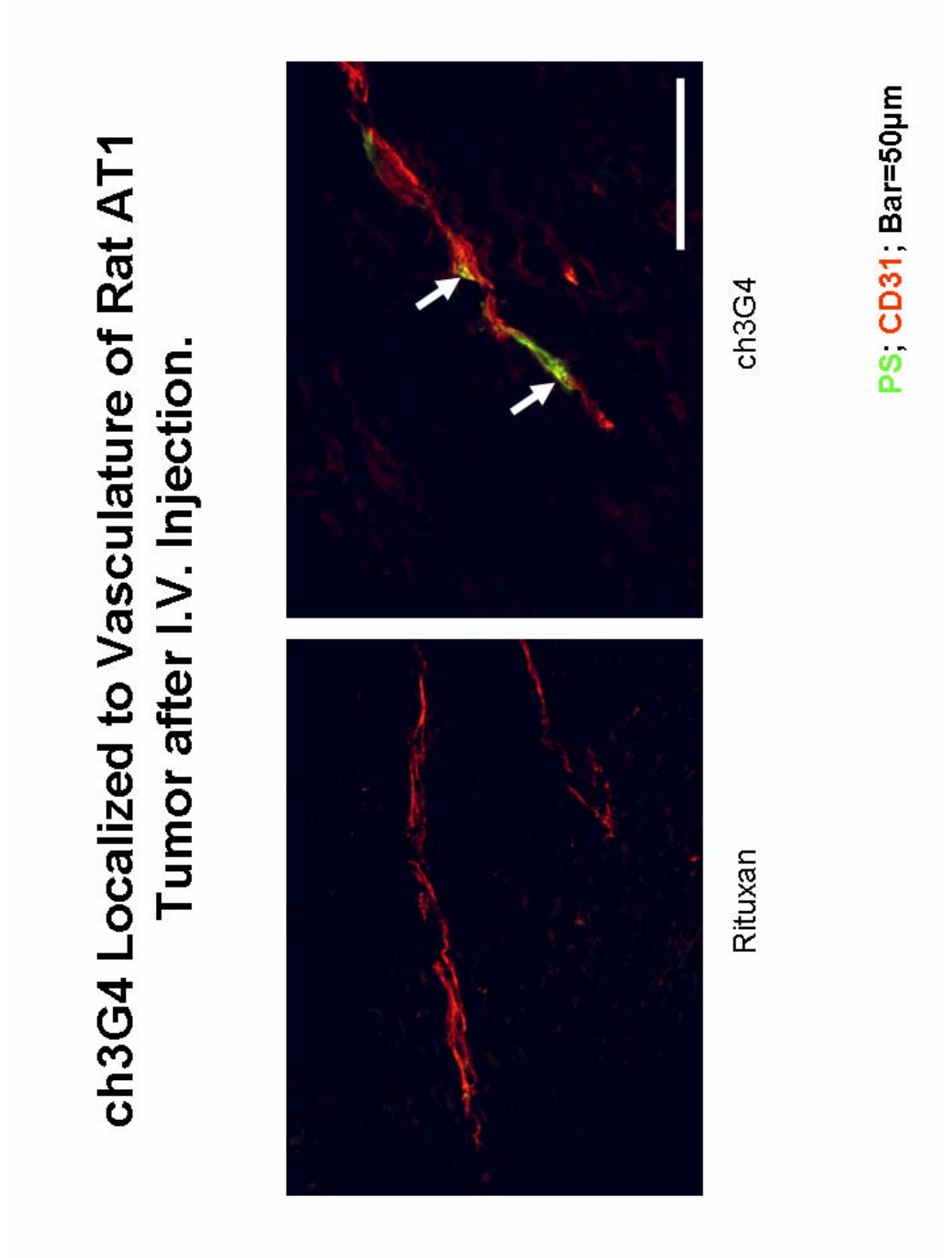
ch3G4 Localized to Vasculature of Rat AT1
Tumor after I.V. Injection.
ch3G4
Rituxan
PS; CD31; Bar=50µm

FIGURE 5.

Localization of ch3G4 to tumor vessels after injection into rats bearing syngeneic Dunning R3227 AT1 prostate tumors.

Male Copenhagen rats bearing 1 cm diameter R3227 Dunning prostate AT1 tumors implanted subcutaneously in their thigh were injected i.v. with 1 mg ch3G4 or control Rituxan. 1 h and 24 h later, the rats were exsanguinated and their tumors were removed. Fig. a) shows a typical area of tumor vasculature and Fig. b) shows the corresponding magnification of a single vessel in a frozen section of tumor at high magnification. The sections were stained with biotinylated goat anti-rat IgG followed by FITC-streptavidin (green) to detect localized ch3G4 and rat anti-mouse CD31 followed by Cy3 goat anti-rat IgG (red) to detect vascular endothelium. Images were merged images of ch3G4 localized to CD31 positive endothelium (arrows).

In addition to the molecular biology findings, this study demonstrates that ^{74}As[SATA]ch3G4, the corresponding SATA-modified antibody conjugated to the positron emitting isotope ^{74}As, can be used to serially image PS expression in the vasculature of Dunning prostate R3327 AT1 cancer in rats, that express high levels of this surface molecule.

As the labelling chemistry for the attachment of radioarsenic isotopes to mabs is new, the in vitro stability of the label had to be studied. No degradation of the label was observed for incubation times in serum for up to 72 h. This reflects the covalent bound of the arsenic to the antibody. Attempts to bind arsenic via complexation to biomolecules, like a lot of other nuclides employed in radiopharmacy and nuclear medicine, always failed because of the low in vitro stability due to chemical exchange with free thiols in the blood.

The developed labelling chemistry can be applied also to other radioarsenic isotopes, like ^{72}As. The arsenic isotopes are preferable to other PET isotopes for the images of whole antibodies in that they have longer half-lives of 26 h for ^{72}As, which could be well suitable for human application, and 18 d for ^{74}As, which enables the observation of extremely long-term pharmacokinetics. In addition, the abundance of positrons for ^{72}As is 85%, much higher than for other isotopes which are currently employed, like e.g. ^{64}Cu (17.4 % β^+ and

$T_{1/2}$ = 12.7 h) or ^{124}I (22.8 % β^+ and $T_{1/2}$ = 4.2 d). Also, iodine-labelled compounds often lead to enormous thyroid uptake, with a high irradiation burden of this radiation-sensitive organ. Moreover, the combined use of arsenic isotopes and ch3G4 enable the repeated images every 24 h. Smith-Jones et al. [22] describe the use of ^{68}Ga for the labelling of $F(ab')_2$ fragments of the anti-HER2 antibody Herceptin to image HER2 expression in breast cancer xenografts. However, in the clinical use of mabs for cancer treatment, mostly whole mabs are employed. Therefore the information which can be obtained using ^{68}Ga is principally very limited, due to the short half-life of 68 min. Practically, after 4 half-lives post injection of a ^{68}Ga labelled radiopharmaceutical, imaging makes no sense any longer, whereas we demonstrated that we obtain best image quality 72 h p.i., corresponding to the biodistribution data, showing a maximum enrichment of anti-PS in tumor tissue at this time.

The *ex vivo* biodistribution data matches very well with the tumor uptake shown in the images. We also observed a very high spleen uptake, compared to any other organ. As PS is not expressed selectively in the spleen and spleen tissue tested negatively for PS expression *in vitro*, we assume that this high uptake may come from the general metabolism of mAbs which is partly done in the spleen. Also, due to the formation of intermolecular dithiol bridges, there could exist mAb conglomerates, which also would be metabolized in the spleen. The high spleen uptake then would not be a characteristic of the ch3G4, but of the developed labelling method.

In vivo planar scintigraphy of whole animals on photostimulable plates is limited, because quantification is difficult and it is only applicable to subcutaneous tumors, because the source of radiation has to be close to the screen. However, this technique could provide a low-cost, time-effective, high-throughput imaging modality for pre-screening studies, where the qualitative uptake into a tumor of a high number of compounds shall be evaluated before selecting compounds for more detailed imaging studies via e.g. small animal PET. Compared to a negative control, like ^{74}As[SATA]Rituximab in our case, the images are very significant, even if they are only qualitative planar projections of the whole animal.

Our small animal PET pictures show excellent localization of ^{74}As[SATA]ch3G4 in the tumor capsule of the solid Dunning R3227 prostate AT1 tumor. Looking at the 1 cm diameter tumor capsule in magnification, a heterogeneity of activity distribution is

distinguishable. This matches the histologic findings of a necrotic tumor core, surrounded by life and well vascularized tissue. One of the major impediments to the development of rational therapeutic strategies with targeted agents has been the difficulty in determining whether the agent is reaching its target and in addition, to quantify what other organs are reached besides the originally designated target. To date, small animal PET is the only imaging modality where these goals can be achieved.

To summarize, the techniques introduced in this study are noteworthy for several reasons: 1. The developed labelling chemistry gives high yields, is reliable and could easily transferred to automated labelling systems in a clinical environment. 2. They are the first PET imaging studies using radioactive arsenic isotopes, an element first used by the Greek and Chinese more than 2,000 years ago to treat everything from syphilis to cancer [60] but was also the favourite poison of the Savellis, the Borgias [61], Agatha Christie and famous movie classics, like 'Arsenic and Old Lace (1944). 3. After showing the antigen specific targeting of ch3G4 in vivo, the next step can be a radiotherapeutically labelled ch3G4, using synergetic effects of the therapeutic potential of ch3G4 alone [19] and cytotoxic effects of a β^- emitting isotope. Arsenic provides 2 isotopes which could be used for this purpose: ^{76}As ($T_{1/2}$ = 26.2 h, $E_{\beta^- mean}$ = 1070 keV) and ^{77}As ($T_{1/2}$ = 1.6 d, $E_{\beta^- mean}$ = 226 keV) employing the same labelling chemistry. In addition this antibody would be a candidate for labelling with ^{90}Y ($T_{1/2}$ = 3.2 h, $E_{\beta^- mean}$ = 232 keV), at the moment the most common used endoradiotherapeutic isotope for the labelling of mabs in tumor animal models and even in clinic [62-68].

Finally, the described technique may be relevant to other antibodies with slow pharmacokinetics. In addition to antibodies, the technique might be transferred to other problems where the localization, follow-up and imaging of drugs over more then day-long periods is relevant, like e.g. stem-cell trafficking.

Acknowledgements

We thank Linda Watkins, Shuzhen Li, Mary Bennett, Amber Marlet and Janie Iglehart for technical assistance, Drs. Ellen Vitetta, Troy Luster and Chaitanya Nirodi for discussions, P.P. Antich and P.V. Kulkarni for providing the PET and laboratories and Samia Burns for typing the manuscript.

References

1. Thorpe, P.E., *Vascular targeting agents as cancer therapeutics.* Clin Cancer Res, 2004. **10**(2): p. 415-27.
2. Burrows, F.J. and P.E. Thorpe, *Vascular targeting--a new approach to the therapy of solid tumors.* Pharmacol Ther, 1994. **64**(1): p. 155-74.
3. Denekamp, J., *Review article: angiogenesis, neovascular proliferation and vascular pathophysiology as targets for cancer therapy.* Br J Radiol, 1993. **66**(783): p. 181-96.
4. Siemann, D.W., E. Mercer, S. Lepler, and A.M. Rojiani, *Vascular targeting agents enhance chemotherapeutic agent activities in solid tumor therapy.* Int J Cancer, 2002. **99**(1): p. 1-6.
5. Williamson, P. and R.A. Schlegel, *Back and forth: the regulation and function of transbilayer phospholipid movement in eukaryotic cells.* Mol Membr Biol, 1994. **11**(4): p. 199-216.
6. Zwaal, R.F. and A.J. Schroit, *Pathophysiologic implications of membrane phospholipid asymmetry in blood cells.* Blood, 1997. **89**(4): p. 1121-32.
7. Calderon, R.O. and G.H. DeVries, *Lipid composition and phospholipid asymmetry of membranes from a Schwann cell line.* J Neurosci Res, 1997. **49**(3): p. 372-80.
8. Hinkovska-Galcheva, V., D. Petkova, and K. Koumanov, *Changes in the phospholipid composition and phospholipid asymmetry of ram sperm plasma membranes after cryopreservation.* Cryobiology, 1989. **26**(1): p. 70-5.

9. Seigneuret, M. and P.F. Devaux, *ATP-dependent asymmetric distribution of spin-labeled phospholipids in the erythrocyte membrane: relation to shape changes.* Proc Natl Acad Sci U S A, 1984. **81**(12): p. 3751-5.
10. Bombeli, T., A. Karsan, J.F. Tait, and J.M. Harlan, *Apoptotic vascular endothelial cells become procoagulant.* Blood, 1997. **89**(7): p. 2429-42.
11. Boyle, E.M., Jr., T.H. Pohlman, C.J. Cornejo, and E.D. Verrier, *Endothelial cell injury in cardiovascular surgery: ischemia-reperfusion.* Ann Thorac Surg, 1996. **62**(6): p. 1868-75.
12. Bevers, E.M., P. Comfurius, and R.F. Zwaal, *Changes in membrane phospholipid distribution during platelet activation.* Biochim Biophys Acta, 1983. **736**(1): p. 57-66.
13. Rote, N.S., J. Chang, H. Katsuragawa, A.K. Ng, T.W. Lyden, and T. Mori, *Expression of phosphatidylserine-dependent antigens on the surface of differentiating BeWo human choriocarcinoma cells.* Am J Reprod Immunol, 1995. **33**(1): p. 114-21.
14. Bitbol, M., P. Fellmann, A. Zachowski, and P.F. Devaux, *Ion regulation of phosphatidylserine and phosphatidylethanolamine outside-inside translocation in human erythrocytes.* Biochim Biophys Acta, 1987. **904**(2): p. 268-82.
15. Zhao, J., Q. Zhou, T. Wiedmer, and P.J. Sims, *Level of expression of phospholipid scramblase regulates induced movement of phosphatidylserine to the cell surface.* J Biol Chem, 1998. **273**(12): p. 6603-6.
16. Hamon, Y., C. Broccardo, O. Chambenoit, M.F. Luciani, F. Toti, S. Chaslin, J.M. Freyssinet, P.F. Devaux, J. McNeish, D. Marguet, and G. Chimini, *ABC1 promotes engulfment of apoptotic cells and transbilayer redistribution of phosphatidylserine.* Nat Cell Biol, 2000. **2**(7): p. 399-406.
17. Williamson, P., A. Kulick, A. Zachowski, R.A. Schlegel, and P.F. Devaux, *Ca2+ induces transbilayer redistribution of all major phospholipids in human erythrocytes.* Biochemistry, 1992. **31**(27): p. 6355-60.
18. Ran, S., A. Downes, and P.E. Thorpe, *Increased exposure of anionic phospholipids on the surface of tumor blood vessels.* Cancer Res, 2002. **62**(21): p. 6132-40.
19. Ran, S. and P.E. Thorpe, *Phosphatidylserine is a marker of tumor vasculature and a potential target for cancer imaging and therapy.* Int J Radiat Oncol Biol Phys, 2002. **54**(5): p. 1479-84.

20. Balasubramanian, K. and A.J. Schroit, *Aminophospholipid asymmetry: A matter of life and death.* Annu Rev Physiol, 2003. **65**: p. 701-34.
21. Contreras, F.X., A.V. Villar, A. Alonso, R.N. Kolesnick, and F.M. Goni, *Sphingomyelinase activity causes transbilayer lipid translocation in model and cell membranes.* J Biol Chem, 2003. **278**(39): p. 37169-74.
22. Smith-Jones, P.M., D.B. Solit, T. Akhurst, F. Afroze, N. Rosen, and S.M. Larson, *Imaging the pharmacodynamics of HER2 degradation in response to Hsp90 inhibitors.* Nat Biotechnol, 2004. **22**(6): p. 701-6.
23. Cullen, W.R. and K.J. Reimer, *Arsenic speciation in the environment.* Chem Rev, 1989. **89**: p. 713-764.
24. Evans, C.D., K. LaDow, B.L. Schumann, R.E. Savage, Jr., J. Caruso, A. Vonderheide, P. Succop, and G. Talaska, *Effect of arsenic on benzo[a]pyrene DNA adduct levels in mouse skin and lung.* Carcinogenesis, 2004. **25**(4): p. 493-7.
25. Bode, A.M. and Z. Dong, *The paradox of arsenic: molecular mechanisms of cell transformation and chemotherapeutic effects.* Crit Rev Oncol Hematol, 2002. **42**(1): p. 5-24.
26. Huff, J., P. Chan, and A. Nyska, *Is the human carcinogen arsenic carcinogenic to laboratory animals?* Toxicol Sci, 2000. **55**(1): p. 17-23.
27. Zhu, J., Z. Chen, V. Lallemand-Breitenbach, and H. de The, *How acute promyelocytic leukaemia revived arsenic.* Nat Rev Cancer, 2002. **2**(9): p. 705-13.
28. Zhu, J., M.H. Koken, F. Quignon, M.K. Chelbi-Alix, L. Degos, Z.Y. Wang, Z. Chen, and H. de The, *Arsenic-induced PML targeting onto nuclear bodies: implications for the treatment of acute promyelocytic leukemia.* Proc Natl Acad Sci U S A, 1997. **94**(8): p. 3978-83.
29. Zhu, J., V. Lallemand-Breitenbach, and H. de The, *Pathways of retinoic acid- or arsenic trioxide-induced PML/RARalpha catabolism, role of oncogene degradation in disease remission.* Oncogene, 2001. **20**(49): p. 7257-65.
30. Zhu, J., H. Okumura, S. Ohtake, S. Nakamura, and S. Nakao, *Arsenic trioxide induces apoptosis in leukemia/lymphoma cell lines via the CD95/CD95L system.* Oncol Rep, 2003. **10**(3): p. 705-9.
31. Wang, Z.Y., *Arsenic compounds as anticancer agents.* Cancer Chemother Pharmacol, 2001. **48 Suppl 1**: p. S72-6.

32. Kwong, Y.L. and D. Todd, *Delicious poison: arsenic trioxide for the treatment of leukemia.* Blood, 1997. **89**(9): p. 3487-8.

33. Kim, J.H., Y.S. Lew, A. Kolozsvary, S. Ryu, and S.L. Brown, *Arsenic trioxide enhances radiation response of 9L glioma in the rat brain.* Radiat Res, 2003. **160**(6): p. 662-6.

34. Chen, G.Q., X.G. Shi, W. Tang, S.M. Xiong, J. Zhu, X. Cai, Z.G. Han, J.H. Ni, G.Y. Shi, P.M. Jia, M.M. Liu, K.L. He, C. Niu, J. Ma, P. Zhang, T.D. Zhang, P. Paul, T. Naoe, K. Kitamura, W. Miller, S. Waxman, Z.Y. Wang, H. de The, S.J. Chen, and Z. Chen, *Use of arsenic trioxide (As2O3) in the treatment of acute promyelocytic leukemia (APL): I. As2O3 exerts dose-dependent dual effects on APL cells.* Blood, 1997. **89**(9): p. 3345-53.

35. Chen, G.Q., J. Zhu, X.G. Shi, J.H. Ni, H.J. Zhong, G.Y. Si, X.L. Jin, W. Tang, X.S. Li, S.M. Xong, Z.X. Shen, G.L. Sun, J. Ma, P. Zhang, T.D. Zhang, C. Gazin, T. Naoe, S.J. Chen, Z.Y. Wang, and Z. Chen, *In vitro studies on cellular and molecular mechanisms of arsenic trioxide (As_2O_3) in the treatment of acute promyelocytic leukemia: As_2O_3 induces NB4 cell apoptosis with downregulation of Bcl-2 expression and modulation of PML-RAR alpha/PML proteins.* Blood, 1996. **88**(3): p. 1052-61.

36. Basile, D., C. Birattari, M. Bonardi, L. Goetz, E. Sabbioni, and A. Salomone, *Excitation functions and production of arsenic radioisotopes for environmental toxicology and biomedical purposes.* Int J Appl Radiat Isot, 1981. **32**(6): p. 403-10.

37. Byrne, A.R., *Simple production of ^{77}As from reactor irradiated germanium.* Int Conf on Nuc Radiochem, 1984: p. 239.

38. Mausner, L.F., S.O. Kurczak, and D.J. Jamriska, *Production of ^{73}As by irradiation of Ge target.* J Nucl Med, 2004. **45**(5S): p. 471P.

39. Ward, T.E., D.L. Swindle, R.J. Wright, and P.K. Kuroda, *Radiochemical procedure for arsenic and germanium.* Radiochimica Acta, 1970. **14**(2): p. 70-72.

40. Jennewein, M., A. Schmidt, A.F. Novgorodov, S.M. Qaim, and F. Rösch, *A no-carrier-added $^{72}Se/^{72}As$ radionuclide generator based on distillation.* Radiochimica Acta, 2004. **92**: p. 245-249.

41. Browne, E. and R.B. Firestone, *Table of Radioactive Isotopes*, ed. V.S. Shirley. 1986, New York: John Wiley & Sons.

42. Sweet, W.H. and G.L. Brownell, *Localization of intracranial lesions by scanning with positron-emitting arsenic.* J Am Med Assoc, 1955. **157**(14): p. 1183-1188.
43. Leicester, J. and G.K. Vanderfield, *The detection of cerebral lesions by the newer forms of encephalography: positron scanning and echoencephalography.* Med J Aust, 1966. **2**(15): p. 680-3.
44. Mealey, J., Jr., *Radioisotopic Localization in Subdural Hematomas. An Experimental Study with Arsenic-74 and Radioiodinated Human Serum Albumin in Dogs.* J Neurosurg, 1963. **20**: p. 770-6.
45. Wilcke, O., *[The diagnosis of brain tumors using isotopes].* Nervenarzt, 1965. **36**(12): p. 508-14.
46. Wilcke, O., *[Scintigraphy of brain tumors].* Radiologe, 1965. **5**(10): p. 393-400.
47. Wilcke, O. and M. Brock, *[Positrocephalography. Results in 1,400 cases. Comparative study with angiography, pneumoencephalography and electroencephalography].* Arq Neuropsiquiatr, 1965. **23**(4): p. 261-70.
48. Pierce-Biotechnology, *SATP, SATA.* Instruction Files, 2003. **26100, 26102**.
49. Duncan, R.J., P.D. Weston, and R. Wrigglesworth, *A new reagent which may be used to introduce sulfhydryl groups into proteins, and its use in the preparation of conjugates for immunoassay.* Anal Biochem, 1983. **132**(1): p. 68-73.
50. Cooke, D.B., V.E. Quarmby, D.D. Mickey, J.T. Isaacs, and F.S. French, *Oncogene expression in prostate cancer: Dunning R3327 rat dorsal prostatic adenocarcinoma system.* Prostate, 1988. **13**(4): p. 263-72.
51. Tennant, T.R., H. Kim, M. Sokoloff, and C.W. Rinker-Schaeffer, *The Dunning model.* Prostate, 2000. **43**(4): p. 295-302.
52. Shepp, L.A. and Y. Vardi, *Maximum likelihood reconstruction for positron emission tomography.* IEEE Transactions in Medical Imaging, 1982. **1**: p. 113-122.
53. Jennewein, M., S.M. Qaim, P.V. Kulkarni, R.P. Mason, A. Hermanne, and F. Roesch, *A no-carrier-added ^{72}Se/^{72}As radionuclide generator based on solid phase extraction.* Radiochimica Acta, 2005.
54. Jennewein, M., R. Schirrmacher, S. Maus, and F. Rösch, *Macroscopic synthesis of arsenoorganic precursors and first no-carrier-added radioarsenic labelling.* J Lab Comp Radiopharm, 2003. **46**(S1): p. 42.
55. Jennewein, M., R. Schirrmacher, S. Maus, and F. Rösch, *Synthesis of 1,3-dimercaptopropyl arsenic-BOC-cysteine-O-Bzl and diphenyl arsenic-BOC-*

cysteine-O-Bzl and first radioarsenic labelling. J Lab Comp Radiopharm, 2003. **46**(S1): p. 283.

56. Zulueta, J.J., F.S. Yu, I.A. Hertig, V.J. Thannickal, and P.M. Hassoun, *Release of hydrogen peroxide in response to hypoxia-reoxygenation: role of an NAD(P)H oxidase-like enzyme in endothelial cell plasma membrane.* Am J Respir Cell Mol Biol, 1995. **12**(1): p. 41-9.
57. Soares, F.A., S.G. Shaughnessy, W.R. MacLarkey, and F.W. Orr, *Quantification and morphologic demonstration of reactive oxygen species produced by Walker 256 tumor cells in vitro and during metastasis in vivo.* Lab Invest, 1994. **71**(4): p. 480-9.
58. Shaughnessy, S.G., M.R. Buchanan, S. Turple, M. Richardson, and F.W. Orr, *Walker carcinosarcoma cells damage endothelial cells by the generation of reactive oxygen species.* Am J Pathol, 1989. **134**(4): p. 787-96.
59. van Gorp, R.M., J.L. Broers, C.P. Reutelingsperger, N.M. Bronnenberg, G. Hornstra, M.C. van Dam-Mieras, and J.W. Heemskerk, *Peroxide-induced membrane blebbing in endothelial cells associated with glutathione oxidation but not apoptosis.* Am J Physiol, 1999. **277**(1 Pt 1): p. C20-8.
60. Waxman, S. and K.C. Anderson, *History of the development of arsenic derivatives in cancer therapy.* Oncologist, 2001. **6 Suppl 2**: p. 3-10.
61. Micca, G., *Arsenic, or rather arsenious anhydride, the preferred poison of the Borgias.* Minerva Med, 1969. **60**: p. IX-XI.
62. Li, L., C.A. Wartchow, S.N. Danthi, Z. Shen, N. Dechene, J. Pease, H.S. Choi, T. Doede, P. Chu, S. Ning, D.Y. Lee, M.D. Bednarski, and S.J. Knox, *A novel antiangiogenesis therapy using an integrin antagonist or anti-Flk-1 antibody coated 90Y-labeled nanoparticles.* Int J Radiat Oncol Biol Phys, 2004. **58**(4): p. 1215-27.
63. Clayton, J., *Nursing a patient during and after ^{90}Y-ibritumomab tiuxetan (Zevalin) therapy.* Leuk Lymphoma, 2003. **44 Suppl 4**: p. S49-55.
64. Stein, R., M. Juweid, M.J. Mattes, and D.M. Goldenberg, *Carcinoembryonic antigen as a target for radioimmunotherapy of human medullary thyroid carcinoma: antibody processing, targeting, and experimental therapy with 131I and 90Y labeled MAbs.* Cancer Biother Radiopharm, 1999. **14**(1): p. 37-47.

65. Richman, C.M., S.J. DeNardo, R.T. O'Donnell, D.S. Goldstein, S. Shen, D.L. Kukis, L.A. Kroger, A. Yuan, G.R. Boniface, I.J. Griffith, and G.L. DeNardo, *Dosimetry-based therapy in metastatic breast cancer patients using ^{90}Y monoclonal antibody 170H.82 with autologous stem cell support and cyclosporin A.* Clin Cancer Res, 1999. **5**(10 Suppl): p. 3243s-3248s.

66. Macklis, R.M., B.A. Beresford, and J.L. Humm, *Radiobiologic studies of low-dose-rate ^{90}Y-lymphoma therapy.* Cancer, 1994. **73**(3 Suppl): p. 966-73.

67. Morton, B.A., B.G. Beatty, A.P. Mison, P.M. Wanek, and J.D. Beatty, *Role of bone marrow transplantation in ^{90}Y antibody therapy of colon cancer xenografts in nude mice.* Cancer Res, 1990. **50**(3 Suppl): p. 1008s-1010s.

68. Washburn, L.C., T.T. Hwa Sun, J.E. Crook, B.L. Byrd, J.E. Carlton, Y.W. Hung, and Z.S. Steplewski, *^{90}Y-labeled monoclonal antibodies for cancer therapy.* Int J Rad Appl Instrum B, 1986. **13**(4): p. 453-6.

69. *National Nuclear Data Center, Brookhaven National Laboratory*. 2004, http://www.nndc.bnl.gov/nudat2/index.jsp.

VII.

Projection and Pinhole based Data Acquisition for Small Animal SPECT using Storage Phosphor Technology

Projection and Pinhole based Data Acquisition for Small Animal SPECT using Storage Phosphor Technology

M. A. Lewis, G. Arbique, E. Richer, N. Slavine, M. Jennewein[†], A. Constantinescu, R. Brekken, J. Guild, E.N. Tsyganov, R.P. Mason and P.P. Antich

The University of Texas Southwestern Medical Center at Dallas

1. Introduction

Three-dimensional Single Photon Emission Computed Tomography (SPECT) can provide high-resolution insight into biomolecular distribution and pharmacokinetics. However, instrument availability and distribution is limited at present, and imaging times can be considerable. To evaluate the large array of novel agents which are becoming available, we find that storage phosphor-based in vivo imaging can provide an important, rapid-throughput transition from the traditional ex vivo sacrifice/gamma-counting and autoradiography to full time-course SPECT.

Storage phosphor (SP) technology has found wide-spread usage in both the radiology clinic and in the molecular biology laboratory. With a linear sensitivity latitude exceeding that of plain film, photostimulable luminescence (PSL) screens can facilitate high-throughput screening and autoradiography for a variety of small animal models. Despite the impressive growth and improvement in small animal nuclear imaging, the determination of appropriate growth and improvement in small animal nuclear imaging, the determination of appropriate time and duration of imaging for a given animal model and imaging agent is still crucial in study design and analysis. Storage phosphor technology is well-suited for addressing this issue, either by producing quantitative planar projection or lowresolution tomographic images.

[†] primary affiliation: Johannes Gutenberg-Universität Mainz, Germany

With γ-ray stopping cross-sections that are not radically different from film/screen systems, the phosphor image plate is well-suited for low energy gamma detection, especially for imaging studies with iodine-125 (^{125}I) where tissue scattering is minimized.

2. Background

2.1 Storage phosphor technology

Photostimulable storage phosphor (PSP[2]) screens were developed and introduced in the 1980s [Sonoda et al., 1983] as a replacement for film/screen x-ray detection systems. Today, SP technology is the key component in commercial film-less imaging systems grouped under the generic term Computed Radiography (CR) [Arbique et al., 2003]. This technology is distinct from so-called Digital Radiography, where x-ray detection is digital from the moment of detection. Subsequently, SP technology was adopted by most suppliers of autoradiography equipment [Johnston et al., 1990]. While the average molecular biologist today does not have ready access to a small animal SPECT system, he or she most likely possesses or has available an SP scanner or reader that is routinely used for gel and blot applications. Compared to the standard CR reader in a radiology clinic, these scanners typically have higher spatial resolutions (down to 50 μm) and greater digital resolution (16 vs. 12 bit). Although the current trend is towards more expensive scanners that can also read direct- or chemi-fluorescence assays, a multipurpose SP system can be obtained for a fraction of the cost of a minimal small animal SPECT system.

A full physical description of SP technology, including image performance parameters (MTF, NPS, DQE) can be found elsewhere [von Seggern, 1999; Rowlands, 2002]. In summary, the interaction of a highenergy photon with a BaF(Br,I):Eu^{2+} phosphor grain generates electrons and holes that are trapped in the immediate fluorohalide matrix area. A latent image is formed in proportion to the density of the trapped carriers. Upon subsequent photostimulation using a red light source (typically a laser at 590-680 nm), the electron is liberated from its trap and recombines with a hole. The energy generated in this process is resonantly transferred to a doped Europium ion, which then decays with characteristic luminescence (390 nm). This luminescence is captured using a photomultiplier tube and

digitized. With an appropriate reader, a typical SP image plate will have a linear dynamic range up to a thousand times greater than film, spanning 4-5 orders of magnitude, and reusable for tens of thousands of exposures. Due to thermal stimulation, the latent image does fade (decay constant approximately 9 hours), so immediate reading of PSL screens is advisable.

2.2 Low energy-integrating SPECT

The hypothesis of low energy-integrating SPECT is that reasonable images can be obtained using γ-ray detectors that integrate activity counts and have no energy discrimination for scatter rejection. Monte Carlo simulations [Tenney, 2002] have shown that for ^{125}I in a mouse sized cylinder of water the scatter fraction remains below 40% and the detective quantum efficiency (DQE) is in the reasonable range of 0.6-0.7, which can exceed the DQE of the SP screen [Rowlands, 2002]. Although dual isotope imaging is precluded, energy-integration imaging shifts the burden of work to image reconstruction, where scatter correction represents a significant challenge, but is an active area of research for all nuclear medicine modalities.

A CCD-based gamma camera has been recently proposed as an efficient energy-integrating detector for small animal SPECT. Although a CCD-based camera will in general be less expensive than the traditional position-sensitive PMT, the intrinsic resolution of the CCD design will be significantly better, with characteristic resolutions below 400 μm [Antich et al., 2003]. At these low intrinsic resolutions, parallel-hole collimators are not well-matched. In addition, compared to a non-magnifying pinhole geometry, the packing of multiple, static projection is limited.

For lower resolution, high-throughput screening, we find that SP image plates and screens are an acceptable alternative to CCDs in an energy-integrating detector. If an infrastructure for reading SP technology is already in place, then the relative cost for detectors is further reduced, with no sacrifice in intrinsic resolution. With this saving, we believe that small animal SPECT using SP technology may be possible for routine low-resolution, high-throughput screening.

3. Prototype

Recently, a prototype system using CR image plates for co-registered I-125 planar scintigraphy and x-ray radiography was introduced [Boone et al., 2003]. In this scheme, half of the image plate is used for a planar emission image. After exposure, the image plate is precisely translated so that a transmission radiography can be taken with the other half of the plate. These two images are subsequently co-registered in software, using the known displacement.

Our approach differs in that we have utilized custom-sized SP image plates as energy-integrating detectors in a low-resolution small-animal pinhole emission computed tomography geometry. As shown in Figure 26.1, a 30 mm inner diameter/5 mm thick brass cylinder serves as a support for eight 1.5 mm diameter pinholes (also in brass, with 90° cone of acceptance), spaced in 45° increments around a ring. In this geometry, the field-of-view in a plane intersecting the axis of the cylinder is equivalent to the 30 mm diameter of the cylinder. A strip of 8 small SP image plates is attached to the support structure at fixed points of known distance from the pinhole centers. Each detector is placed 10 mm from the corresponding pinhole center. In this geometry, reading of the SP screen at 100 μm resolution will produce 128x128 and 256x128 projections for 60° and 90° cone-of-acceptance pinholes, respectively. For ^{125}I energies (< 35.5 keV), brass is sufficient for collimation (HVL ¼ 80 μm).

Eight 24 mm by 50 mm SP screens were cut from a 25.2x30.3 cm Fuji CR ST-VN Imaging Plate (Fuji Photo Film, Tokyo). Attachment holes of 1.6 mm diameter were milled at the end of each screen for attachment to the imaging system. The imaging plates were connected in a continuous strip using black insulating tape.

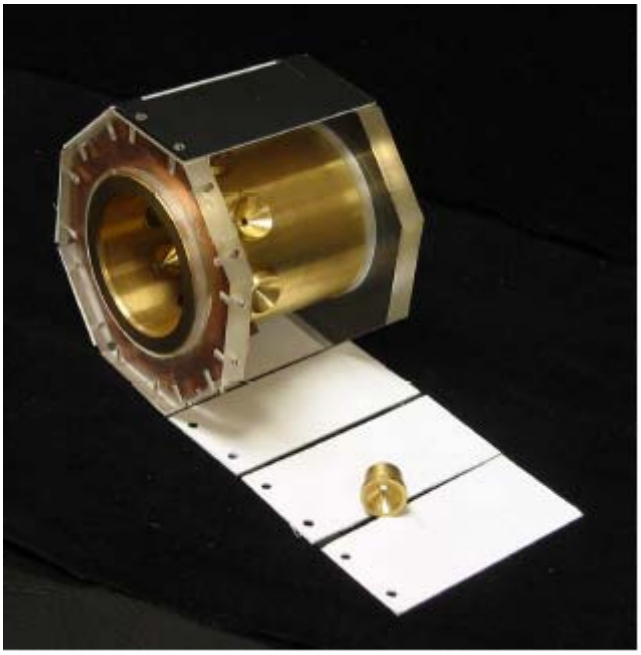

FIGURE 26.1. Prototype murine pinhole emission computed tomography system using using energy-integrating storage phosphor technology

The system is placed in a light-tight enclosure with the phantom or animal placed inside the cylinder. After exposure[3], the SP detector is carefully removed and transported in a light-tight envelope to the SP reader. An SP scanner with the ability to read arbitrary size screens, such at the Molecular Dynamics Storm (Amersham Biosciences, Piscataway, NJ), is preferred, but in practice other systems may work. Special attention to the relationship between the detector coordinate system and the angular position of the detector should be maintained, as different SP readers may report data in mirror orientations.

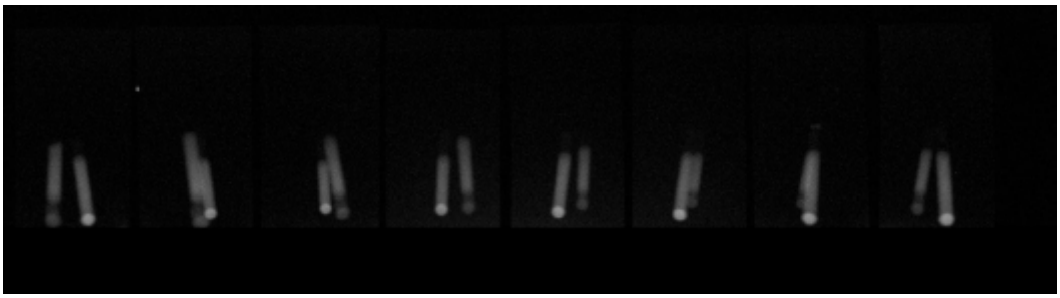

FIGURE 26.2. Eight pinhole projections from two 1.85 MBq ^{125}I capillaries (0.8 mm inner diameter). 15 minutes integration exposure. Signal-to-noise ratio ≈ 10. Heterogeneities due to air bubbles in capillaries and infiltration of sealant.

4. Results

To evaluate the prototype system, two non-uniform 1.85 MBq ^{125}I capillaries with inner diameter of 0.8 mm were prepared. The line sources were placed off-center in the field-of-view for the ring of pinholes, and were non-parallel with an average separation of 8 mm. The sources were imaged for 15 minutes, followed by prompt reading of the SP image plates. Eight pinhole projections of the line source can be found in Figure 26.2.

Using unexposed regions of the SP image plates, background noise levels were determined for windowing. Since the attachment holes appear as voids on the raw projection images, detector coordinate origins were calculated as the midpoint, and projections were corrected for rotation.

A 3D image (48x48x60, 0.5 mm voxels) was reconstructed from these eight projections using the maximum-likelihood estimation maximization (MLEM) algorithm with convolution for resolution modelling [Reader et al., 2002; Zinchenko et al., 2003]. Figure 26.3 provides a maximum intensity projection (MIP) of the reconstructed volume that is consistent with the projections in Figure 26.2. For a non-magnifying pinhole geometry, the standard pinhole collimator resolution expression (a is the pinhole to detector distance, b is the pinhole to object distance) indicates that the pinhole point-spread function (full-width half maximum) at the imaging volume center is 2.5 times the pinhole diameter. Figure 26.4

demonstrates the observed and expected line broadening due to the non-magnifying geometry.

$$R_c = \frac{a+b}{a} d_e$$

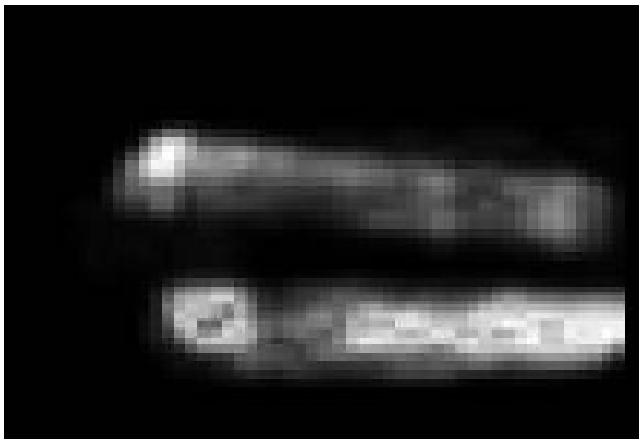

FIGURE 26.3. Maximum intensity projection for reconstructed, heterogenous line sources

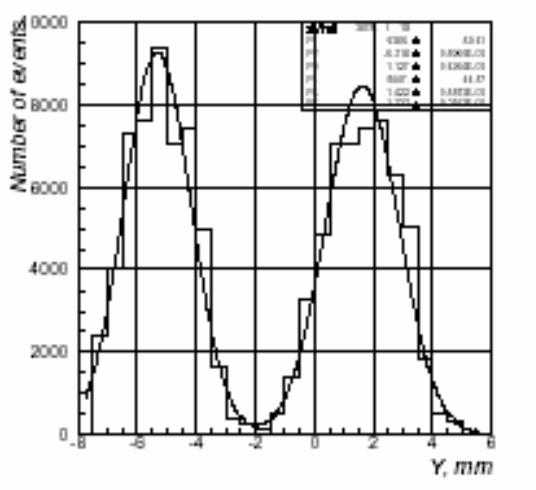

FIGURE 26.4. Cross section through line sources with expected broadening due to pinhole geometry

5. Conclusions and Open Issues

Low resolution imaging with a static pinhole geometry and energy-integrating storage phosphor detectors is a feasible, low cost alternative for high-throughput evaluation of imaging agents and for determining optimal timing of high resolution, small animal SPECT studies. High resolution is not limited by the intrinsic resolution or sensitivity of the SP detector, but is due to limited angular sampling with small numbers of projections.

The current prototype possesses detector areas that allow for expansion to 2 rings of 90° or 3 rings of 60° pinholes. The challenge for higher resolution is to increase angular sampling by increasing the number of projections in the static geometry. Sixty projections have been reported as sufficient for imaging [Palmer and Wollmer, 1990], but multiplexed multi-pinholes [Schramm et al., 2001], coded-apertures [Schellingerhout et al., 2002], and relaxed collimation [Prior et al., 1993] are possible solutions for efficient projection packing.

For low exposures with PS image plates, it has been shown that noise levels obey the expected Poisson statistics [Arbique et al., 2003]. However, at uniform higher exposures, it has been demonstrated that structured noise source in the image plate contributes to spatial-variant signal-to-noise ratio [Nishikawa and Yaffe, 1990]. A procedure for correcting projection images in the pre-processing stage has not been addressed.

$BaF(Br,I):Eu^{2+}$ SP imaging plates are optimized for 80 kVp radiography. Unfortunately, a large K-edge at 40 keV reduces the sensitivity of SP detectors to ^{125}I emissions. The future commercial availability of storage phosphors more suitably matched to low energy emissions ($RbCs:Tl^{+}$ and $CsBr:Eu^{2+}$) will increase the efficiency of energy-integrated imaging with ^{125}I. As stated above, the primary challenge remains development of image reconstruction algorithms that provide scatter correction. Inevitably, this will probably require knowledge of the mouse topography (size and shape) for modelling scatter on a per-animal basis.

Acknowledgments

This work was supported in part by NCI P20 CA 86354.

Notes

1) The terms screen and image plate are synonymous in the context of this paper.
2) The terms storage phosphor (SP), photostimulable luminescence (PSL), and photostimulable storage phosphor (PSP) are synonymous in the context of this paper.
3) Exposure time will depend upon collimation. Our experience is that 1 minute per 2 μCi is typically sufficient

References

1. Antich, P. P., Lewis, M. A., Richer, E., Kulkarni, P. V., Smith, B. J., and Mason, R. P. (2003). A novel multi-pinhole/CCD-coupled CsI(Tl) crystal gamma camera for fully 3D μSPECT/μCT small-animal imaging. *Journal of Nuclear Medicine*, 44(5 (Supplement)):161P. No. 523. Presented at 2003 SNM Annual Meeting, New Orleans, LA, June 21–25.
2. Arbique, G., Guild, J., Anderson, J., Blackburn, T., Lane, T., and Wang, J. (2003). Clinical experience with a FUJI computed radiography quality assurance program. *Medical Physics*, 30(6):1344. Presented at 2003 AAPM Annual Meeting, San Diego, California, August 10–14.
3. Boone, J. M., Abbey, C. K., and Cherry, S. R. (2003). A combined I-125 nuclear emission and transmission radiography system for coregistered imaging of mouse function and anatomy. *Medical Physics*, 30(6):1438–1439. Presented at 2003 AAPM AnnualMeeting, San Diego, California, August 10–14.
4. Johnston, R. F., Pickett, S. C., and Barker, D. L. (1990). Autoradiography using storage phosphor technology. *Electrophoresis*, 11(5):355– 360.
5. Nishikawa, R. M. and Yaffe, M. J. (1990). Effect of various noise sources on the detective quantum of phosphor screens. *Medical Physics*, 17(5):887– 893.

6. Palmer, J. and Wollmer, P. (1990). Pinhole emission computed tomography: method and experimental evaluation. *Phys. Med. Biol*., 35(3):339– 350.

7. Prior, J. O., Antich, P. P., Fernando, J., Anderson, J. A., Kulkarni, P. V., and Parkey, R. W. (1993). Imaging stategies with scintillating fibers detectors: issues and preliminary results. In *Scintillating Fiber Technology and Applications. SPIE.*, volume 2007, pages 116–124.

8. Reader, A. J., Ally, S., Bakatselos, F., Manavaki, R., Walledge, R. J., Jeavons, A. P., Julyan, P. J., Zhao, S., Hastings, D. L., and Zweik, J. (2002). One-pass list-mode em algorithm for high resolution 3D pet image reconstruction into large arrays. *IEEE Trans. Nucl. Sci*., 49:693–699.

9. Rowlands, J. A. (2002). The physics of computed radiography. *Phys. Med. Biol*., 47(23):R123–R166.

10. Schellingerhout, D., Accorsi, R., Mahmood, U., Idoine, J., Lanza, R. C., and Weissleder, R. (2002). Coded aperture nuclear scintigraphy: A novel small animal imaging technique. *Molecular Imaging*, 1(4):344– 352.

11. Schramm, N., Wirrwar, A., and Halling, H. (2001). Development of a multi-pinhole detector for high-sensitivity SPECT imaging. In *IEEE Nuclear Science Symposium*, volume 3, pages 1585–1586.

12. Sonoda, M., Takano, M., Miyahara, J., and Kato, H. (1983). Computed radiography utilizing scanning laser stimulated luminescence. *Radiology*, 148(3):833–888.

13. Tenney, C. R. (2002). On the use of an energy-integrating detector for small-animal pinhole emission computed tomography. Presented at 2002 Annual Conference of the Academy of Molecular Imaging, San Diego, CA, October 22–27.

14. von Seggern, H. (1999). Photostimulable X-ray storage phosphors: a review of present understanding. *Brazilian Journal of Physics*, 29(2):254– 268.

15. Zinchenko, A., Tsyganov, E. N., Slavine, N. V., Kulkarni, P. V., Lewis, M. A., Mason, R. P., Oz, O. K., Parkey, R. W., and Antich, P. P. (2003). Expectation maximization algorithm with resolution deconvolution for 3-D image reconstruction in a small animal PET imager. *Journal of Nuclear Medicine*, 44(5 (Supplement)):161P. No. 528. Presented at 2003 SNM Annual Meeting, New Orleans, LA, June 21–25.

VIII.

Performance of the Dallas Small Animal PET Imager

Performance of the Dallas Small Animal PET Imager

Edward N.Tsyganov, *Member, IEEE*, Pietro P. Antich, Gary Arbique, Anca Constantinescu, Johan Fernando, Marc Jennewein, Padmakar V. Kulkarni, Ralph P. Mason, Roderick W. McColl, Orhan Öz, Robert W. Parkey, Edmond Richer, Frank Rösch, Serguei Y. Seliounine, Nikolai V. Slavine, Philip Thorpe, George Thambi, Alexander I. Zinchenko

This work is supported in part by the Cancer Imaging Program (an NCI Pre-ICMIC) 1P 20 CA 86354.

Edward N. Tsyganov is with the University of Texas Southwestern Medical Center at Dallas, Texas 75390 USA, phone: 214-648-3689, fax: 214-648-7513, e-mail: edward.tsyganov@utsouthwestern.edu.

Pietro P. Antich is with the University of Texas Southwestern Medical Center at Dallas, Texas 75390 USA, e-mail: pietro.antich@utsouthwestern.edu

Gary Arbique is with the University of Texas Southwestern Medical Center at Dallas, Texas 75390 USA, e-mail: gary.arbique@utsouthwestern.edu

Anca Constantinescu is with the University of Texas Southwestern Medical Center at Dallas, Texas 75390 USA, e-mail: anca.constantinescu@utsouthwestern.edu

Marc Jennewein is with Institute of Nuclear Chemistry, University of Mainz, D-55128 Mainz, Germany, e-mail: jennewein@mail.kernchemie.uni-mainz.de

Padmakar V. Kulkarni is with the University of Texas Southwestern Medical Center at Dallas, Texas 75390 USA, e-mail: padmakar.kulkarni@utsouthwestern.edu

Ralph R. Mason is with the University of Texas Southwestern Medical Center at Dallas, Texas 75390 USA, e-mail: ralph.mason@utsouthwestern.edu

Roderick W. McColl is with the University of Texas Southwestern Medical Center at Dallas, Texas 75390 USA, e-mail: roderick.mccoll@utsouthwestern.edu

Orhan Öz is with the University of Texas Southwestern Medical Center at Dallas, Texas 75390 USA, e-mail: orhan.oz@utsouthwestern.edu

Robert W. Parkey is with the University of Texas Southwestern Medical Center at Dallas, Texas 75390 USA, e-mail: robert.parkey@utsouthwestern.edu
Edmond Richer is with the University of Texas Southwestern Medical Center at Dallas, Texas 75390 USA, e-mail: edmond.richer@utsouthwestern.edu
Frank Rösch is with Institute of Nuclear Chemistry, University of Mainz, D-55128 Mainz, Germany, e-mail: frank.roesch@uni-mainz.de
Serguei Y. Seliounine is with the University of Texas Southwestern Medical Center at Dallas, Texas 75390 USA, e-mail: seruei.seliounine@utsouthwestern.edu
Nikolai V. Slavine is with the University of Texas Southwestern Medical Center at Dallas, Texas 75390 USA, e-mail: nikolai.slavine@utsouthwestern.edu
Philip Thorpe is with the University of Texas Southwestern Medical Center at Dallas, Texas 75390 USA, e-mail: philip.thorpe@utsouthwestern.edu
Alexander I. Zinchenko is with the University of Texas Southwestern Medical Center at Dallas, Texas 75390 USA, e-mail: alexandre.zintchenko@cern.ch

Abstract

Parameters of the Dallas Small Animal PET Imager are evaluated with phantoms and in small animal images. Spatial resolution and sensitivity of the system are characterized. Different algorithms of 3D image reconstruction are tested.

Index Terms

Image Reconstruction, Positron Emission Tomography, Small Animal Imaging.

1. Introduction

Nuclear imaging is a well recognized diagnostic modality. Single Photon Emission Computed Tomography (SPECT) and Positron Emission Tomography (PET) now are widely used in the clinic and in the laboratory. The technique detects radio labeled agents quantitatively at the picomolar level and detects normal and disturbed biochemical and physiological functions noninvasively and quantitatively that are not available otherwise. PET in animal research is a powerful technique capable of answering basic and applied questions in biology and pharmacology.

This paper presents a basic description of the Dallas Small Animal Imaging (SAI) PET system built in the Advanced Radiological Sciences Division of the University of Texas Southwestern Medical Center at Dallas [1] and presents the main parameters of the system. Results are illustrated with phantom and small animal studies.

2. Dallas Small Animal Imaging System Design

Fig. 1 is a schematic design of the Dallas SAI system. The system comprises two plastic fiber scintillator detectors [1-6], the position sensitive photo multiplier tube (PSPMT) light sensors, PET coincidence trigger electronics, and a custom-built FADC crate to digitize detector signals. The current Data Acquisition (DAQ) system is based on a multistandard platform: a custom back plane for the Analog-to-Digital Convertor (ADC) modules and a PXI (the Compact PCI standard from National Instruments) enclosure for the data readout from the ADCs. Two interface modules (PXI-6508 for slow control, and PXI-6533 for the fast data transfer) are included in this enclosure. The current data transfer rate is about 6 MB/s (~40 K events per second), with the possibility to attain a final data transfer rate of 40 MB/s. Small animal scans are usually performed with activity of 1-3 mCi and take from 20 to 40 minutes.

As shown in Fig. 1, each detector assembly and its two associated PSPMTs are enclosed in a housing, and both housings are mounted on a gantry with rotational and translational degrees of freedom. Objects to be imaged are placed between the detector pair and the separation adjusted to satisfy geometric constraints and to optimize sensitivity and field of view requirements.

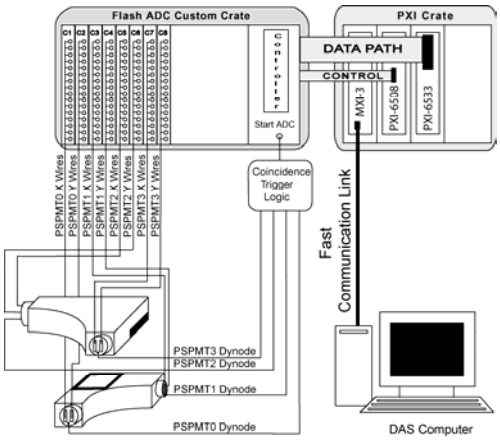

FIGURE 1. Schematic of System Hardware.

The detectors were fabricated using BCF-10 (Bicron Corp, Newbury, Ohio) scintillating plastic fibers. The fiber core is polystyrene $(C_8\ H_8)_n$ doped with butyl-PBD and dPOPOP. The fibers are clad in a non-scintillating Lucite cladding. Generally, the scintillation mechanism is via excitation of π-electrons in the butyl-PBD benzene ring. These ~365 nm photons penetrate through a plastic scintillator by a distance of ~1 mm and produce so-called X-Y "conferencing" effect firing the neighboring fibers due to wave-shifting mechanism with the dPOPOP to ~420 nm. This wavelength provides high fiber transparency and is also more compatible with the optimal spectral response of standard photo multiplies cathodes. At 511 keV PET, photon energy in plastic scintillator, the photo fraction is small and Compton scatter interactions dominate. The scatter electrons give up their energy well within a 1 mm range.

The detectors consist of an epoxied stack of 28 layers each containing 135 fibers. The criss-crossed overlap region forms a 13.5x13.5x2.8 cm^3 detector volume. Fig. 2 shows schematics of the PSPMT-to-detector fiber layout.

The high density of fiber intersection results in a near isotropic photon response for the detector. The fast response of plastic scintillators allows for high count-rate and low-noise performance. The fibers from a particular face are split into three equal blocks and stacked to form the optical interface to the tube. Light levels from the detector fibers are expected to be low. The average energy deposition from Compton scatter is ~175 keV. Therefore,

the PMT photo cathode emissions can range up to ~50 pe's for primary fibers and up to ~10 pe's for conferencing fibers.

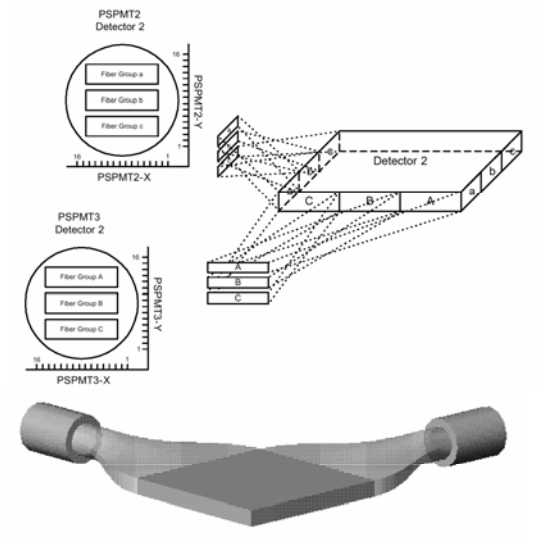

FIGURE 2. Scheme of PSPMT-to-Fiber Detector Layout.

PET events are detected by photon coincidences in the detector pair. The system is triggered by the coincidence of the signals from all four PSPMT. Signals from the dynodes of the PSPMTs are used for triggering. At present configuration, resolution time of the system is about 18 ns. Although scintillation light in fibers has fast decay time of 1-2 ns, preamplifiers receiving anode wires have a limiting bandwidth, and amplitude spread of signals degrades potential timing resolution. It is the obvious subject for further improvement.

A detector gantry provides for three-dimensional positioning and rotation of the detectors. Figure 3 shows the scanner assembly.

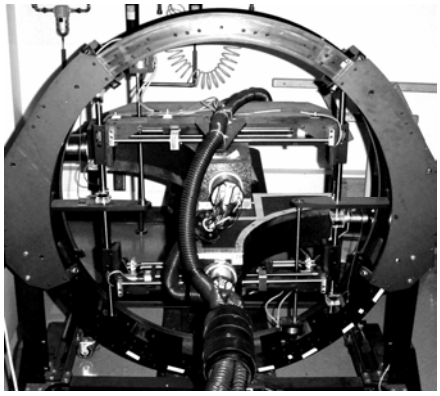

FIGURE 3. Overall view of detector assembly.

3. Analysis software and test results with phantoms

Data from the Small Animal Imager are recorded in list-mode. Analysis software starts with a primary information decoding step. The optimal algorithm of centroid finding that gives the position of a light cluster on the PSPMT face was based on fitting a Gaussian plus an offset to the wire amplitude profile, after pedestal subtraction. In the case of two clusters, the highest amplitude cluster is chosen. Several other simplified versions of centroid finding algorithms were also tested. Then conversion from the coordinate on the phototube to the three coordinates in the detector is made. Further analysis includes 3D reconstruction, and several approaches were tried. First, we have reconstructed three-dimensional radio labeling distribution using a so-called line-clustering algorithm [7]. This is a novel algorithm giving an excellent spatial resolution. However, it is rather slow in computation. We used also an approach [8, 9, 10] based on Defrise's extended back projection filtered reconstruction algorithm developed for the truncated geometries provided by practical detectors. We found that Maximum Likelihood - Expectation Maximization (ML-EM) algorithm [11] is one of the most reliable 3D reconstruction approaches for scanner like ours. Furthemore, a system modeling modification of the algorithm [12] provides high quality images and quantification. We further developed ML-EM with a deblurring algorithm [13] and used it for data analysis. Having reconstructed lines, some parameters of the system can be easily evaluated. First, a ^{22}Na 7 μCi point-like

(1 mm in diameter) positron source was used for the tests. With a 90 mm separation between the detector surfaces and 10 mV trigger discriminator thresholds the trigger rate for the source placed in the center was 4100 cps (620 c/μCi), i.e. 1.7%. The Monte Carlo dependence of the efficiency of the detector upon position is illustrated in Fig. 4.

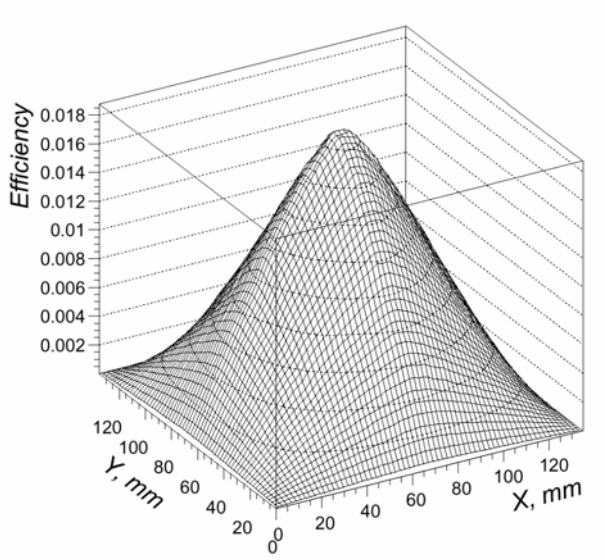

FIGURE 4. X-Y efficiency plot (Monte Carlo, smoothed). Detector separation is 90 mm.

Efficiency of the reconstruction of lines from the recorded data depends on software cuts applied (minimal amplitude of cluster, etc.) and varies from a 90% to a typical 30%. Fig. 5 shows results obtained with the standard analysis. The left plot is a two-dimensional planar back projection X-Y distribution of the events from the ^{22}Na positron source in the source Z-plane. The right plot is the Y-projection of the distribution; the graph is fitted to a Gaussian plus an offset. Gaussian σ_y is 1.5 mm, and the noise-to-signal ratio is about 10% (Y-view). The point source image shown in Figure 5, top panel, exhibits a "cross-like" artifact. One of the most common causes for incorrect calculation of the coordinate is a double light cluster on a PSPMT photo cathode.

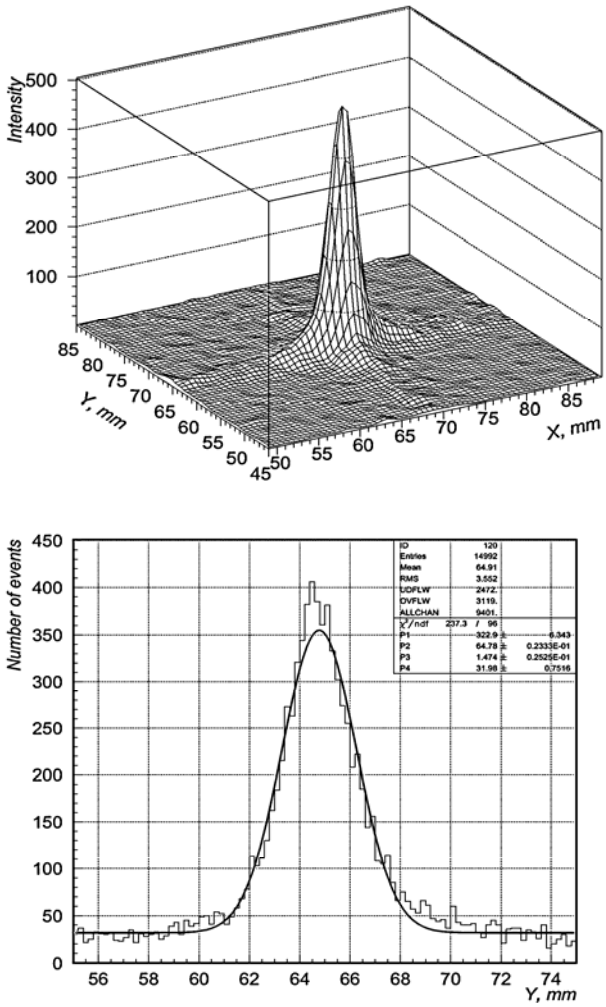

FIGURE 5. Point-like ^{22}Na source image parameters. Detector separation is 100 mm. Upper graph - two-dimensional X-Y distributions, lower graph – Y-distribution of reconstructed events fitted to a Gaussian plus an offset. σ_y is 1.5 mm; noise-to-signal ratio is about 10%.

This could happen in the case of double Compton interaction of a photon in the detector. In the case of ^{22}Na source it could also happen when interaction of a 511 keV photon accompanies the interaction of a 1275 keV photon. Since double interaction in either of two detectors can lead to incorrect line reconstruction, this fraction may be significant. As we mentioned earlier, the coordinate finding algorithm chooses the cluster with the higher amplitude, which does not necessarily coincide with the first Compton interaction of 511

keV photon, which provides the correct line. If the coordinate is corrupted in only one phototube of the detector, it gives a typical “cross-like” behavior arises in the background. Figure 6 illustrates such an event.

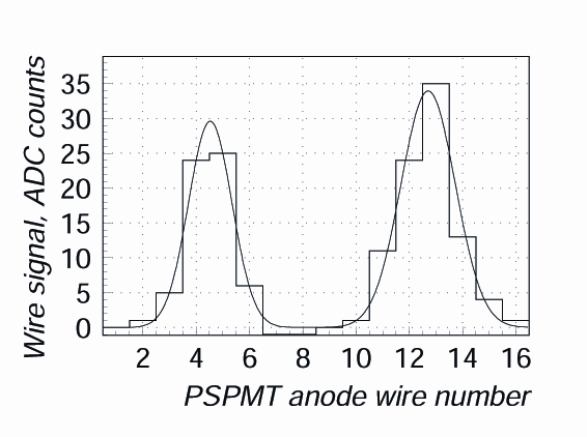

FIGURE 6. Example of an event profile in X-direction (along the fiber blocks) produced by double interaction.

Fig. 7 shows results when the two detectors were separated by 270 mm. In addition, the lines were selected within $\pm 11^{o}$ in the X- and Y-view. The effect of double Compton scattering and of third photon here artificially reduced by the angular cuts. σ_y is 1.2 mm, noise-to-signal ratio is 3%.

We compare the data collected with ^{22}Na point-like source (1 mm in size) and point-like source with ^{18}F (about 1.5 mm in size). Fig. 8 presents these data with detector separation of 200 mm. The background for ^{22}Na source is visibly higher than for ^{18}F.

Figure 9 shows fraction of the events *vs* radius of circle around the center of source position in the X-Y plane for ^{22}Na and ^{18}F sources. Data suggest that background counts outside the central peak (a circle of 6 mm radius around the peak in X-Y plane, which is about 3.5 FWHM) are ~50% for ^{22}Na source and ~30% for ^{18}F source. Double Compton scattering contributes to the background, as also some misidentification of fiber blocks on PSPMTs. An additional part of background events from ^{22}Na source is due to the presence of third gamma.

Figure 10, top, presents X-distribution of reconstructed line intersections with the Z-plane of the^{18}F line phantom in 60 mm diameter Lucite cylinder, imitating a body of a rat. Comparison with a “neck" line phantom results on Fig. 10, bottom, gives the Compton scatter fraction in 60 mm diameter Lucite phantom of about 15%.

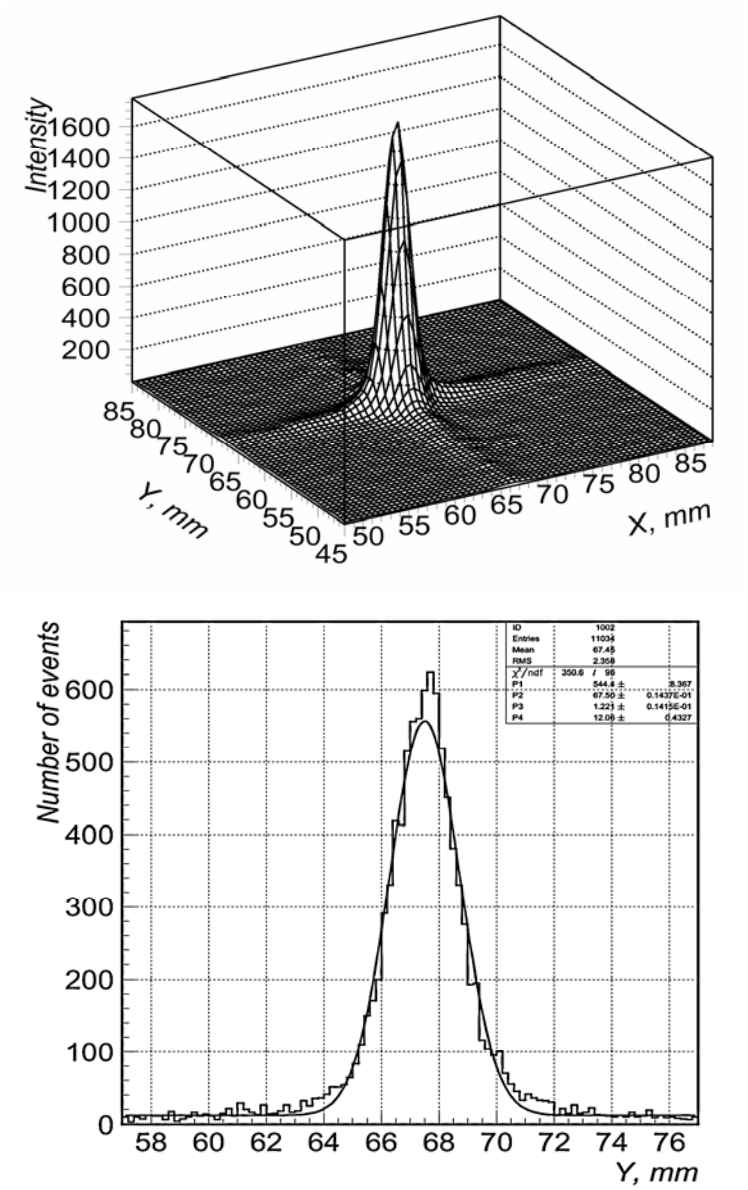

FIGURE 7. Point-like ^{22}Na source image, separation between detectors 270 mm, lines selected within $\pm 11^{o}$ of vertical. Upper graph - two-dimensional X-Y distribution, lower graph – Y-distribution of reconstructed events fitted to a Gaussian plus an offset. σ_y is 1.2 mm, noise-to-signal ratio is 3%.

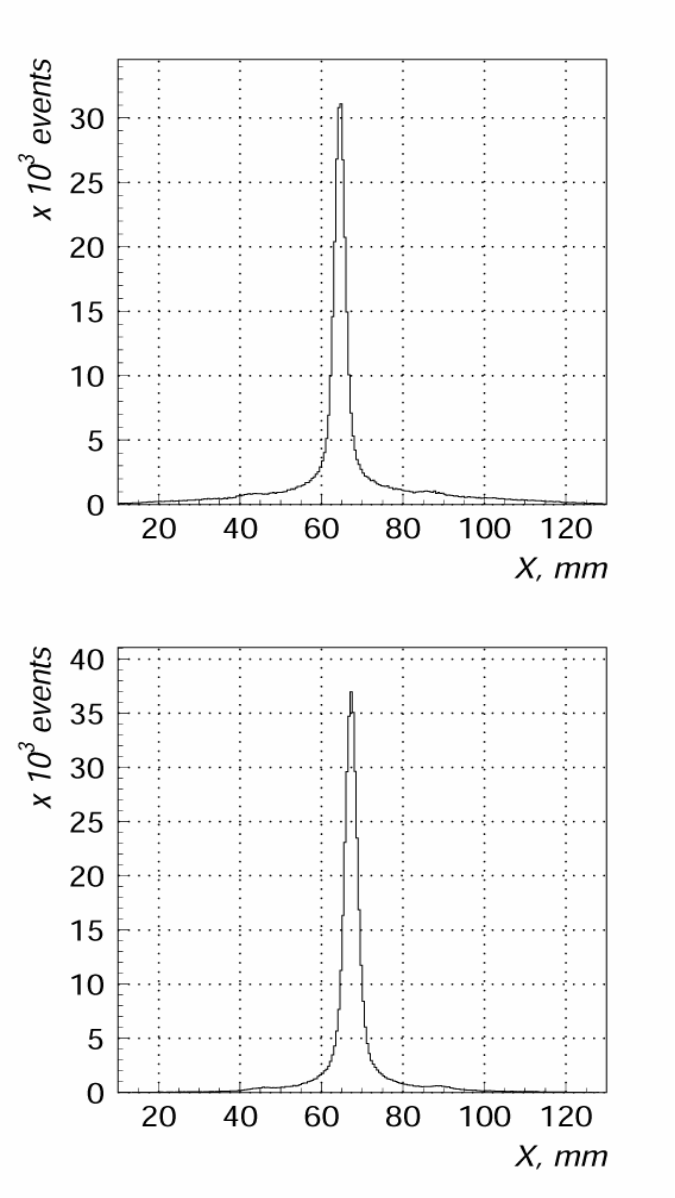

FIGURE 8. Upper graph: X-distribution of line intersections with a source plane in the case of point-like (1 mm) ^{22}Na source. Lower graph: similar distribution for point-like (1.5 mm) ^{18}F source. The background for ^{22}Na source is visibly higher than for ^{18}F.

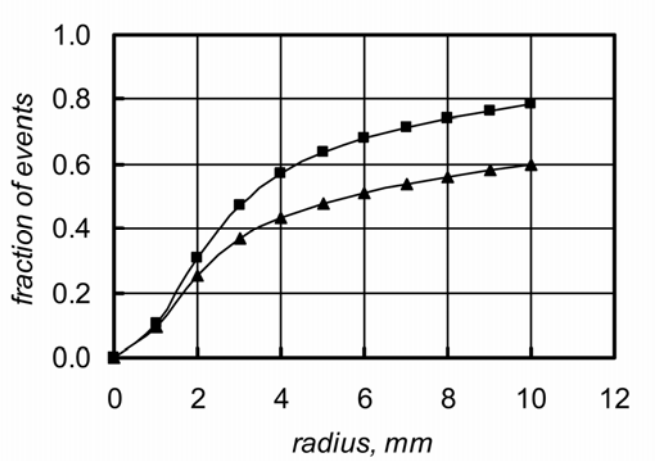

FIGURE 9. Fraction of the events *vs* radius of circle around the center of source position in the X-Y plane for ^{18}F and ^{22}Na sources. Data suggest that background counts outside the central peak (a circle of 12 mm diameter in X-Y plane, which is about 3.5 FWHM) are ~50% for ^{22}Na source and ~30% for ^{18}F source.

Fig. 11 presents the resolution data from the line phantoms, thin glass tubes filled with ^{18}F. The upper graph presents the data from a single line phantom. FWHM of the distribution is about 2 mm. The lower graph presents the data when a center-to-center separation of the two tubes placed in proximity of each other is 2.05 mm. The initial separation is noticeable.

Figure 12 presents results of the reconstruction of transaxial images of a Hoffman brain phantom, showing good spatial correspondence between the PET (top) and X-ray projection (bottom) images. 3D reconstruction in a phantom slice is performed using the line-clustering algorithm [7]. The method of obtaining a single image of an object larger than the field of view, involving multiple motions of the detectors in the gantry, is currently being perfected, and this is only a preliminary result partially affected by summation and calibration imperfections.

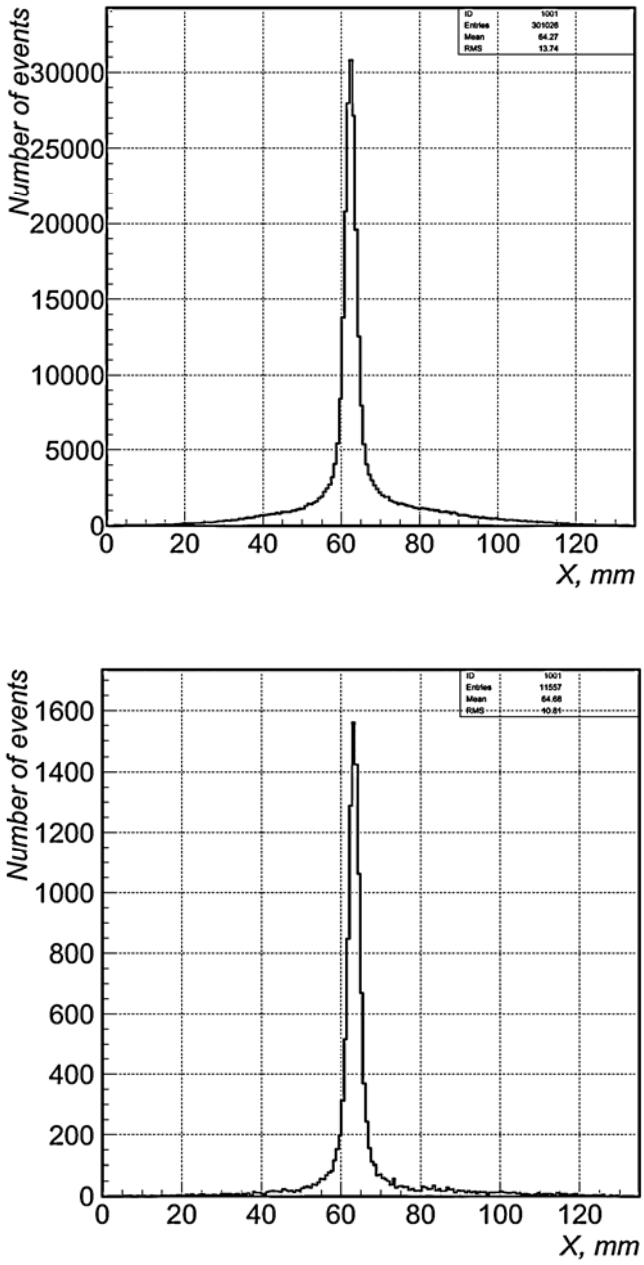

FIGURE 10. Upper graph: X-distribution of line intersections with the ^{18}F 2 mm line plane in 60 mm diameter Lucite phantom. Comparison with a "neck" ^{18}F 1 mm line phantom results (lower graph) gives the Compton scatter fraction in 60 mm diameter acrylic phantom of less than 15%.

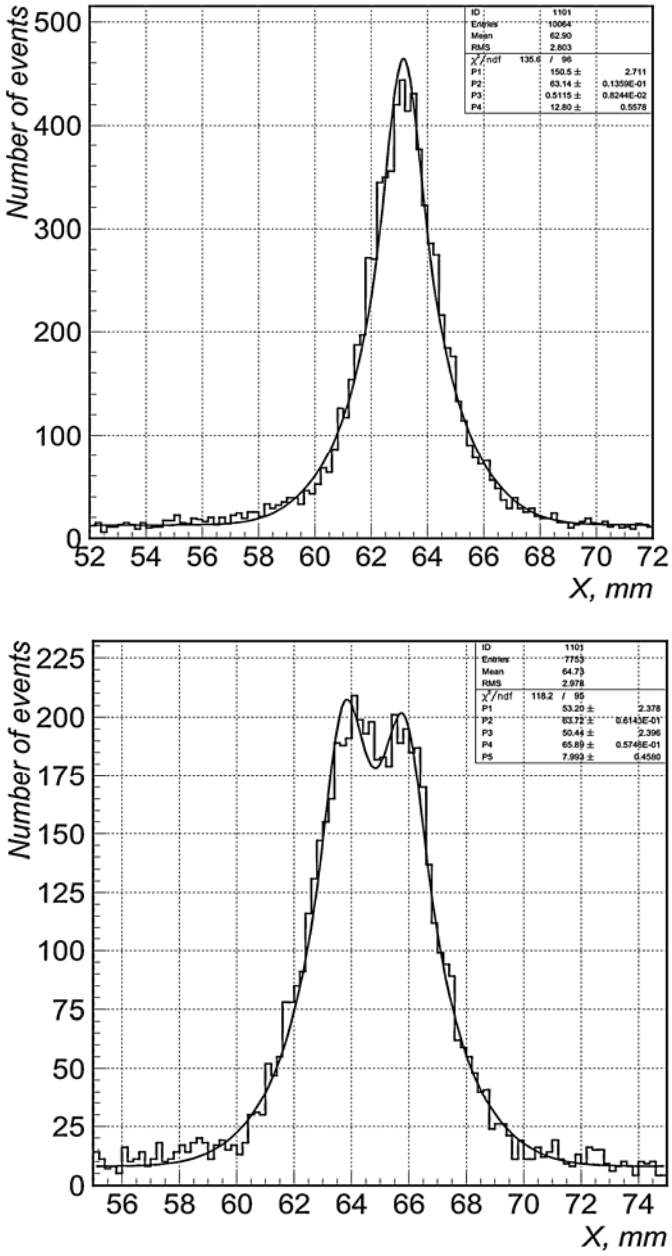

FIGURE 11. Upper graph: single thin glass tube filled with ^{18}F, lower graph: double line with center-to-center separation of 2.05 mm. The initial separation is noticeable.

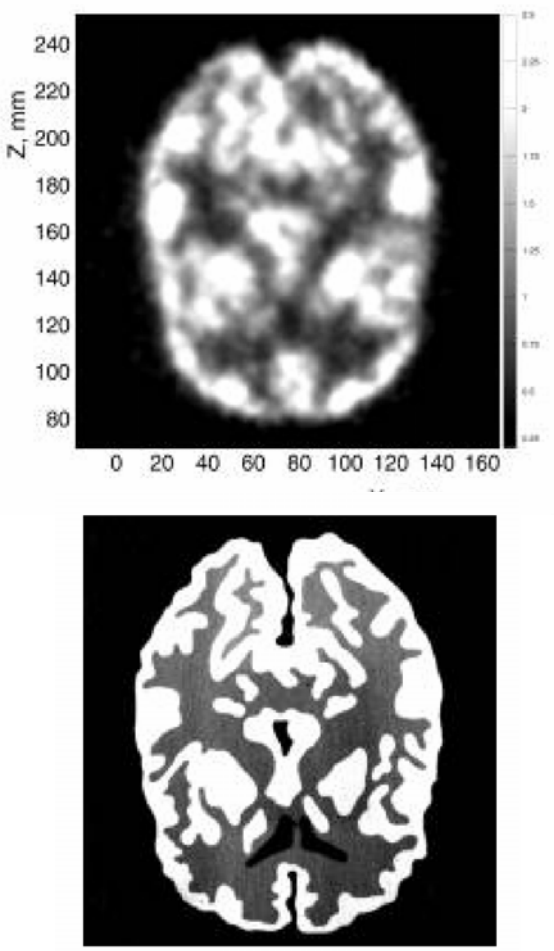

FIGURE 12. Transaxial images of a Hoffman human brain phantom, showing good spatial correspondence between the PET (upper) and X-ray projection (lower) images.

Figure 13 presents results of reconstruction of an ^{18}F FDG 2 mm diameter line in a 60 mm diameter Lucite phantom for five different line source intensities. This test was done to evaluate saturation of our detectors and electronics. The images are normalized to the maximum. Although line is reconstructed even at 13 mCi source, practical range of intensity is below 3 mCi. Above this intensity, the quality of an image degrades, as also efficiency of line reconstruction. As we mentioned earlier, the bandwidth of the PSPMT

preamplifiers is a most limiting factor in our system. We are going to upgrade this electronics.

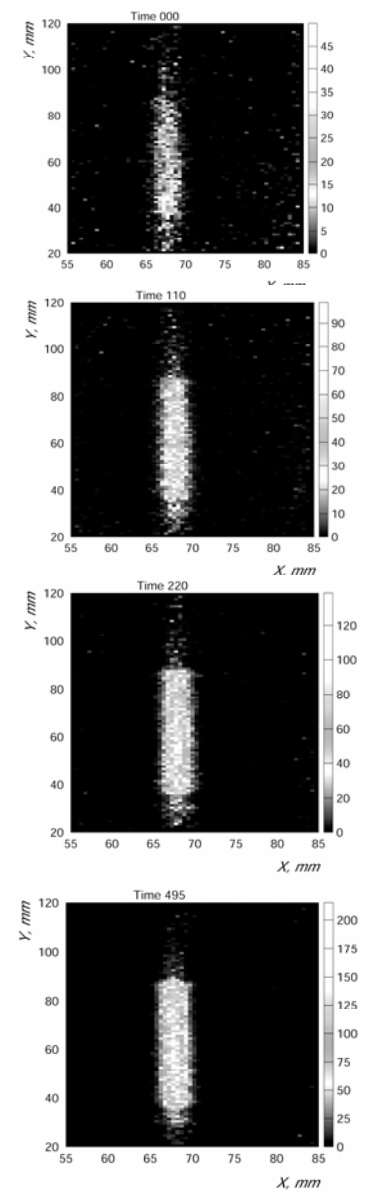

To test the reconstruction characteristics of the Small Animal Imager, a hot-spot resolution phantom was imaged. The phantom is an 11.5 cm diameter by 2 cm thick Lucite disc, with holes of differing diameters. Fig. 14 (top) shows a transaxial projection through a 3D reconstruction of an imaging experiment using an ^{18}F activity fill (~500 μCi). For the experiment, 2 mm, 4 mm and 10 mm diameter holes were filled with activity. The phantom was placed coaxial with the detector rotation axis, and the detectors were rotated to acquire a complete 3-D data set (~2 million valid events were collected in a 2.8 hr acquisition).

The reconstruction software for the list-mode acquisition data from the Small Animal Imager planar detectors was based on Defrise's extended back projection filtered reconstruction algorithm developed for the truncated geometries provided by practical detectors. The extended back-projection filtered reconstruction (BFR) algorithm of Defrise et al: [8], [9], [10] was developed and implemented.

As shown in Fig 14 (up), all activity locations in the phantom were resolved in the reconstruction of the experimental data. These locations included a pair of 2 mm diameter holes with a 2 mm edge-to-edge separation. Fig 14 (down) shows an iso-surface rendering, thresholded to display maximum detail. The general features of the activity distribution are apparent, and the detail is sufficient to reveal an air bubble that was discovered in one of the holes (in the 2

mm diameter hole segment).

Intensity differences in Fig 14 reflect activity concentration differences in the holes. Fig. 15 shows a bar chart comparing the ideal source activity concentrations to cylindrical region-of-interest (ROI) voxel amplitude sums from the reconstruction. After background scatter corrections, the percentage differences between the measured and expected concentrations are in very good agreement (better than ~5%), demonstrating the quantitative ability of the Small Animal Imager.

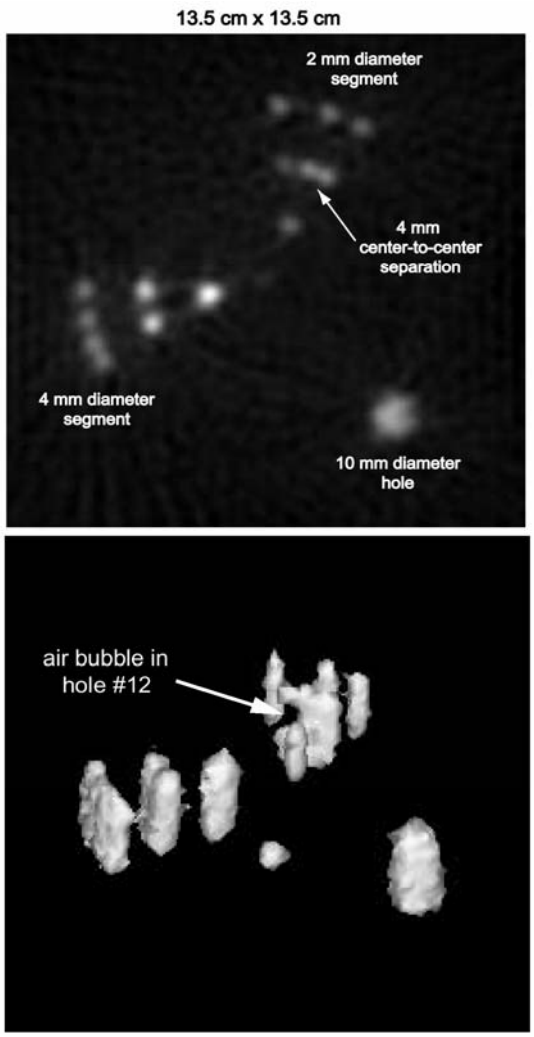

FIGURE 14. Hot-Spot Phantom Reconstructions. Top picture - transaxial projection, bottom picture - iso-surface rendering.

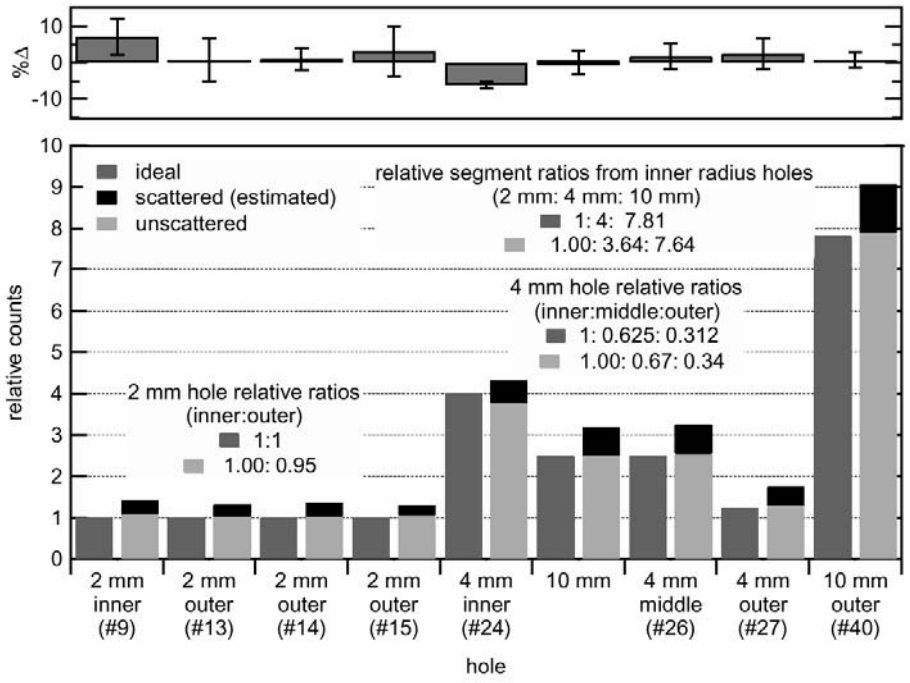

FIGURE 15. Summed ROI voxel signals from the Hot-Spot Phantom reconstruction.

4. Spatial Resolution

To obtain a spatial resolution of the system, we scanned a ^{22}Na source of 1 mm in diameter locating it in 9 different places across the median plane between the two detectors. 400,000 events were detected for each position of the source. Data were processed by the ML-EM algorithm. Results are presented in Table 1. Upper rows – position of the source, lower rows – FWHM resolution in X-direction (the first line) and Y-direction (the second line). All dimensions are in millimeters. Taking into account the size of the source and other smearing effects like positron range in a media we can conclude that the spatial resolution of our PET scanner is better or about equal to 2 mm in entire volume.

x = 0	x = 0	x = 0	x = 0	x = 0	x = -50	x = -25	x = 25	x = 50
y = -50	y = -25	y = 0	y = 25	y = 50	y = 0	y = 0	y = 0	y = 0
1.9	2.0	2.5	2.5	2.2	2.7	2.6	2.4	2.3
2.4	2.1	2.2	2.3	2.3	2.0	2.1	2.0	1.9

TABLE 1. ML-EM algorithm results of data processing

As we mentioned earlier, system modeling modification of the algorithm [12] provides high quality images and quantification. With system modeling spatial resolution of our scanner is better than 0.6 mm.

5. Small Animal Imaging

The Small Animal Imager was used recently for bone research, cancer studies, brain tumor imaging and lung metastases [15], [16], [17]. Some results are presented here as an illustration of the scanner parameters. In addition, recent studies on the in vivo characteristics of ^{74}As-labelled antibodies are described.

Figure 17 presents a 10 mm coronal slice of a mouse with two melanoma tumors implanted. 700 μCi FDG is used to scan the mouse in about 30 minutes. 3D PET reconstruction is performed by the line-clustering algorithm [7]. Figure 17, top, PET X-Y slice is shown with x-ray image superimposed. Left and right side tumors are perfectly visible. For comparison, bottom – the only x-ray image presented.

Bone studies with mice were performed using $^{18}F^{-}$. Figure 18 presents most intense voxel projections (MIP) image of a normal mouse with ^{18}F. 3D reconstruction was carried out with ML-EM algorithm using system modeling [13, 16]. Scull, ribs, spine, femur details are obviously visible.

FIGURE 17. Top - mouse with FDG, two melanoma tumors are implanted. PET X-Y slice is shown with X-ray image superimposed. Left and right side tumors are perfectly visible. For comparison, bottom – the X-ray image.

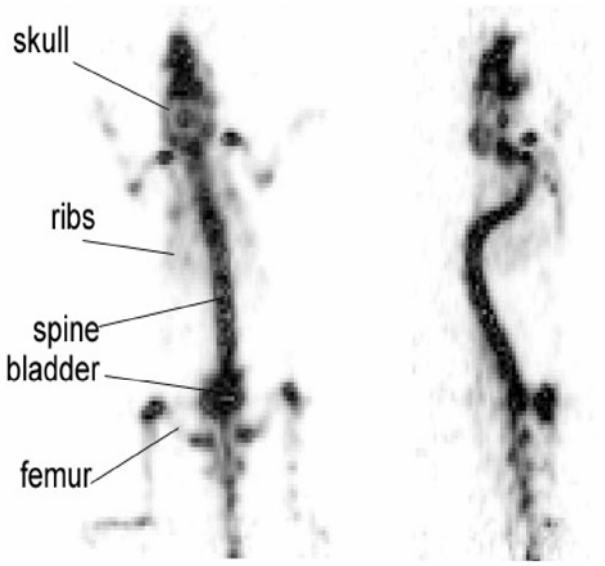

FIGURE 18. Posterior and lateral mages of a normal mouse with $^{18}F^{-}$.

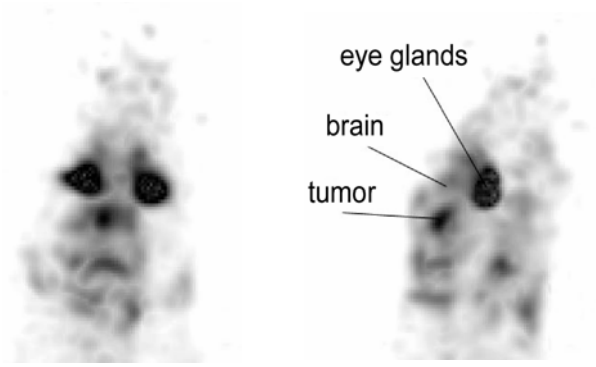

FIGURE 19. Posterior and lateral MIP images of a Copenhagen rat with FDG. Tumor is implanted in the brain.

FDG scans are very effective for cancer studies. Figure 19 shows two orthogonal most intense voxel projections (MIP) of the 3D image of a Copenhagen rat brain with FDG. Tumor is implanted in the brain.

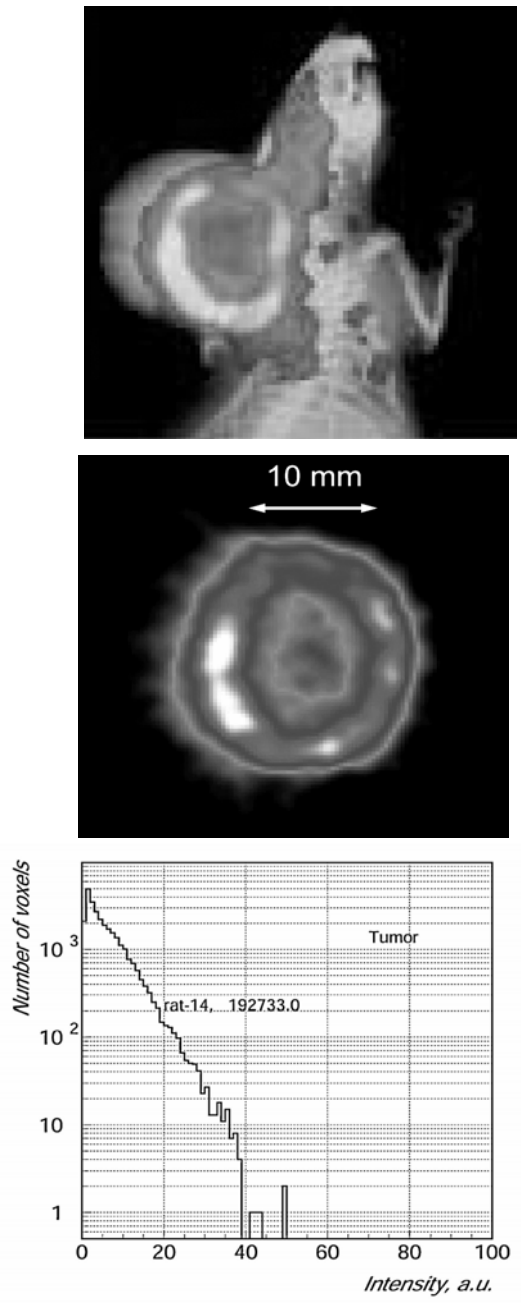

FIGURE 20. Upper image - Copenhagen rat with melanoma cancer implanted, PET with X-ray image overlaid. Middle – a 2 mm slice of another melanoma Copenhagen rat, the FDG PET image. A metabolic activity of the FDG is seen predominantly on the surface of the tumor. A typical activity distribution in tumor presented in the lower graph.

Figure 20 presents Copenhagen rat with melanoma cancer implanted. Top – a slice of the FDG PET image and the X-ray image are overlaid. Middle – an example of a slice of a melanoma cancer in a rat. A metabolic activity of the FDG is seen on the surface of the tumor. A typical activity distribution in tumor is presented in the bottom graph.

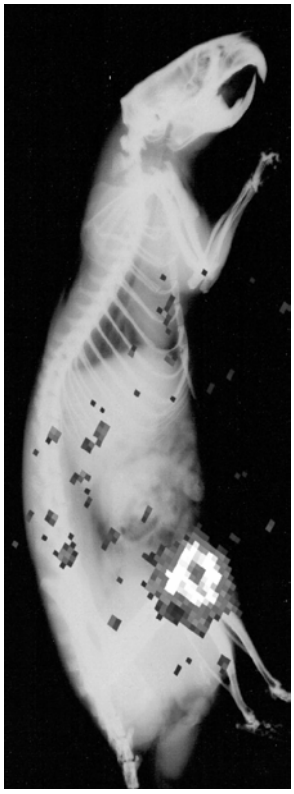

FIGURE 21. A Dunning prostate R3327-AT1 tumor bearing male Copenhagen rat with [^{74}As]SATA-ch3G4. Lateral view, 72h post injection.

We also studied the positron emitting isotope ^{74}As. Radioactive arsenic isotopes, such as ^{74}As and ^{72}As have promising properties for eventual application in radiopharmaceuticals [26,27]. The antibody and vascular targeting agent Vatuximab® (Anti-PS, ch3G4) was chosen as a model system for the first *in vivo* experiments. ^{74}As has a positron emission rate of 29% and positron energies of $E_{\beta+max}$ = 1.5 MeV; $E_{\beta+mean}$ = 0.9 MeV. The long physical half-life of 17.8 days makes the isotope convenient for multiple scans in small animal models. ^{74}As and ^{72}As are representing possible PET isotopes of choice for biochemical/physiological processes with longer biological half-lives, like immunoimaging and receptor mapping. The versatile chemistry of arsenic permits the radiolabeling of a broad spectrum of potentially valuable pharmaceuticals. Figure 21 shows a Dunning prostate R3327-AT1 tumor bearing male Copenhagen rat which was injected with 300 μCi of [^{74}As]SATA(N-Succinimidyl-S-acetylthioacetate)-ch3G4. The image was taken 72h post injection and overlayed with an X-ray picture. Tumor and enrichment and heterogeneity of activity distribution inside the tumor can be clearly observed.

Figure 22 shows the image of the rat brain activity in our experiments with cocaine addiction. Left: PET image of the rat brain slice of 1.6 mm thick. Right: for comparison, a photograph of a rat brain.

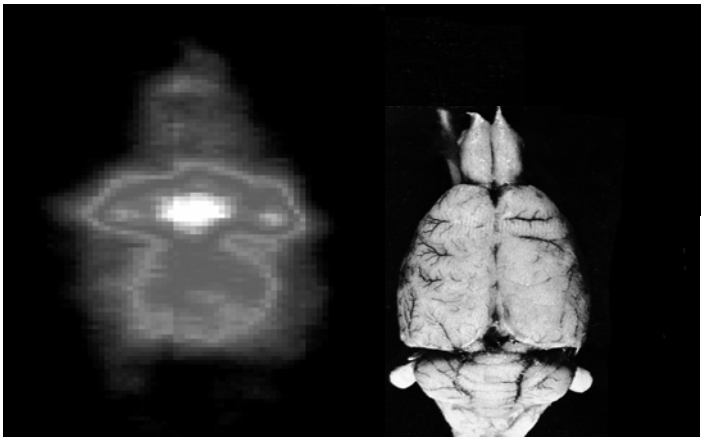

FIGURE 22. Left: PET image of the rat brain slice of 1.6 mm thick, from our experiments with cocaine addiction. Right: for comparison, a photograph of a rat brain.

6. Conclusion

Small animal PET scanners become very popular instruments for biological interrogations. Genetically modified animals revolutionized biological research, and noninvasive imaging of reporter gene expression with new radiolabeled agents widens possibilities for scientific research and for tests of new drugs. Among most succesful PET scanners for small animals is the microPET family: microPET, microPET II, P4, R4, Focus [18-25]. Based on a ring of high density small size LSO crystals, these scanners provide spatial resolution under 1 mm and have a good sensitivity.

In our SAI scanner probability of detection of 511 keV photon in one detector is about 20% instead of about 90% typical for LSO crystal elements. However, the area of the detectors in SAI is much larger than the detector elements in microPET family, and that compensates lower detection efficiency. Measurement of the Depth Of Interaction (DOI) in microPET family is limited, and spatial resolution usually degrades with radial offset. In SAI spatial information from detectors is truly three dimensional, which completely eliminates so-called parallax errors. MicroPET family scanners use a full energy deposition window to reduce scattering background to some degree. SAI is based on Compton

interaction, full energy deposition measurements therefore are limited, and an energy window cut is not applicable. However, in the case of small animals background due to scattering is not a serious problem and could be modelled during 3D reconstruction [14]. SAI is much simpler system and correspondingly more robust.

The following parameters characterize the Small Animal Imaging scanner:

Detector type	Scintillating optical fibers
Dimensions (mm)	135x135x28 (3780 fibers)
Detection	4 PSPMTs, 128 channels
Equivalent radius	Variable 5-45 cm
Spatial resolution without system modeling	~2 mm, isotropic
Spatial resolution with system modeling	~0.6 mm, isotropic
Sensitivity (ID=17 cm)	6.5 cps/kBq
Scatter fraction	15% for Lucite of 6cm diameter

TABLE 20. Parameters of the Dallas Small Animal Imaging System

Small Animal Imager of our design provides good images for biological research. Cancer of different types, bone studies, brain activity research are performed at SAI routinely. Good sensitivity and sub-millimeter spatial resolution make SAI perfect instrument for biological studies. The scanner is reasonably fast, reliable and simple in operation. Besides the biological value of the device, it is good test bed for software modification and improvements. The system is relatively inexpensive.

Acknowledgement

We appreciate very much the help from Dr. M. Lewis, Mr. B. Smith and Mr. T. Nguyen. The work was supported in part by the Cancer Imaging Program (an NCI Pre-ICMIC).

References

1. P. V. Kulkarni, J. A. Anderson, P. P. Antich, J. O. Prior, Y. Zhang, J. Fernando, "New approaches in medical imaging using plastic scintillating detectors", *Nuclear Instruments and Methods in Physics Research B79* (1993) 921-925.
2. Anderson J, Fernando J, Nguen T, Prior JO, Constantinescu A, Parkey RW, Antich PP, Chaney RC, Hammock H, and Fenyves EJ, "Constructing a Small Laboratory Animal Imaging Device Based on Scintillating Fibers", *Scintillating Fiber Technology and Applications, Proc. SPIE*, 2007 (1993) 125-131.
3. Prior JO, Antich PP, Fernando J, Anderson JA, Kulkarni PV, Parkey RW, Chaney RC, and Fenyves EJ, "Imaging Strategies with Scintillating Fiber Detectors: Issues and Preliminary Results", *Scintillating Fiber Technology and Applications, Proc. SPIE*, 2007 (1993) 116-124.
4. Kulkarni PV, Antich PP, Constantinescu A, Prior J, Nguen T, Fernando J, Anderson JA, Weitman SD, Kamen BA, Parkey RW, Chaney RC, and Fenyves EJ, "Folate Receptor Imaging with ^{125}I Labeled Folic Acid with a Whole Body Small Animal Imaging Device Built with Plastic Scintillating Optical Fibers", *Nuclear Instruments and Methods in Physics Research,* B99 (1995) 800-803.
5. PP Antich, R Parkey, and J Anderson, "Position Sensitive Gamma-Ray Detector", U.S. Patent No. 5,281,821 issued 25 January 1994.
6. J Anderson and PP Antich, "Position Sensitive Radiation Detector", U.S. Patent No. 5,334,839 issued 2 August 1994.
7. P. Antich, R. Parkey, N. Slavine, E. Tsyganov, A. Zinchenko, "Compact Compton Camera Design: Parameters and Imaging Algorithm", *IEEE Nuclear Science Symposium & MIC-2000*, Conference Record, Paper N225, October 14- 20, 2000, Lyon, France.
8. Defrise, M., Kuijk, S., and Deconinck, F., "A new three-dimensional reconstruction method for positron cameras using plane detectors", *Physics in Medicine and Biology* 33, 1 (1988), 43-51.
9. Clack, R., Townsend, D., and Jeavons, A., "Increased sensitivity and field of view for a rotating positron camera", *Physics in Medicine and Biology* 29, 11 (1984), 1421-1431.

10. G. M. Arbique, *Ph.D. thesis*, "Three-Dimensional Reconstruction for a Positron Annihilation Volume Imager", University of Texas Southwestern Medical Center at Dallas, Dallas, TX, May 2000.
11. L. A. Shepp and Y. Vardi, "Maximum likelihood reconstruction for emission tomography", *IEEE Transaction in Medical Imaging*, v.1, 1982, pp.113-122.
12. Andrew J. Reader et al., "One-Pass List-Mode EM Algorithm for High Resolution 3D PET Image Reconstruction into Large Arrays", *IEEE Transactions on Nuclear Science*, v.49, no 3, June 2002, p. 693.
13. P. Antich, R. Parkey, S. Seliounine, N. Slavine, E. Tsyganov, A. Zinchenko, "Application of Expectation Maximization Algorithms for Image Resolution Improvement in PET Systems", *IEEE Transactions on Nuclear Science*, accepted for publication.
14. Reader, A.J.; Sha Zhao; Julyan, P.J.; Hastings, D.L.; Zweit, J., "Adaptive correction of scatter and random events for 3-D backprojected PET data", *IEEE Transactions on Nuclear Science*,Volume: 48 , Issue: 4 , Aug. 2001 pp. 1350 – 1356
15. Öz OK, Hirasawa G, Lawson J, Nanu L, Constantinescu A, Antich PP, Mason RP, Tsyganov EN, Parkey RW, Zerwekh JE, Simpson ER: "Bone phenotype of aromatose deficient mouse", *Journal of Steroid Biochemistry and Molecular Biology*, 2001, 79:49-59.
16. E. N. Tsyganov, A. I. Zinchenko, N. V. Slavine, P. P. Antich, S. Y. Seliounine, O. K. Oz, P. V. Kulkarni, M. A. Lewis, R. P. Mason, R. W. Parkey, "Reconstruction Algorithm With Resolution Deconvolution For 3-D Image In A Small Animal Pet Imager", *Chapter 10 in book on the University of Arizona SPECT Workshop*, Tucson, Arizona, January 2004.
17. P. Antich P., A. Constantinescu, R. Mason, R. McColl, O. K. Oz, P. Kulkarni, S. Seliounine, N. Slavine, E. Tsyganov, "FDG Imaging of Lung Metastases in Copenhagen Rats on a Small Animal PET System with Position-Encoding Fiberoptic Detectors", *Journal of Nuclear Medicine*, 43(5) (2002) 216.
18. Chatziioannou, AF, Cherry, SR, Shao, Y, et al. Performance Evaluation of microPET: A High-Resolution Lutetium Oxyorthosilicate PET Scanner for Animal Imaging. *Journal of Nuclear Medicine*, 40, 1164-1175, 1999.

19. Y-C Tai, Chatziioannou, A.F., Dahlbom, M., Cherry, S.R. System design for a 1mm3 resolution animal PET scanner: microPET II. *2000 IEEE Nuclear Science Symposium Conf. Rec*., vol.3, p.21/52.

20. A. F. Chatziioannou, "PET scanner dedicated to molecular imaging of small animal models," *Molecular Imaging and Biology*, vol. 4, no. 1, pp. 47-63, 2002.

21. Y. C. Tai, A. F. Chatziioannou, Y. Yang, R. W. Silverman, K. Meadors, S. Siegel, D. F. Newport, and J. R. Cherry, "MicroPET II: design, development and initial performance of an improved microPET scanner for small-animal imaging," *Phys. Med. Biol.*, vol. 48, pp. 1519-1537, 2003.

22. Y.-C. Tai *et al.*, "MicroPET II: design, development and initial performance of an improved microPET scanner for small-animal imaging," *Physics in Medicine and Biology*, **48**, pp. 1519–1537, 2003.

23. Chatziioannou, A. F., S. R. Cherry, Y. Shao, R. W. Silverman, K. Meadors, T. H. Farquhar, M. Pedarsani and M. E. Phelps "Performance evaluation of microPET: a high-resolution lutetium oxyorthosilicate PET scanner for animal imaging." *J. Nuc. Med.* **40**(7) (1999) 1164-1175.

24. Y. C. Tai, A. Chatziioannou, S. Siegel, J. Young, D. Newport, R. N. Goble, R. E. Nutt, and S. R. Cherry, "Performance evaluation of the microPET P4: a PET system dedicated to animal imaging," *Physics in Medicine and Biology*, vol. 46, pp. 1845-1862, 2001.

25. Cherry SR, Shao Y, Silverman RW, Meadors K, Siegel S, Chatziioannou A, Young JW, Jones WF, Moyers JC, Newport D, Boutefnouchet A, Farquhar TH, Andreaco M, Paulus MJ, Binkley DM, Nutt R, Philps ME: MicroPET: A high resolution PET scanner for imaging small animals. *IEEE Transactions on Nuclear Science*, vol.44, No. 3:1161-1166, 1997.

26. Jennewein, M., A. Schmidt, A.F. Novgorodov, S.M. Qaim, F. Rösch, *A no-carrier-added $^{72}Se/^{72}As$ radionuclide generator based on distillation*, Radiochimica Acta, 92, 245-249 (2004)

27. Jennewein, M., Schirrmacher, R, Maus , S. Rösch, F., *Macroscopic Syntheses of Arsenoorganic Precursors and first no-carrier-added Radioarsenic Labelling,* J. Lab. Comp. Radiopharm. 46, S42 (2003)

IX.

Verfahren zur Herstellung von trägerfreiem ^{72}As und Vorrichtung zur automatischen Herstellung von trägerfreiem ^{72}As und trägerfreiem ^{72}As (III)-Halogenid sowie deren Verwendung

Verfahren zur Herstellung von trägerfreiem ^{72}As und Vorrichtung zur automatischen Herstellung von trägerfreiem ^{72}As und trägerfreiem ^{72}As (III)-Halogenid sowie deren Verwendung

Deutsches Patent Nr.: DE 103 44 101 B3

Die Erfindung betrifft ein Verfahren zur Herstellung von trägerfreiem ^{72}As und eine Vorrichtung zur automatischen Herstellung von trägerfreiem ^{72}As und trägerfreiem ^{72}As(III)-Halogenid, welche in der Chemie und Radiopharmazie sowie Nuklearmedizin verwendet werden. Insbesondere betrifft die Erfindung die Gewinnung von und Synthesechemie mit trägerfreiem (im Folgenden bezeichnet mit ‚no-carrier-added' bzw. ‚nca' ^{72}As und ^{72}As(III)-Halogeniden.

Hintergrund der Erfindung

Mit Hilfe der Positronen-Emissions-Tomographie (PET) ist es möglich, biochemische Prozesse *in vivo* zu quantifizieren. Dazu sind beispielsweise neurobiologisch oder tumorbiologisch relevante Moleküle mit solchen geeigneten Radioisotopen zu markieren, die eine hohe Positronen-Emissionsrate haben. Diese Positronen treffen in unmittelbarer Nähe ihres Emissionsortes auf Elektronen und werden beim Zusammenstoß mit diesen vernichtet. Die dabei entstehende Annihilationsstrahlung besteht zum größten Teil aus zwei γ-Strahlen mit einer Energie von jeweils 511 keV. Die beiden Photonen werden in einem Winkel von 180 Grad ausgestrahlt. Diese Tatsache ermöglicht, tomographisch den Ort des Zusammenstoßes zu berechnen. Mit Hilfe einer Koinzidenzschaltung werden die beiden Photonen von zwei gegenüberliegenden Detektoren registriert. Die erhaltenen Informationen werden mit Hilfe tomographischer Algorithmen in Bilder und Zeit-Aktivitäts-Daten umgerechnet. Wendet man die PET zum Beispiel beim Menschen an, liefern die dabei entstehenden Aufnahmen Informationen über Stoffwechselvorgänge einzelner Organe.

Die meisten PET-Pharmaka enthalten kurzlebige Radioisotope wie zum Beispiel Fluor-18, Kohlenstoff-11, Stickstoff-13 oder Sauerstoff-15. Sind die zu untersuchenden Vorgänge viel langsamer als die Halbwertszeit der genannten Radioisotope, können die mit solchen Radioisotopen markierten Radiopharmaka nicht eingesetzt werden. Ein längerlebiges Radioisotop könnte in solchen Fällen sehr hilfreich sein, langsam ablaufende Stoffwechselvorgänge zu untersuchen.

Arsen-72 ist ein potentielles PET-Radioisotop zur Untersuchung langsam ablaufender Stoffwechselvorgänge. Die Halbwertszeit von Arsen-72 beträgt 26 h und es emittiert mit einer hohen Rate von 88% Positronen mit $E_{\beta+\ max.}$ = 2,5 MeV. Es kann direkt über verschiedene Kernreaktionen an Zyklotronen produziert werden; z. B. über die Reaktionen ^{72}Ge(p,n), ^{72}Ge(d,2n), ^{69}Ga(α,n), ^{71}Ga(α,3n), ^{71}Ga(^{3}He,2n).

Zur Herstellung kurzlebiger Radioisotope verwendet man entweder Nuklear-Reaktoren oder ein Zyklotron, welches dann aber in der Nähe des Tomographen stehen muss. Eine Alternative zur Erzeugung vor Ort ist die Darstellung mit Hilfe eines Isotopen-Generators. Der Vorteil des Generators liegt darin, dass die Produktion des in der Regel relativ langlebigen Generator-Mutterisotops nicht in der Nähe des PET-Tomographen stattfinden muß.

Arsen-72 entsteht auch bei dem radioaktiven Zerfall von Selen-72. Selen-72 mit einer Halbwertszeit von 8,5 d dient somit als Generator-Mutterisotop für ^{72}As. Das ^{72}Se selbst läßt sich ebenfalls über verschiedene Kernreaktionen herstellen. Dazu zählen vor allem Spallationsreaktionen mit Protonen, beispielsweise an RbBr [Phillips D.R., United States Patent, Nr.: 5,371,372, Dez. 6, (1994); WO 93/04768, 18.03.1993] oder die Direkt-Prozesse ^{70}Ge(α,2n) bzw. ^{72}Ge(^{3}He,2n); *(Ward, Swindle et al. 1970; Hara, Tilbury et al. 1973; Al-Kourashi and Boswell 1978; Guillaume, Lambrecht et al. 1978; Basile, Birattari et al. 1981; Blessing, Weinreich et al. 1982; Byrne 1984; Mushtaq, Qaim et al. 1988; Mushtaq and Qaim 1990; Blessing, Lavi et al. 1992; Novgorodov, Schmidt et al. 2001; Blessing, Lavi et al. 2002; Mukhopadhyay, Nayak et al. 2002; Rösch, Novgorodov et al. 2002).*

Bislang ist ein Generatorprinzip publiziert worden [S.H. Al-Kouraishi, G.G.J. Boswell, Int. J. Appl. Rad. Isot. 29 (1978) 607], das auf einer säulenchromatographischen Elution des ^{72}As beruht, während ^{72}Se als Se^{o} auf dem Säulenmaterial verbleibt. Dazu wird ^{72}Se vorher mit Se-Trägerzusatz reduziert. Die Elutionsausbeuten betragen 70 %, was auf den Se-Trägergehalt zurückzuführen ist. Das Elutionsvolumen ist mit ca. 15 ml sehr groß.
Zwei weitere $^{72}Se/^{72}As$-Generatorprinzipien sind in den Dokumenten Phillips D.R., United States Patent 5 371 372, Dez. 6, (1994); WO 93/04768, 18.03.1993, Rösch, F., DE 100 28 056 A beschrieben. Das ^{72}Se wird gemäß dem US Patent 5 371 372 aus mit Protonen bestrahltem RbBr gewonnen. Bei diesem Verfahren sind jedoch viele Reinigungsschritte von Nöten, um ^{72}Se in reiner Form darzustellen. Der zyklische Abtrennschritt des ^{72}As erfolgt dadurch, dass jedesmal zuerst selenige Säure zugegeben, danach mit Hydrazinhydrochlorid das Trägerselen zusammen mit ^{72}Se zu metallischem Selen reduziert und abfiltriert wird. ^{72}As verbleibt in der Lösung. Zur Vorbereitung des nächsten Trennzyklus muß das reduzierte Selen wieder oxidativ mittels H_2O_2 in Lösung gebracht werden. Dann wird über zwei Tage ^{72}As in dieser Lösung generiert.

Gemäß der DE 100 28 056 wird das ^{72}As als $^{72}AsCl_3$ im HCl-Gasstrom von einer ^{72}Se-haltigen Lösung abdestilliert. Nachteile dieses Systems sind die Redoxinstabilität des Generators, der vor jedem Abtrennungsvorgang zunächst mit Königswasser reoxidiert werden muss, sowie der apparative Aufwand einer radioaktiven Destillation im HCl-Gasstrom. Des Weiteren wird dort das ^{72}As primär in Aktivkohle aufgefangen und steht nicht unmittelbar für radiopharmazeutische Synthesen zur Verfügung.

Im Hinblick auf diese Nachteile stellt sich für die Erfindung die Aufgabe ein Verfahren zur Herstellung von trägerfreiem ^{72}As und eine Vorrichtung zur Herstellung von trägerfreiem ^{72}As und trägerfreiem ^{72}As(III)-Halogeniden in solchen Formen zu schaffen, die für anschließende nca ^{72}As-Synthesen und Verwendung als Radiopharmaka für PET-Untersuchungen und Radiotherapeutika (analoge Chemie mit ^{77}As) geeignet sind.

Diese Aufgabe löst erfindungsgemäß ein Verfahren zur Herstellung von trägerfreiem ^{72}As durch folgende Verfahrensschritte:

(a) Bestrahlen eines Targets aus Germanium oder Germaniumverbindungen, mit natürlicher Isotopenzusammensetzung des Germaniums oder Isotop angereichertem Germanium,

(b) chemisches Abtrennen von ^{72}Se von dem bestrahltem Target,

(c) Reduktion von trägerfreiem ^{72}Se zu $^{72}Se^{(0)}$,

(d) Überführen und Fixieren des trägerfreien $^{72}Se^{(0)}$ auf einen Radionuklidgenerator in Gestalt einer Festphasenextraktionskartusche, auf der ^{72}As durch radioaktiven Zerfall von $^{72}Se^{(0)}$ generiert wird, und

(e) chemisches Abtrennen des trägerfreien ^{72}As von $^{72}Se^{(0)}$ mit Hilfe eines protischen (protogenen) Lösungsmittels.

Die Verfahrensschritte (a) bis (e) werden mit trägerfreiem ^{72}Se ausgeführt, können aber ebenso mit geträgertem ^{72}Se durchgeführt werden.

Die weitere Ausgestaltung des Verfahrens ergibt sich aus den Merkmalen der Ansprüche 3 bis 9.

Im Rahmen der zu lösenden Aufgabe wird auch ein Verfahren zur Weiterverarbeitung von trägerfreiem ^{72}As, hergestellt nach den Ansprüchen 1 bis 8, zu trägerfreiem $^{72}As(III)$-Halogenid, durch folgende Verfahrensschritte angegeben:

(a) Hinzufügen eines Halogenids wie KI zu dem trägerfreiem ^{72}As, das als Eluat mit Hilfe von konzentrierter Flußsäure HF_{konz} gewonnen wurde,

(b) Erwärmen der konzentrierten Flußsäure HF_{konz} und des Eluats auf eine Temperatur von 35 bis 45 °C und Einwirken der konzentrierten Flußsäure HF_{konz} über eine Zeitspanne von 10 bis 15 min bis zur Bildung von Arsenhalogenid,

(c) Überführen und Fixieren des Arsenhalogenids auf einer Festphasenextraktionskartusche, die vor dem Aufgeben der Lösung von Arsenhalogenid gemäß Schritt (b) mit einem organischen Lösungsmittel und Wasser konditioniert wird,

(d) Spülen mit einem organischen Lösungsmittel, wie Chloroform oder Ethanol, der aufgegebenen Lösung von Arsenhalogenid, und

(e) Trocknen des eluierten Arsenhalogenids mit einem Trocknungsmittel, wie Calciumchlorid, in einer Trocknungskartusche und Auffangen des Arsenhalogenids in einem Produktgefäß.

Als Target zur Erzeugung des Mutternuklides für einen ^{72}Se / ^{72}As Radionuklidgenerator wird natürliches Germanium oder hochangereichertes ^{70}Ge verwendet werden. Die Darstellung des ^{72}Se erfolgt hier über (α,2n)- oder (^{3}He,3n)-Reaktionen an Germanium oder Germanium-Verbindungen. Das bestrahlte Germaniumtarget wird beispielsweise in HF_{konz} bei einer Temperatur von 50 °C gelöst. Dabei bildet sich $[GeF_6]_2$-. Das in der Lösung vorhandene ^{72}Se wird ohne Se-Trägerzusatz zu ^{72}Se(0) reduziert. Der wesentliche Unterschied zu dem oben genannten Verfahren *(Al-Kourashi and Boswell 1978; Phillips, Hamilton et al. 1991; Phillips, Hamilton et al. 1992; Blessing, Lavi et al. 2002)* ist damit der Verzicht auf Selen-Trägerzugabe. Dieses trägerfreie $^{72}Se^{(0)}$ wird auf einer Festphasenextraktionskartusche fixiert.

Zur zyklischen Abtrennung des trägerfreien ^{72}As von ^{72}Se und zur Umwandlung von nca ^{72}As zu nca ^{72}As(III)-Halogeniden, wobei nca trägerfrei (no carrier added) bedeutet, wird eine Vorrichtung zur automatischen Herstellung von trägerfreiem ^{72}As und trägerfreiem ^{72}As(III) Halogenid eingesetzt, enthaltend:

(a) ein erstes Reaktionsgefäß, das mit einer Anzahl von Eingabeeinrichtungen und einer Inertgaszufuhr verbunden ist,
(b) einen Radionuklidgenerator, der mit dem ersten Reaktionsgefäß in Verbindung steht,
(c) eine Zufuhrleitung, die den Ausgang des Radionuklidgenerators mit dem Eingang eines zweiten Reaktionsgefäßes verbindet, dessen Eingang mit den Eingabeeinrichtungen in Verbindung ist,
(d) eine Festphasenextraktionskartusche, die an den Ausgang des zweiten Reaktionsgefäßes angeschlossen ist;
(e) ein Abfallgefäß, das mit dem Radionuklidgenerator verbunden ist,
(f) ein Produktgefäß, das über eine Trocknungseinrichtung an den Ausgang der Festphasenextraktionskartusche angeschlossen ist, und

(g) eine Heizeinrichtung zum Beheizen der Reaktionsgefäße, des Radionuklidgenerators und der Festphasenextraktionskartusche.

Das durch das auf der Festphasenextraktionskartusche fixierte ^{72}Se generierte ^{72}As kann mit verschiedenen protischen Lösungsmitteln, z.B. HF_{konz} von der Kartusche eluiert werden. Mit HF_{konz} sind 60% der Aktivität schon im ersten Milliliter Eluat (im Gegensatz zu 15 ml bei Al-Kourashi (Al-Kourashi and Boswell 1978)) separierbar. Dieser Vorgang kann bei Bedarf jederzeit zur Gewinnung des Generatorprodukts ausgeführt werden.

Im Gegensatz zu den bis jetzt bekannt gewordenen Verfahren ermöglichen die erfindungsgemäßen Verfahren, das nca ^{72}As in eine für weitere chemische Synthesen praktikable Form überzuführen. Hierzu werden zu dem Generatoreluat geringe Mengen eines Halogenids (z.B. KI) hinzugefügt. Es bildet sich eine nca $^{72}AsI_3$-Lösung, die über eine weitere Festphasenextraktionskartusche aufgegeben wird, wobei das nca $^{72}AsI_3$ zu mehr als 99 % an der stationären Phase fixiert bleibt. Zur Entfernung der HF wird die Kartusche mit Argon aus einer Inertgaszufuhr 1 trockengeblasen. Danach kann das nca $^{72}AsI_3$ in einem organischen Lösungsmittel zu mehr als 99 % eluiert werden. Diese Fraktion wird abschließend über einer mit Trocknungsmittel gefüllten Kartusche getrocknet. Im Unterschied zu dem bisher bekannten Stand der Technik kann ^{72}As in einem organischen Lösungsmittel eluiert werden. Der zeitliche Aufwand zum Aufbau der Generatorvorrichtung und zur Abtrennung ist extrem niedrig und beträgt etwa 1 h für den Aufbau und ca. 30 min für die Abtrennung. Im Gegensatz hierzu benötigt das in der DE 100 28 056 A1 beschriebene Verfahren zum Aufbau einen Tag und zur Abtrennung 5 h.

An Hand der einzigen Figur wird die Vorrichtung zur automatisierten Herstellung von trägerfreiem ^{72}As und von trägerfreien ^{72}As(III)-Halogeniden erläutert.

Die Vorrichtung enthält zwei Reaktionsgefäße 8, 9, die Inertgaszufuhr 1, eine Anzahl von Eingabeeinrichtungen 2 bis 7, einen Radionuklidgeneratorkartusche 10, eine Festphasenextraktionskartusche 11, eine Trocknungskartusche 12, ein Abfallgefäß 13 und ein Produktgefäß 14. Jedes der beiden Reaktionsgefäße 8, 9 ist mit einem Rührwerk 17, 18 ausgerüstet. Die Reaktionsgefäße 8, 9 bestehen aus einem Kunststoff auf Basis von Polytetrafluorethylen oder Perfluoroalkoxy, d. h. aus einem Kunststoff, der gängigerweise

als Teflon bekannt ist. Die Eingabeeinrichtungen 2 bis 7 sind Spritzpumpen, wobei über die Eingabeeinrichtung 2 ein organisches Lösungsmittel, über die Eingabeeinrichtung 3 Wasser, über die Eingabeeinrichtung 4 konzentrierte Flußsäure HF_{konz} und ein Halogenid, z.B. KI, über die Eingabeeinrichtung 5 konzentrierte Flußsäure HF_{konz} und ein Reduktionsmittel, z.B. Hydrazindihydrochlorid, nach Bedarf, in die Reaktionsgefäße 8, 9 bzw. in den Radionuklidgenerator 10 und die Festphasenextraktionskartusche 11 einleitbar sind. Über die Eingabeeinrichtung 7 gelangt ein bestrahltes Germaniumoxidtarget in das erste Reaktionsgefäß 8, das der Targetaufbereitung dient. Der Radionuklidgenerator 10 ist eine Festphasenextraktionskartusche. Das erste Reaktionsgefäß 8 ist mit den Eingabeeinrichtungen 2 bis 7 und mit der Inertgaszufuhr 1 verbunden. Der Ausgang des ersten Reaktionsgefäßes 8 ist an den Radionuklidgenerator 10 angeschlossen. Dessen Ausgang steht über einer Leitung 15 in Verbindung mit dem zweiten Reaktionsgefäß 9. Des Weiteren ist der Ausgang des Radionuklidgenerators 10 verzweigt einerseits über die Trocknungskartusche 12 mit dem Produktgefäß14 in Verbindung und andererseits direkt an das Abfallgefäß 13 angeschlossen. Das zweite Reaktionsgefäß 9 steht in Verbindung mit der Festphasenextraktionskartusche 11, deren Ausgang gleichfalls an die Trockungskartusche 12 angeschlossen ist. Die Trocknungskartusche 12 ist eine z. B. mit $CaCl_2$ gefüllte Trocknungskartusche, in der das in der Festphasenextraktionskartusche eluierte trägerfreie ^{72}As-Halogenid trocknet und danach in das Produktgefäß 14 abfüllbar ist. Zum Beheizen sowohl der Reaktionsgefäße 8, 9 als auch des Radionuklidgenerators 10 und der Kartusche 11 ist eine Heizeinrichtung 16 vorgesehen.

Ausführungsbeispiel:

Ein über (^{3}He,xn) bestrahltes 100 mg Germaniumoxidtarget wird zur Abtrennnung des ^{72}Se zunächst in 3 ml $HF_{konz.}$, zugeführt über die Eingabeeinrichtung 5, bei T = 50 °C in dem ersten Reaktionsgefäß 8 gelöst. Dieser Vorgang dauert etwa 30 min. Zu dieser Targetlösung werden 50 mg Hydrazindihydrochlorid, gleichfalls über die Eingabeeinrichtung 5, gegeben und anschließend wird kräftig für 5 min durchmischt und 20 min inkubiert. Das reduzierte $^{72}Se^{(0)}$ wird anschließend auf dem Radionuklidgenerator 10, der Festphasenextraktionskartusche aus Polystyrol ENV fixiert. Dazu wird der Radionuklidgenerator mit Acetonitril, H_2O und $HF_{konz.}$ aus den Eingabeeinrichtungen 2, 3 und 5 konditioniert, die Lösung aufgegeben und mit 5 ml $HF_{konz.}$ gespült. Die Elution der

gebildeten ^{72}As-Aktivität erfolgt mit 1ml $HF_{konz.}$ direkt in dem zweiten Reaktionsgefäß 9, in dem sich unter Zugabe von 10 mg KI nach etwa 10 min Inkubation bei T = 35 □C AsI_3 bildet. Dieses wird auf der Festphasenextraktionskartusche 11 aus Polystyrol ENV fixiert. Hierzu wird die Kartusche mit Acetonitril und H_2O konditioniert, die Lösung aufgegeben und anschließend mit 2 ml Chloroform aus der Eingabeeinrichtung 6 gespült. Das so eluierte $^{72}AsI_3$ in Chloroform wird über die Trocknungskartusche 12 zur Trocknung gespült und in dem Produktgefäß 14 aufgefangen.

Mit der Erfindung wird der Vorteil erzielt, dass ein sehr einfaches und schnelles Verfahren zur Darstellung von trägerfreiem $^{72}AsI_3$ an einem trägerfreien $^{72}Se/^{72}As$-Radionuklidgenerator zur Verfügung steht. Das nca ^{72}Se wird dabei zuerst auf naßchemischem Weg von bestrahlten Germaniumtargets abgetrennt. Es erfolgt die Trennung $^{72}Se/^{72}As$ in einer einfach aufgebauten Vorrichtung, die Synthese von ^{72}As(III)-Halogeniden, bzw. generell die automatisierte Herstellung von trägerfreiem $*AsX_3$; (*=70, 71, 72, 74, 76, 77; X=Cl, Br, I), sowie nachfolgende Synthesen von nca As-Pharmaka damit.

Die Erfindung beinhaltet dabei ein Generatorkonzept, in dem das ^{72}Se trägerfrei auf einer Festphasenextraktionskartusche fixiert bleibt, und ^{72}As als ^{72}As(III)-Halogenid in einem organischen Lösungsmittel gewonnen werden kann. Die ^{72}As-Trennausbeuten liegen höher als 60 % in einem Milliliter, die ^{72}Se-Kontaminationen final unter 0,001%.

Des Weiteren sind die Verfahrensschritte und die Vorrichtung zur automatisierten Herstellung von trägerfreiem $^{72}AsI_3$ auf andere Arsenisotope und weitere As(III)-Halogenide ($*AsX_3$; *=70, 71, 72, 74, 76, 77; X=Cl, Br, I) übertragbar.

Für das trägerfreie Arsenhalogenid wird ein Arsenisotop aus der Gruppe mit den Atomgewichten 70, 71, 72. 74, 76, 77 ausgewählt. Trägerfreie Arsenhalogenide $*AsX_3$ mit * = 70, 71, 72. 74 und X = Cl, Br, I werden zur Herstellung von Radiopharmaka für die Positronen-Emissions-Tomographie verwendet, während Arsenhalogenide mit * = 76, 77 und X = Cl, Br, I bei der Herstellung von Radiotherapeutika Anwendung finden.

Patentansprüche

1. Verfahren zur Herstellung von trägerfreien ^{72}As durch folgende Verfahrensschritte:
   (a) Bestrahlen eines Targets aus Germanium oder Germaniumverbindungen, mit natürlicher Isotopenzusammensetzung des Germaniums oder isotop angereichertem Germanium oder bestrahlen eines Targets zur Produktion von ^{72}Se über eine der alternativen Produktionswege
   (b) chemisches Abtrennen von ^{72}Se von dem bestrahltem Target,
   (c) Reduktion von trägerfreiem ^{72}Se zu $^{72}Se^{(0)}$,
   (d) Überführen und Fixieren des trägerfreien $^{72}Se^{(0)}$ auf einer Festphasenextraktionskartusche, auf der ^{72}As durch radioaktiven Zerfall von $^{72}Se^{(0)}$ generiert wird, und
   (e) chemisches Abtrennen des trägerfreien ^{72}As von $^{72}Se^{(0)}$ mit Hilfe eines protischen (protogenen) Lösungsmittels.

2. Verfahren nach Anspruch 1, dadurch gekennzeichnet, dass die Verfahrensschritte (a) bis (e) sowohl mit trägerfreiem als auch mit geträgertem ^{72}Se durchgeführt werden.

3. Verfahren nach Anspruch 2, dadurch gekennzeichnet, dass das chemische Abtrennen von ^{72}Se mit protischen (protogenen) Lösungsmitteln vorgenommen wird.

4. Verfahren nach Anspruch 3, dadurch gekennzeichnet, dass als protisches (protogenes) Lösungsmittel konzentrierte Flußsäure HF_{konz} eingesetzt wird.

5. Verfahren nach Anspruch 3 oder 4, dadurch gekennzeichnet, dass das protische (protogene) Lösungsmittel auf eine Temperatur von 45 bis 55 °C erwärmt wird und 25 bis 45 min auf das Target einwirkt.

6. Verfahren nach Anspruch 5, dadurch gekennzeichnet, dass zur Reduktion von ^{72}Se dem protischen Lösungsmittel ein geignetes Reduktionsmittel hinzugegeben und mit dem Lösungsmittel einige Minuten durchmischt wird.

7. Verfahren nach Anspruch 1, dadurch gekennzeichnet, dass das trägerfreie ^{72}Se auf der Festphasenextraktions-Kartusche durch Konditionierung der Kartusche mit einer Mischung aus organischem Lösungsmittel, HF_{konz} und Wasser fixiert wird.

8. Verfahren nach Anspruch 7, dadurch gekennzeichnet, dass als organisches Lösungsmittel für die Konditionierung Acetonitril eingesetzt wird.

9. Verfahren nach einem der Ansprüche 1 bis 8, dadurch gekennzeichnet, dass das chemische Abtrennen des trägerfreien ^{72}Se durch Elution mit konzentrierter Flußsäure HF_{konz} vorgenommen wird.

10. Verfahren zur Weiterverarbeitung von trägerfreiem ^{72}As, hergestellt nach den Ansprüchen 1 bis 9, zu trägerfreiem ^{72}As(III)-Halogenid, durch folgende Verfahrensschritte:
    (a) Hinzufügen eines Halogenids wie KI zu dem trägerfreiem ^{72}As, das als Eluat mit Hilfe von konzentrierter Flußsäure HF_{konz} gewonnen wurde,
    (b) Erwärmen der konzentrierten Flußsäure HF_{konz} und des Eluats auf eine Temperatur von 35 bis 45°C und Einwirken der konzentrierten Flußsäure HF_{konz} über eine Zeitspanne von 10 bis 15 min bis zur Bildung von Arsenhalogenid,
    (c) Überführen und Fixieren des Arsenhalogenids auf einer Festphasenextraktionskartusche, die vor dem Aufgeben der Lösung von Arsenhalogenid gemäß Schritt (b) mit einem organischen Lösungsmittel und Wasser konditioniert wird,
    (d) Spülen mit einem organischen Lösungsmittel, z. B. Chloroform oder Ethanol, der aufgegebenen Lösung von Arsenhalogenid, und
    (e) Trocknen des eluierten Arsenhalogenids mit einem Trocknungsmittel, z.B. Calciumchlorid, in einer Trocknungskartusche und Auffangen des Arsenhalogenids in einem Produktgefäß.

11. Verfahren nach Anspruch 10, dadurch gekennzeichnet, dass das trägerfreie Arsenhalogenid aus den Halogeniden Chlor, Brom, Iod ausgewählt wird.

12. Verfahren nach Anspruch 10, dadurch gekennzeichnet, dass als Arsenhalogenid Arsen(III)-iodid $^{72}AsI_3$ eingesetzt wird.

13. Verfahren nach Anspruch 10 oder 11, dadurch gekennzeichnet, dass für das trägerfreie Arsenhalogenid ein Arsenisotop aus der Gruppe mit den Atomgewichten 70, 71, 72, 74, 76, 77 ausgewählt wird.

14. Verwendung von trägerfreien Arsenhalogeniden $*AsX_3$ mit * = 70, 71, 72, 74 und X = Cl, Br, I, zur Herstellung von Radiopharmaka für die Positronen-Emissions-Tomographie.

15. Verwendung von trägerfreien Arsenhalogeniden $*AsX_3$ mit * = 76, 77 und X = Cl, Br, I, zur Herstellung von Radiotherapeutika.

16. Vorrichtung zur automatischen Herstellung von trägerfreiem ^{72}As und trägerfreiem ^{72}As(III)-Halogenid enthaltend:
    (a) ein erstes Reaktionsgefäß (8), das mit einer Anzahl von Eingabeeinrichtungen (2 bis 7) und einer Inertgaszufuhr (1) verbunden ist,
    (b) einen Radionuklidgenerator (10), der mit dem ersten Reaktionsgefäß (8) in Verbindung steht,
    (c) eine Zufuhrleitung (15), die den Ausgang des Radionuklidgenerators (10) mit dem Eingang eines zweiten Reaktionsgefäßes (9) verbindet, dessen Eingang mit den Eingabeeinrichtungen (1 bis 6) in Verbindung ist,
    (d) eine Festphasenextraktionskartusche (11), die an den Ausgang des zweiten Reaktionsgefäßes (9) angeschlossen ist;
    (e) ein Abfallgefäß (13), das mit dem Radionuklidgenerator (10) verbunden ist,
    (f) ein Produktgefäß (14), das über eine Trocknungseinrichtung (12) an den Ausgang der Festphasenextraktionskartusche (11) angeschlossen ist, und
    (g) eine Heizeinrichtung (16) zum Beheizen der Reaktionsgefäße (8, 9), des Radionuklidgenerators (10) und der Festphasenextraktionskartusche (11).

17. Vorrichtung nach Anspruch 16, dadurch gekennzeichnet, dass jedes Reaktionsgefäß (8; 9) mit einem Rührwerk (17; 18) ausgerüstet ist und dass das Material der Reaktionsgefäße ein Kunststoff auf Basis von Polytetrafluorethylen oder Perfluoroalkoxy ist.

18. Vorrichtung nach Anspruch 16, dadurch gekennzeichnet, dass die Eingabeeinrichtungen (2 bis 7) Spritzpumpen sind und dass über die Eingabeeinrichtung (2) ein organisches Lösungsmittel, über die Eingabeeinrichtung (3) Wasser, über die Eingabeeinrichtung (4) konzentrierte Flußsäure HF_{konz} und ein Halogenid wie KI, über die Eingabeeinrichtung (5) konzentrierte Flußsäure HF_{konz} und ein Reduktionsmittel, wie Hydrazindihydrochlorid, bei Bedarf, in die Reaktionsgefäße (8, 9) bzw. in den Radionuklidgeneratoren (10) einleitbar sind.

19. Vorrichtung nach Anspruch 16, dadurch gekennzeichnet, dass über die Eingabeeinrichtung (7) ein bestrahltes Target in das erste Reaktionsgefäß (8) einbringbar ist.

20. Vorrichtung nach Anspruch 16, dadurch gekennzeichnet, dass über die Eingabeeinrichtung (6) Chloroform zum Spülen in die Festphasenextraktionskartusche (11) einleitbar ist.

21. Vorrichtung nach Anspruch 16, dadurch gekennzeichnet, dass der Radionuklidgenerator (10) eine Festphasenextraktionskartusche ist, wobei auf dem Radionuklidgenerator (10) trägerfreies $^{72}Se^{(0)}$ fixierbar ist, das durch radioaktiven Zerfall trägerfreies ^{72}As generiert und auf der Festphasenextraktionskartusche (11) ein ^{72}As-Halogenid fixierbar ist.

22. Vorrichtung nach Anspruch 16, dadurch gekennzeichnet, dass die Trocknungseinrichtung (12) eine mit einem Trocknungsmittel wie Calziumchlorid, gefüllte Kartusche ist, in der das in der Festphasenextraktionskartusche (11) eluierte trägerfreie ^{72}As-Halogenid trocknet, und danach in das Produktgefäß (14) abfüllbar ist.

Zusammenfassung

Verfahren zur Herstellung von trägerfreiem ^{72}As und Vorrichtung zur automatischen Herstellung von trägerfreiem ^{72}As und trägerfreiem ^{72}As (III)-Halogenid sowie deren Verwendung

Die Darstellung von trägerfreiem ^{72}As erfolgt an einem Radionuklidgenerator 10, ausgehend von einem Germaniumtarget, das in einem ersten Reaktionsgefäß 8 gelöst wird. Das trägerfreie ^{72}As-Eluat wird in einem zweiten Reaktionsgefäß 9 mit KI umgesetzt und das Produkt $^{72}AsI_3$ über eine Festphasenextraktionskartusche 11 abgetrennt. Die Umsetzung der ^{72}As-Eluat kann neben Iod auch mit den Halogeniden Br und Cl vorgenommen werden. Aus den gewonnenen Arsenhalogeniden werden Radiopharmaka und Radiotherapeutika hergestellt.

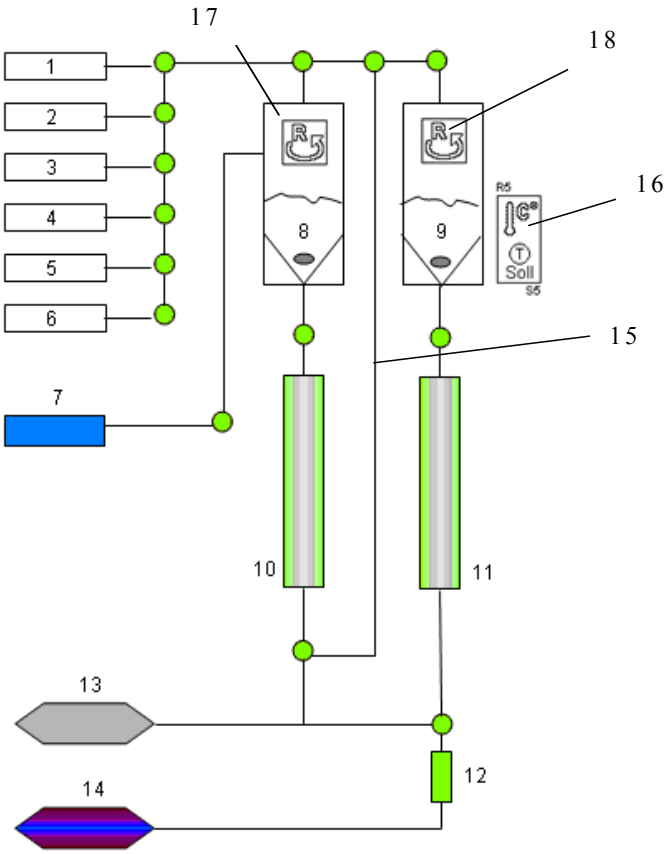

X.

Radioaktives Arsentriiodid und dessen Verwendung zur radioaktiven Markierung

Radioaktives Arsentriiodid und dessen Verwendung zur radioaktiven Markierung

Deutsches Patent Nr.: DE 103 50 397.8

Die vorliegenden Erfindung betrifft radioaktives Arsentriiodid sowie ein Verfahren zur Markierung mit radioaktivem Arsentriiodid.

Radioisotope haben eine große Bedeutung in der nuklearmedizinischen Diagnostik und Therapie. Die nuklearmedizinische Diagnostik umfaßt zwei bildgebende Verfahren, die single-photon-emission-tomography (SPET) und die positron-emission-tomography (PET). In dem erstgenannten Verfahren kommen Radioisotope zum Einsatz, die bei ihrem radioaktiven Zerfall gamma-Strahlung im Energiebereich von etwa 100 bis 300 keV emittieren. Die am häufigsten eingesetzten Nuklide sind ^{99m}Tc (6,02 h Halbwertszeit, 141 keV), ^{111}In (2,81 d; 245 keV) und ^{123}I (13,2 h; 159 keV). Für die PET sind Nuklide erforderlich, die unter Aussendung eines Positrons zerfallen. Diese Bedingung erfüllen insbesondere die Radioisotope ^{11}C (20,4 min; 99,8 % β^+), ^{13}N (9,96 min; 100 % β^+), ^{15}O (2,03 min; 99,9 % β^+) und ^{18}F (109,7 min; 96,9 % β^+). Für Prozesse mit längeren biologischen Halbwertszeiten werden allgemein Positronen-emittierende Metalle wie ^{86}Y (14,7 h; 34 % β^+) oder ^{64}Cu (12,7 h; 50 % β^+) sowie die Halogene ^{76}Br oder ^{124}I eingesetzt. Diese werden mit Hilfe von geeigneten Komplexbildnern an die Zielmoleküle koordinativ gebunden. Gerade bei der Anwendung von nuklearmedizinisch relevanten, tumoraffinen Peptiden, Antikörpern oder Fragmenten davon sind häufig Radionuklide mit einer längeren Halbwertszeit erforderlich. Solche Radionuklide sind für Therapie und Diagnostik von besonderem Interesse. Aufgrund der längeren Halbwertszeiten und der in vivo-Stabilitäten gelten Yttrium-, Kupfer- und Arsen-Radioisotope als besonders vielversprechend. Besonders hervorzuheben sind hierbei ^{70}As (52,6 min Halbwertszeit; 90 % β^+), ^{71}As (64,8 h; 30 % β^+), ^{72}As (26 h; 88 % β^+), ^{74}As (17,78 d; 29 % β^+),^{76}As (26,4 h; β^-) und ^{77}As (38,8 h; β^-). Arsen bildet mit den meisten Nichtmetallen starke kovalente Bindungen. Arsenhaltige Pharmaka sind zudem seit Jahrhunderten bekannt. Solche Pharmaka werden auch heute noch entwickelt.

In der DE 100 28 056 A1 ist ein Verfahren sowie eine Vorrichtung zur Abtrennung von trägerfreiem Arsen-72 aus einem Gemisch von Selen-72 und Arsen-72 offenbart. In einer Quarz- oder Glasapparatur wird dabei eine ^{72}Se enthaltende Lösung beispielsweise mit

Kaliumchlorid und konz. Salzsäure versetzt und die Mischung auf etwa 100℃ erhitzt. Über die heiße Lösung läßt man dann einen Strom von HCl-Gas streichen, der das aus der Mischung abdestillierende $^{72}AsCl_3$ (Siedepunkt: 130,2 ℃) aufnimmt. Das als Mutternuklid fungierende ^{72}Se verbleibt dagegen in der salzsauren Lösung. Der Gasstrom wird dann durch eine Adsorberkartusche geleitet, die beispielsweise Aktivkohle enthält. Das Arsen-72-Radionuklid wird an den Adsorber gebunden und kann anschließend mit einem wäßrigen oder nicht-wäßrigen Lösemittel als trägerfreies ^{72}As herausgespült werden.

Ein Verfahren zur Abtrennung von Arsen-72 von einem geträgerten (carrier added) Vorläufer Selen-72 ist in der US 5,371,372 offenbart. In dem Verfahren wird das ca-Selen-72, das in Form von seleniger Säure vorliegt, mit Hydrazin-dihydrochlorid zu elementarem Selen reduziert, das durch Filtrieren abgetrennt wird, während das Arsen in Lösung bleibt. Das Selen muß anschließend durch Oxidation erneut in eine lösliche Form überführt werden. Das Verfahren ist aufwendig und dementsprechend schwierig zu handhaben.

Weiterhin bekannt ist ein Dimethylchlorarsin, $(H_3C)_2AsCl$, das radioaktives Arsen-76 enthält. Beschrieben ist auch die Umsetzung des radioaktiven Dimethylchlorarsins mit Mercapto-Gruppen enthaltenden Biomolekülen (*Int. J. Appl. Radiat. Isotop.* **33** [1982] 1477 - 1478).

Zur Markierung von Molekülen, insbesondere solchen, die in biologisch aktivem Material vorkommen, sind Arsen-Radioisotope von besonderem Interesse. Es stehen jedoch bis heute keine einfach zu handhabenden trägerfreien (no-carrier-added, nca) oder geträgerten (carrier-added, ca) Arsenverbindungen zur Verfügung, mit denen eine solche Markierung durchgeführt werden könnte.

Gefunden wurde nunmehr, daß diese Aufgabe gelöst werden kann mit radioaktiven Arsentriiodid, $*AsI_3$, und davon abgeleiteten Verbindungen, in denen 2 der 3 Iodatome durch Substituenten ersetzt sind, die unter den bei Markierungsreaktionen herrschenden Bedingungen unverändert bleiben.

Gegenstand der vorliegenden Erfindung ist demgemäß radioaktives $*AsI_3$, wobei *As für Arsen-70, -71, -72, -74, -76 oder -77 steht. In einer besonderen Ausführungsform ist das $*AsI_3$ geträgert, d.h. mit nicht- radioaktivem AsI_3 vermischt.

Herstellen läßt sich das radioaktive Arsentriiodid beispielsweise nach folgendem Verfahren Ein bestrahltes Target aus Germaniumoxid (je nach zu produzierendem Isotop in einem Kernreaktor oder einem Cyclotron bestrahlt) wird in konz. HF gelöst. Es bildet sich Germaniumhexafluorat GeF_6^{2-}. Durch Zugabe von KI wird nun AsI_3 gebildet. Das nca- oder ca-*AsI_3 wird zweckmäßig in einer Festphasenextraktionskartusche fixiert, während das GeF_6^{2-} in der mobilen Phase verbleibt. Mit einem organischen Lösungsmittel, wie z.B. Methylenchlorid, Dimethylformamid oder Ethanol kann es dann schnell (in maximal etwa 30 min) und praktisch quantitativ von dem Adsorbens in der Kartusche eluiert werden.

Arsentriiodid kann prinzipiell dreimal mit Nucleophilen reagieren. Das sind insbesondere Verbindungen, die mindestens eine Amino-, Hydroxy- und/oder Mercapto-Gruppen aufweisen. In einer bevorzugten Ausführungsform sind daher 2 der 3 Halogenatome ersetzt durch Atome oder Gruppen, die unter den Bedingungen, die bei den Markierungsreaktionen herrschen, nicht reagieren. Das sind beispielsweise Alkylgruppen, insbesondere Methyl-, Ethyl-, Propyl- oder Isopropylgruppen oder Phenyl- und/oder Alkylsulfanylgruppen, insbesondere Methylsulfanyl- oder Ethylsulfanyl-Gruppen. Die 2 Gruppen können auch untereinander verbunden sein, beispielsweise durch eine oder mehrere Methylengruppen. Das ist beispielsweise der Fall bei einer Propan-1,3-diylbissulfanyl-Gruppe (-S-CH_2-CH_2-CH_2-S-).

Diese Derivate mit nur noch einer reaktionsfähigen As-I-Bindung sind auf einfache und dem Fachmann prinzipiell bekannte Art erhältlich. So kann nca- oder ca-*AsI_3 mit Propan-1,3-dithiol in Gegenwart von Pyridin als Base bei tiefer Temperatur zu nca- oder ca-Propan-1,3-diylbissulfanyl-arseniodid umgesetzt werden. Pyridin fällt dabei im Laufe der Reaktion als unlösliches Pyridiniumiodid aus. Das ca-Propan-1,3-diylbissulfanyl-arseniodid ist empfindlich gegenüber Licht und Sauerstoff. Es kann durch Hochdruck-Flüssigkeitschromatographie (HPLC) isoliert werden und danach für Reaktionen mit den zu markierenden Verbindungen eingesetzt werden. Die zu markierenden Verbindungen sind wiederum solche, die SH- und/oder NH_2-Gruppen enthalten, beispielsweise eine Aminosäure mit Thiolgruppen, wie Cystein. Ebenso gut können auch Peptide oder Proteine markiert werden, die SH-Gruppen und/oder primäre Aminogruppen enthalten. Die markierte Verbindung wird zweckmäßig wiederum mit Hilfe der HPLC isoliert. Des

weiteren können in relevanten Biomolekülen durch chemische Modifikationen geeignete SH-Bindungsstellen geschaffen werden. Hier bieten sich vor allem zwei Möglichkeiten an: zum einen die Schaffung zusätzlicher SH-Funktionalisierungen, z.B. durch Umsetzung mit SATA (N-Succinimidyl S-Acetylthioacetat), und zum anderen eine schonende Reduktion vorhandener Disulfidbrücken mit gängigen Reduktionsmethoden, wie dem Zusatz von Sn^{2+} oder Mercaptoethanol.

Die entsprechenden, nicht-radioaktiven Arsenverbindungen lassen sich in gleicher Weise erhalten.

Zwischen dem radioaktiven Arsen und der zu markierenden Verbindung kann noch eine Brückengruppe angeordnet sein. Beispielsweise kann das oben genannte geträgerte oder nichtgeträgerte Propan-1,3-diylbissulfanyl-arseniodid zunächst unter Ausschluß von Licht und Sauerstoff mit mit 4-Mercapto-buttersäure in Gegenwart einer Base, wie Pyridin, umgesetzt werden. Im Verlauf der Reaktion fällt Pyridiniumiodid aus. Die mit dem radioaktiven Arsen substituierte Buttersäure kann dann unter Zuhilfenahme von einem Standard-Aktivierungsreagens, wie Tetramethyluronium-hexafluorophosphat (HATU), mit einem Peptid umgesetzt werden. Als Resultat davon wird ein mit radioaktivem Arsen markiertes Peptid erhalten.

Eine weitere Möglichkeit besteht darin, große SH-haltige Moleküle, z.B. Antikörper, auch direkt mit nca $*AsI_3$ umzusetzen. Hierzu wird das Molekül mit nca $*AsI_3$ bei T=37,5℃ für eine bestimmte Zeit inkubiert. Das markierte Molekül kann über HPLC aufgereinigt werden.

Zahlreiche der erfindungsgemäß markierten Verbindungen sind von besonderem Wert bei der Diagnose und Therapie von Krankheiten.

Das folgende Beispiel dient zur Illustration der Erfindung.

Beispiel

a) No-carrier-added *AsI_3 wurde in 5 ml wasserfreiem Methylenchlorid gelöst. Die Lösung wurde unter einer Argon-Schutzgasatmosphäre in einem mit Aluminiumfolie vor Licht geschützten Kolben gerührt und auf -10 °C abgekühlt. Zu der gekühlten Lösung wurden dann nacheinander jeweils 1 µl Propan-1,3-dithiol und Pyridin gegeben. Nach dem Auftauen wurde zur Vervollständigung der Reaktion noch weitere 15 min gerührt. Das Propan-1,3-diylbissulfanyl-arseniodid wurde dann durch HPLC aufgereinigt.

b) Das gemäß a) erhaltene Propan-1,3-diylbissulfanyl-arseniodid wurde ohne Reinigung weiter umgesetzt. Dazu wurde die Lösung erneut auf -10 °C abgekühlt und 5 mg N-*tert*.-Butoxycarbonyl-cystein-benzylester sowie 1 µl Pyridin hinzugefügt. Anschließend wurde die Lösung auf Raumtemperatur erwärmt und noch 15 min nachgerührt. Die Reaktionsmischung wurde anschließend auf Eis gegeben. Die organische Phase wurde abgetrennt, auf 2 ml eingeengt und durch präparative HPLC gereinigt (Luna C18(2), 250 x 30 mm, 5 micron, unter Verwendung eines Wasser/Methanol-Gemisches, 1 : 9 v/v).

c) Erhalten wurde auf diese Weise ein radioaktiv markiertes, mit Schutzgruppen versehenes Cystein (N-*tert*.-Butoxycarbonyl-S-(propan-1,3-diylbissulfanyl)-arsanyl-cystein-benzylester), dessen Schutzgruppen nun mit dem Chemiker geläufigen Standard-Methoden entfernt werden können. Am Schluß erfolgt noch ein letzter Aufreinigungschritt mittels HPLC

b) Das gemäß a) erhaltene Propan-1,3-diylbissulfanyl-arseniodid wurde ohne Reinigung weiter umgesetzt. Dazu wurde die Lösung erneut auf -10 °C abgekühlt und 5 mg N-*tert*.-Butoxycarbonyl-cystein-benzylester sowie 1 µl Pyridin hinzugefügt. Anschließend wurde die Lösung auf Raumtemperatur erwärmt und noch 15 min nachgerührt. Die Reaktionsmischung wurde anschließend auf Eis gegeben. Die organische Phase wurde abgetrennt, auf 2 ml eingeengt und durch präparative HPLC gereinigt (Luna C18(2), 250 x 30 mm, 5 micron, unter Verwendung eines Wasser/Methanol-Gemisches, 1 : 9 v/v).

Patentansprüche

Radioaktives Arsentriiodid der Formel *AsI_3, wobei * für 70, 71, 72, 74, 76 oder 77 steht.

1. Verfahren zur radioaktiven Markierung organischer Verbindungen, dadurch gekennzeichnet, dass sie mit radioaktivem Arsentriiodid der Formel *AsI_3, wobei *As für ^{70}As, ^{71}As, ^{72}As, ^{74}As, ^{76}As oder ^{77}As steht, umgesetzt werden, wobei mindestens eine reaktive Gruppe in den zu markierenden Verbindungen mit dem Arsen(III)halogenid unter Ausbildung einer kovalenten Bindung reagiert.

2. Verfahren gemäß Anspruch 2, dadurch gekennzeichnet, dass das radioaktive Arsentriiodid im Gemisch mit nicht-radioaktivem Arsentriiodid eingesetzt wird (carrier-added).

3. Verfahren gemäß Anspruch 2 oder 3, dadurch gekennzeichnet, dass zwei der drei Iodatome in dem nca- oder ca-Arsentriiodid vor der Umsetzung mit der zu markierenden Verbindung ersetzt werden durch Reste, die bei der Markierungsreaktion unverändert bleiben oder daß das nca- oder ca-Arsentriiodid direkt als Markierungsagens eingesetzt wird.

4. Verfahren gemäß einem oder mehreren der Ansprüche 2 bis 4, dadurch gekennzeichnet, dass zwischen dem Arsen und der zu markierenden Verbindung eine Brückengruppe eingefügt wird.

5. Verfahren gemäß einem oder mehreren der Ansprüche 2 bis 5, dadurch gekennzeichnet, dass die zu markierende Verbindung mindestens eine Thiol- und/oder eine primäre Aminogruppe umfasst.

6. Verfahren gemäß Anspruch 6, dadurch gekennzeichnet, dass die zu markierende Verbindung eine Aminosäure, ein Peptid oder ein Protein ist.

Zusammenfassung:

Radioaktives Arsentriiodid und dessen Verwendung zur radioaktiven Markierung

Beschrieben ist radioaktives Arsentriiodid der Formel *AsI_3, wobei * für 70, 71, 72, 74, 76 oder 77 steht, sowie ein Verfahren zur radioaktiven Markierung organischer Verbindungen, wobei mindestens eine reaktive Gruppe in den zu markierenden Verbindungen mit dem Arsen(III)halogenid unter Ausbildung einer kovalenten Bindung reagiert. Die zu markierende Verbindung ist vorzugsweise eine Aminosäure, ein Peptid oder ein Protein. Sie enthält vorzugsweise Mercaptogruppen und/oder primäre Aminogruppen. Gegebenenfalls wird sie auf bekannte Weise chemisch so modifiziert, daß geeignete Bindungsstellen entstehen.

4. Conclusion

This thesis describes the implementation of radioactive arsenic isotopes for life-sciences, molecular imaging and nuclear medical diagnosis and therapy, beginning with nuclear reactions for isotope production, over radiochemical separations of nca radioarsenic from irradiated targets or ^{72}Se as a radionuclide generator mother, development and evaluation of a labeling chemistry, *in vitro, ex vivo* and *in vivo* evaluation of the labeled compounds, namely serum stability, immunoreactivity and biodistribution and, finally, to first *in vivo* imaging experiments related to apoptosis.

The major achievements are:

- A ^{72}Se/^{72}As radionuclide generator utilising a distillation concept could be optimised. The system could be suitable for future application as a biomedical generator. At an optimum temperature of 105°C, more than 99% of the nca ^{72}As is separated in less than 10 minutes at a nca ^{72}Se contamination level below 0.05%.
- Following radiochemical separation of ^{72}Se from irradiated Ge or GeO_2 targets, nca ^{72}Se was used to design a second radionuclide generator based on solid phase extraction. After initial reduction of radioselenium, nca $Se^{(0)}$ is fixed on a polysterene based solid phase extraction column. Macroscopic Ge is separated as $[GeF_6]^{2-}$. Depending on the eluent, ^{72}As can be obtained with yields > 60% and a selenium contamination of less then 0.1%. The method presented in this thesis allows (A) an efficient route to ^{72}As labelling of molecules relevant to biochemistry and medicine via the labelling synthon $[^{72}As]AsI_3$ and represents (B) a convenient technological realisation with rather low operation costs, easy to automate for routine use.
- A new method was developed to separate radioactive arsenic isotopes from reactor or cyclotron irradiated germanium oxide targets. Following initial target dissolution, the arsenic reacts on addition of KI to form $[*As]AsI_3$. This nca radioarsenic triiodide is fixed on a polystyrene based solid phase extraction column. Macroscopic Ge is separated as $[GeF_6]^{2-}$. Nca $[*As]AsI_3$ can be obtained in yields > 85% with a contamination from germanium of less than 0.01%. This approach suggests a convenient technological realisation with rather low operation costs, and

would be easy to automate for routine use. Compared to previously described radioarsenic separations from macroscopic germanium, the method allows an efficient route to *As labelling of molecules relevant to biochemistry and medicine via the labelling synthon [*As]AsI_3. This approach might be in particular relevant to the cyclotron-based large-scale production of ^{72}As following $^{72}Ge(p,n)^{72}As$ reaction on highly enriched $^{72}GeO_2$.

- The nca synthesis of dimercapto arsenic and diphenyl arsenic iodides was established. These radioarsenic precursors were coupled to a biprotected cysteine, giving 1,3-dimercaptopropyl arsenic-boc-cysteine-O-bzl and diphenyl arsenic-boc-cysteine-O-bzl. The synthesis was performed using macroscopic AsI_3 and radioactive using nca $^{77}AsI_3$ with ≈ 60 % radiochemical yields.
- A new chimeric IgG_3 monoclonal antibody, ch3G4 (Tarvacin®), directed against anionic phospholipids was raised. A method for the labeling of antibodies with radioactive arsenic isotopes was developed and the radioarsenic labeled antibody was tested for its ability in terms of localization to tumor vessels and imaging qualities. *In vitro* and *ex vivo* evaluations showed, that ch3G4 recognized anionic phospholipids on the external membrane of R3227 Dunning prostate solid tumors in male Copenhagen rats.
- The tumors could be imaged with planar scintigraphy techniques and with Positron Emission Tomography *in vivo*, showing excellent and antigen-specific localization. In addition, the experiments proved the concept of the radiochemical separations applied and the developed labeling chemistry and demonstrated the potential benefits of the use of arsenic radioisotopes for molecular imaging of antibodies. The biomedical use of radioactive arsenic isotopes was exemplified for the first time in a multi-modality molecular imaging approach *in vivo*.
- Radioarsenic labeled compounds were used for basic science studies on the determination of imaging qualities and resolution enhancement for both planar scintigraphy- and small animal PET techniques.

To summarize, all the questions raised in the introduction have been discussed extensively and arsenic isotopes were brought from their nuclear production to first *in vivo* studies

providing new technical and chemical answers to multiple problems in the nuclear and radiopharmaceutical chemistry of arsenic isotopes.

As the results of these developments are promising in terms of making radioactive arsenic isotopes useful for molecular imaging, respectively PET, further experiments in the field could be challenging and rewarding:

1. **Isotope production**

   Higher yields for all nuclear reactions could be achieved using enriched target material. As the radiochemical separations suggested here are limited to germanium oxide and enriched targets material is available only in metallic state, a reliable way to oxidize metallic germanium in high yields should be developed. Also a way to recover the expensive target material should be found. Large-scale productions which could be used later on for a satellite-like distribution concept of arsenic radiopharmaceuticals should be evaluated.

2. **Radiochemistry and radiochemical separations**

   The product of the radiochemical separations is nca *AsI_3. Experiments to produce other nca arsenic halides are suggested because they differ in their reactivity and a larger variety of arsenic labeled biomolecules could be achieved.

3. **Labeling of smaller molecules**

   The amino acid cysteine was labeled and a cold arsenocysteine was synthesized. These results could be transferred to smaller thiol-containing peptides like glutathione and finally, a thiol-modified octreotide. Octreotide labeled with various radioactive isotopes is currently in clinical use for the detection and treatment of human somatostatin Typ 2 receptor expressing tumor malignancies.

4. **Labeling of antibodies**

   The results obtained using the PS-selective mab ch3g4 are excellent in terms of antigen specific tumor uptake and imaging qualities. The introduced labeling methods should be verified using additional animals models with various tumor

sorts and other antibodies with tumor targeting qualities. In addition endoradiotherapy studies are recommended using ^{77}As and /or ^{90}Y labeled ch3G4.

5. Mechanism of action of As_2O_3 (ATO)

ATO is currently a very promising agent for the treatment of promyelytic leukaemia and already in international clinical trials. However, the mechanism by which this agent is leading to a high percentage of partial and complete remissions remains unclear. A radioactive arsenic tracer could be used to observe detailed biodistribution and metabolic pathways of arsenic species.

Curriculum Vitae

Name	Marc Jennewein
Geburtsdatum	03.04.1974
Geburtsort	Mainz
Staatsangehörigkeit	deutsch
Familienstand	ledig
Anschrift	Am Eichelwäldchen 15 D-55252 Mainz-Kastel

Schulausbildung

1980 – 1984	Grundschule Martinusschule Weisenau
1984 – 1993	Bischöfliches Willigis Gymnasium, Mainz

Hochschulausbildung / Zivildienst

1993 - 1994		Zivildienst
1994	Okt	Beginn des Chemiestudiums an der Johannes-Gutenberg-Universität, Mainz
1997	Maerz	Vordiplom
1995	Aug	Diplomarbeit bei Prof. Dr. F. Rösch, Institut für Kernchemie, Johannes-Gutenberg-Universität, Mainz „Entwicklung eines nca ^{77}As/Ge-Trennsystems und eines nca ^{72}Se/nca ^{72}As-Radionuklidgenerators“
2002	Juni	Diplom
seit Juli 2002		Dissertation bei Prof. Dr. F. Rösch, Institut für Kernchemie, Johannes Gutenberg-Universität, Mainz „Production, Radiochemical Separation and Chemical Coupling of Radioactive Arsenic Isotopes to Synthesize Radiopharmaceuticals for Molecular Imaging“

Erklärung

Hiermit erkläre ich, dass ich die hier als Dissertation vorgelegte Arbeit selbst angefertigt und alle benutzten Hilfsmittel (z.B. Literatur, Geräte) in der Arbeit angegeben habe. Die aus den Quellen übernommenen Daten wurden unter Angabe der Quellen gekennzeichnet.
Ich habe weder diese Arbeit noch Teile davon bei einer anderen Stelle im In- und Ausland als Dissertation eingereicht.

Mainz, 28. Februar 2005 _____

Marc Jennewein